eman ta zabal zazu
Universidad del País Vasco
Euskal Herriko Unibertsitatea

DESIGN AND CHARACTERIZATION OF HYBRID POLYMERIC MATERIALS BASED ON PE-b-PEO BLOCK COPOLYMER

Sheyla Carrasco Hernández

Donostia-San Sebastián, 2017

UNIVERSITY OF THE BASQUE COUNTRY (UPV/EHU)
FACULTY OF EGINEERING, GIPUZKOA
DONOSTIA-SAN SEBASTIÁN
Department of Chemical and Environmental Engineering
Group `Materials + Technologies´ (GMT)

DESIGN AND CHARACTERIZATION OF HYBRID POLYMERIC MATERIALS BASED ON PE-b-PEO BLOCK COPOLYMER

Sheyla Carrasco Hernández

PhD Program Renewable Materials Engineering

Thesis Supervisor: Dr. Agnieszka Tercjak

Donostia-San Sebastián, 2017

Agradecimientos/Acknowledgments/Eskerrak

En primer lugar, quisiera agradecer al Ministerio de Economía y Competitividad por la financiación para llevar a cabo esta Tesis Doctoral y al Departamento de Ingeniería Química y del Medio Ambiente de la Escuela de Ingeniería de Gipuzkoa, Universidad del País Vasco (UPV/EHU) donde he realizado la misma.

Agradecer especialmente a mi directora Agnieszka Tercjak, por darme la oportunidad de crecer profesionalmente. Gracias por tu apoyo y paciencia durante el desarrollo de esta tesis, no sólo en lo profesional sino también en lo personal.

Gracias a todo el grupo de "Materiales + Tecnologías" y a todos los compañeros que habéis compartido parte de vuestro tiempo conmigo. A Gurutz, con el que siempre tendré pendiente una escapada al monte, a Irati con sus achaques de juventud, a Laida por tantas conversaciones y bueno ya sabes, la vida, a Clara por su mirada de Garfield y especialmente a Junkal, gracias por ser mi mentora de tesis y por hacer siempre lo que ha estado en tu mano para ayudarme, mila esker.

Gracias a Laura Peponi por supervisar mi estancia en el ICTP y a las compañeras que allí me ayudaron. Estuve muy a gusto con vosotras.

Thanks to Michael Morris for giving me the chance to stay at UCC and thanks also to all my colleagues in Cork, Cian, Parvaneh, Elsa and Sibu. Thanks for your help.

Gracias a mis compañeros de piso, a Guiomar por acogerme en mi llegada, a Lucía por ser mi apoyo femenino y a Daniel por las tertulias sobre la vida, la cuántica y los elementos finitos. Y a ti Álex, gracias por mantenerme a flote en tantas situaciones difíciles, por tantas risas y por ser mi familia en Donostia.

Gracias a mi gente de siempre que me ha apoyado desde lejos, en especial a Marta y a Carmen, gracias por estar ahí, en las duras y en las maduras. Gracias a Lucía por escucharme siempre y a Elisa por esas visitas a Donostia tan divertidas. Gracias a tantos amigos que no se han olvidado de mí a pesar de estar lejos.

Gracias a los que desde el principio me habéis hecho un hueco en Donostia, por esas tardes de ensayo y esas reuniones de Chopper. Gracias por contestar a ese email Juancar y por portarte siempre tan bien conmigo. Gracias Julen por esas charlas y por implicarte como un amigo. Gracias Kako por tantas risas y tantos buenos ratos contigo, que sí y por esas plaquitas tan bien hechas, sin ellas el Chapter 4 no hubiera sido posible.

Gracias a ti Jairo, por permanecer a pesar de todo. Espero poder compensarte de ahora en adelante. “Vivir la vida y aceptar el reto, recuperar la risa, ensayar el canto, bajar la guardia y extender las manos, desplegar las alas e intentar de nuevo, celebrar la vida y retomar los cielos”.

Mi agradecimiento más profundo a mi familia, a mi madre y a mi padre por demostrarme que de la tierra, además de hortalizas, también salen licenciados y doctores. Gracias por darnos la oportunidad de estudiar aunque eso supusiera tanto trabajo para vosotros. Gracias mama por enseñarme a resistir aunque las piernas fallen y a ti papa por enseñarme a ponerle cara de perro a la vida. Sois un ejemplo para nosotros. Gracias a mis hermanos, César y Jandro, siempre dispuestos a echar una mano. Gracias también a mi madrina y familia, por apoyarme siempre en la distancia. Sin vosotros esto no hubiera sido posible. Gracias.

Donostia, bat bakarra munduan, nire zati bat uzten dut zugan, zure jendean. Hurrengo bat arte!!

Summary

The main objective of this investigation work was the design and characterization of novel hybrid polymeric materials based on PE-b-PEO block copolymer. On the one hand, polymer dispersed liquid crystal materials based on PE-b-PEO block copolymer and nematic liquid crystals were developed as well as hybrid electrospun fibers fabricated by co-electrospinning. On the other hand, PE-b-PEO block copolymer nanostructured thermosetting systems were used as template for dispersion and localization of TiO_2 nanoparticles.

This dissertation consists of 7 Chapters. The Chapter 1 is a general introduction about liquid crystals, polymer blends with the especial emphasis on polymer dispersed liquid crystal blends and thermosetting systems modified with block copolymers and inorganic nanoparticles.

In the Chapter 2, a brief description of all materials and the experimental techniques employed for the design of the investigated PE-b-PEO block copolymer based polymeric blends and their characterization is exposed.

In the Chapter 3, PDLC blends based on poly(ethylene-b-ethylene oxide) (PE-b-PEO) and modified with 4'-(hexyloxy)-4-biphenylcarbonitrile (HOBC) or N-(4-ethoxybenzylidene)-4-butylaniline (EBBA) nematic liquid crystals were prepared and characterized proving strong influence of used nematic liquid crystals on the miscibility and morphology of the investigated PDLC blends.

The Chapter 4 deals with thermo-optical reversible properties of the PDLC blends studied in the Chapter 3 with high content of HOBC and EBBA nematic liquid crystals. Especial emphasis was placed on the reversible switching process of the PDLC blends studied by spectroscopies techniques.

The Chapter 5 discussed the electrospinning processing-window to fabricate nanostructured PE-b-PEO and hybrid PE-b-PEO/EBBA electrospun fibers. Moreover, hybrid PLA/EBBA and PLA/PE-b-PEO/EBBA electrospun fibers were also fabricated and characterized from the point of view of the compact mat formation.

In the Chapter 6, PE-b-PEO block copolymer nanostructured thermosetting systems was fabricated and used as template for successful dispersion of TiO_2 nanoparticles. The influence of the molecular weight and molar ratio between the blocks of the PE-b-PEO block copolymer on the dispersion and localization of TiO_2 nanoparticles was also addressed.

Finally, the general conclusions of this investigation work are summarized in Chapter 7 as well as future work and scientific contributions related with the results obtained along this dissertation.

Motivation and objectives

Hybrid polymeric materials show outstanding properties if compare to neat components. The synergistic properties of hybrid polymeric materials extend their potential applications as optical devices, sensors, ion-exchanges, solar cells, and others.

Taken into account the applications, polymer dispersed liquid crystals (PDLC) are hybrid polymeric material with interesting thermo-optical properties. Moreover, PDLC materials modified with nematic liquid crystal can switch from opaque to transparent state applying external stimuli such as temperature gradient, electric or magnetic field.

Block copolymers are highly explored polymeric materials able to self-assemble at the nanometric scale. From this point they are excellent components to create novel hybrid polymeric materials.

On the other hand, block copolymer nanostructured thermosetting systems based on epoxy resins can lead to enhancement of the properties if compare with thermosetting systems and broader their applications. These block copolymer nanostructured thermosetting systems can act as template for dispersion and localization of inorganic nanoparticles.

Taking the above into account, the main objective of this work consists of the design and characterization of hybrid polymeric materials based on block copolymers. In particular, the following objectives are proposed:

- Fabrication of PDLC blends based on PE-b-PEO block copolymer and two different nematic liquid crystals with the aim to design materials which maintain the character of the nematic liquid crystals
- Verification of the thermo-optical reversible behavior of the fabricated PDLC blends with nematic liquid crystal matrix as a function of the temperature
- Optimization of the electrospinning processing-window for preparation of hybrid PE-b-PEO/EBBA and PLA/PE-b-PEO/EBBA electrospun fibers with liquid crystal character
- Employment of PE-b-PEO nanostructured thermosetting systems as template for dispersion and localization of TiO_2 nanoparticles

Table of content

Appendix

1 Introduction

1. Introduction

1.1. Liquid crystals (LCs)

Materials in nature can be presented as solid, liquid or gaseous state. The mobility of the individual atoms or molecules marks the difference between each state. The solid materials are directly turned on isotropic liquids during the melting transition. However, exist materials with an intermediate state, named mesophase. This mesophase is the phase transition between solid and liquid state called the liquid crystal state [1-6].

In the case of liquid crystal state, the intermolecular forces, based on dipole-dipole interactions or dispersion forces, are weaker in some directions and maintain the associations between molecules in a preferred orientation. Generally, molecules in liquid crystal state are large and elongated, which allows them to be placed parallel and simultaneously move freely ones with respect to others along their axes. The increase of the temperature (heating process) leads to a molecular movement of the liquid crystals (LCs) able to overcomes the intermolecular weaker forces while stronger ones maintain molecules bound. Consequently, the increase of the temperature provokes a molecular random placement in some directions and a regular one in others (see Figure 1.1).

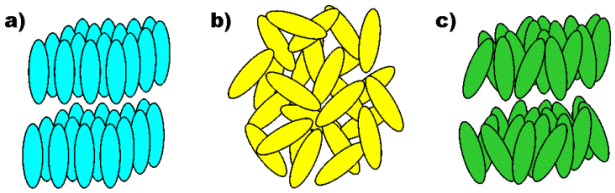

Figure 1.1. Arrangement of the molecules in a a) solid state, b) liquid state and c) liquid crystal state.

LCs are organic mesophases, which exhibits features from both the solid and the liquid state with long-range orientational order [1-6]. They are anisotropic materials due their arrangement [1-9], since display different properties depending on the direction in which they are oriented. By contrast, in an isotropic material, properties are maintained in all directions.

1.1.1. Classification of the LCs

LCs can be broadly divided into two classes, thermotropic and lyotropic LCs. In the case of thermotropic LCs the molecular orientation depends only on temperature, while in the case of lyotropic LCs, formed by aqueous solution of amphiphilic molecules such as surfactants, the molecular orientation is related to the surfactant

concentration [1-15].

In solid state, thermotropic LC molecules present a regular arrangement, with the same pattern in all directions. Intermolecular forces maintain molecules in fixed positions. The increase of the temperature results in energetically vibrated molecules. This movement overcomes the forces responsible for maintain the order of the molecules in the solid state and their start to move into random positions and results in an isotropic phase or liquid state [1-15].

The considered phase transitions in thermotropic LCs are the solid-liquid and crystal-isotropic liquid transitions. The decrease of the temperature (cooling process) from the isotropic liquid provokes reversible phase transitions, which can be repeated during heating/cooling cycles [1-5]. On the one hand, the solid-liquid crystal transition, is associated with the melting temperature, T_m, and on the other hand, the transition liquid crystal-isotropic liquid is associated with the elucidation temperature [5,6].

The orientation of the molecules in a thermotropic LC is characterized by the director axis pointing in the direction of the average molecular alignment. The director axis describes the long-range order of molecules and depends only on the temperature.

Generally, liquid crystal can pass through isotropic, nematic, cholesteric, smectic and crystalline phase transitions as a function of temperature.

At high temperatures, in the isotropic phase, the axes of the liquid crystal molecules are randomly oriented. During the cooling process the nematic phase appears first. The main characteristic of this mesophase is an orientational order without a positional one [1-15].

Taking into account the molecular order, the nematic liquid crystalline phase, can forms calamitic or discotic structures. The molecules of calamitic nematic material present rod-like structure, while the molecules of discotic nematic material present the disc-shaped structure [1-6,8,10,11,13,14].

A nematic phase can be transformed into a cholesteric phase (chiral nematic phase), in which the director axes changes its direction in a helical mode, by means doping the nematic mesophase with a chiral molecule [1-5].

A smectic phase can be also achieved during cooling process. Smectic phase displays a positional ordering, which leads to an additional order into planes.

The classification of the thermotropic LCs as function of the LC molecules arrangement is exposed bellow.

1.1.1.1. Smectic LCs

The smectic liquid crystals (SLCs) form well-defined layers which can slide freely over one another and are positionally ordered along an unique direction.

The elongated rod molecules oriented along the normal layer are denominated smectic A phase. By contrast, in smectic B phase, there is a hexagonal crystalline order within the layers. The molecules inclined out of the normal layer, in which the axis is not perpendicular to the layers form a smectic C phase. They are liquid phases within each layer of different smectic phase [1-10, 16-18].

Different types and degrees of positional and orientational order provide many different smectic phases, which are responsible for different final properties of these materials [19-25]. Figure 1.2 shows different smetic phases which are commonly studied.

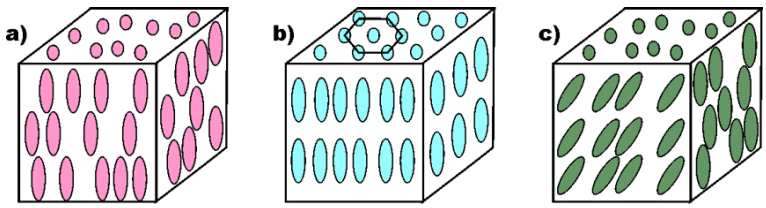

Figure 1.2. Arrangement of the molecules in a a) smectic A, b) smectic B and c) smectic C phase.

1.1.1.2. Cholesteric LCs

Cholesteric liquid crystals (CLCs) present a helical structure due to the chirality of molecules, which impart unique optical properties. CLCs possess a long-range orientational order and not a long-range order in positions of elongated rod molecules and its director axis varies in a regular way. The axis of the molecules is aligned along a single direction in a plane, however in a series of equidistant parallel planes the direction rotates through a fixed angle [1-10,16-18]. A typical structure of a CLC is shown in Figure 1.3.

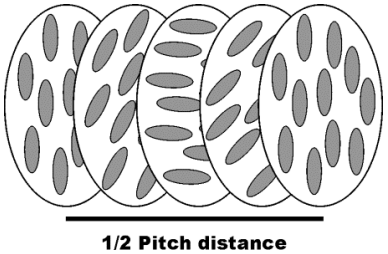

Figure 1.3. Arrangement of the molecules in a cholesteric liquid crystal in the different planes.

The helical pitch of CLCs can be in the same order of magnitude as the

wavelength of visible light and consequently a Bragg reflection takes place. The helical arrangement is responsible for the characteristic colors of CLCs in reflection.

On the other hand, the helix pitch is very sensitive to the influence of external conditions such as temperature, chemical composition, external fields such as magnetic or electric [26-30].

1.1.1.3. Nematic LCs

The molecules of a nematic liquid crystal (NLC), majority elongated rods, have not positional order, however they reveal a long-range orientational order. Thus, the molecules are located in the same direction however some of them are not completely parallel showing a certain deviation.

This property is governed by the director axis pointing in the direction of the average molecular alignment, being long axes approximately parallel [1-10,16,18,31,32].

The fluidity of NLCs is similar to that of ordinary isotropic liquids however, they can be easily aligned by an external field such as magnetic, electric, temperature gradient and others. Aligned NLCs molecules display optical properties of uniaxial crystals. Thus, NLCs possess the ability to switch the director axis and as consequence, the alignment of their rod-like molecules takes place as a response to external stimuli. The NLCs switch from the state of high light dispersion, ON-state, when the director axes are aligned to a transparent state, to OFF-state, when they are not aligned [33,34].

From the point of view of the thermodynamic, the transition between nematic phase and isotropic liquid is a relatively weak first order transition in comparison with the solid crystalline-nematic transition.

Figure 1.4 shows the solid crystalline-nematic and nematic-liquid isotropic transitions of a NLC when a gradient of temperature is applied.

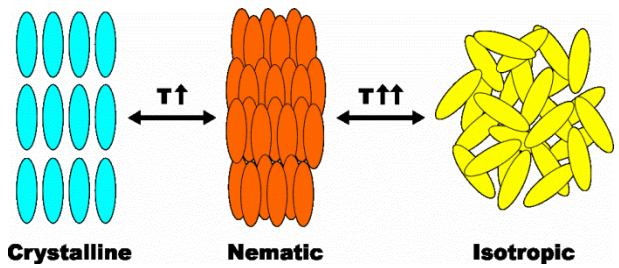

Figure 1.4. Solid crystalline-nematic and nematic-liquid isotropic transitions.

The most common approach to describe the nematic phase and nematic-isotropic

(N-I) phase transition, is based on the continuous decreasing of the order parameter with the increase of the temperature, dropping drastically to zero at the N-I transition temperature (T_{N-I}). This transition can be described theoretically by using Landau equation [1-7,10,11,13,15,16,35].

Several theories have been developed to describe the nematic phase and N-I phase transition. The most widely used approach is the model proposed by de Gennes based on the Laudau's general description of the phase transition. The Laudau-de-Gennes (LDG) theory describes the state of a nematic liquid crystal by macroscopic order parameter defined in terms of macroscopic quantities [1-7].

The reversible switching process makes NLCs interesting to be combined with others materials in order to reach innovative applications.

1.1.2. Applications

Numerous applications of the LC materials have been achieved in many research areas and in technological devices as schematically showed in Figure 1.5. An extensive list of applications such as general digital thermometers, battery testers and other voltage measuring devices, temperature indicators for medical applications, medical thermography, radiation detection, esthetic, ingredients for cosmetic formulations, non-destructive testing/thermal mapping, aerospace, engineering research, gas/liquid level indicators, biomedical, among others provides effective solutions to many different problems [7,16,18,41-50].

Liquid crystal thermometers are one of the most common application of LCs. The color changes are associated directly to the temperature and allow to measure it. The chiral nematic or cholesteric liquid crystals reflect light with a wavelength equal to the pitch as was explained above, the pitch depends on the temperature and hence the reflected color indicates determined temperature values.

Regarding the optical imaging, LCs are also employed. A liquid crystal cell is placed between two layers of photoconductor then light is applied increasing the conductivity of the material and generating an electric field to develop in the liquid crystal corresponding to the intensity of the light.

Liquid crystal displays (LCDs) are another common application of liquid crystal technology. LCD screens use liquid crystals to switch pixels ON and OFF to visualize a determined color by applying an electric current. In LCD displays liquid crystals turn on or turn off a filter responsible for visualize a determinate color or maintain black.

The light emitting diode (LED) screens, are based on LCD displays, the difference lies on the employed lamp. Moreover, in the case of LED displays the contrast is deeper [45-49].

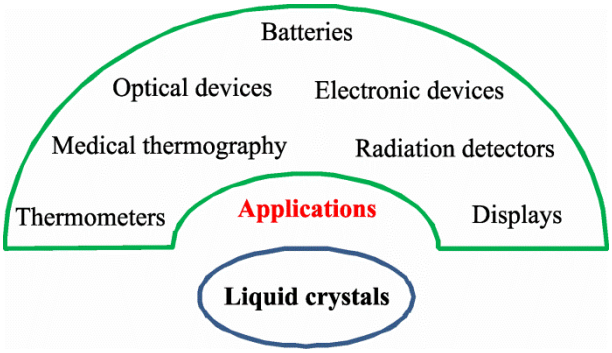

Figure 1.5. Several applications of liquid crystals.

The alignment capacity of the NLCs rod-like molecules under an external stimulus combined with the processability of the polymers is an interesting pathway to develop PDLC blends which are used in a wide range of applications in the field of thermal and electro-optical devices [36-40].

1.2. Polymer dispersed liquid crystal blends (PDLC)

Nowadays, Polymer Blend Technology is one of the main areas of research and development in Polymer and Material Science. Due to the increased interest in the application of Polymer Blends Technology to commercial usefulness, the academic and industrial research has taken an active role. This technology leads to combine synergistically different polymeric materials [51-55].

A polymer blend is a physical mixture in which at least two polymers are combined together to create a new material with different physical properties.

The main goal of the polymer blending is, on the one hand, the achievement of novel materials with improved properties for commercial applications, and on the other hand, the preservation of these improved properties reducing material cost and enhancing the processability of these materials. All these advantages can be reached through the proper selection of the polymer components and overcoming limitations such as the difficulty of the dispersion of one polymer in another due to the high interfacial tension, the weak interfacial adhesion and the instability of the polymer blends [51-55].

Depending on both the Gibbs free energy (ΔG_m) of mixing value and the second

derivative of the Gibbs free energy with respect to the volume fraction value of major component, polymer blends can be classified as miscible, immiscible and partially miscible [55-62].

For a miscible polymer blend, $\Delta G_m < 0$ and the second derivative positive, a homogeneous blend is obtained and an unique phase is observed. The miscibility between components depends strongly on the preparation conditions (temperature and pressure, among others) and formulation of the polymer blends. The preparation of miscible polymer blends guarantees the synergistic properties.

For an immiscible or heterogeneous blend, $\Delta G_m > 0$ and the second derivative of free energy function negative, several phases corresponding to each component of the polymer blend are detected as consequence of macrophase separation.

When $\Delta G_m < 0$ and the second derivative of free energy function is negative, the polymer blends are partially miscible. In this case, some part of one component of the polymer blend is miscible with the other component forming an interface, which is responsible for a good interfacial adhesion [55-62].

The miscibility of the polymer blends can be verified by Fox equation [62-65]. This equation employs the glass transition temperature (T_g) of the polymer blend components to find theoretical T_g of polymer blend. This equation is an easy way to discuss the miscibility of polymer blends. Miscible polymer blend shows only one T_g and if different T_gs are found this means that the polymer blends are immiscible [62-65].

Generally, partially miscible polymer blends offer higher possibility to achieve synergistic properties while an incompatible polymer blends are completely immiscible and as a consequence of macrophase separation, possess poor mechanical properties [52,58,66-70].

The versatility of polymer blends makes them useful in numerous fields of applications such as medical, optical engineering for electronic devices, nanotechnology, cosmetic industry, as well as coatings and adhesives, among others.

The advantages obtained from the mixture of polymeric materials lead to development of new classes of polymer blends, combining polymers with other components.

One of these polymer blends with outstanding synergistic properties, are polymer dispersed liquid crystal (PDLC) blends. PDLC blends combine properties of thermoplastic polymers and properties of liquid crystals to create novel materials with

tailored properties [36-40,48-50].

As was described above, the reversible switching process of the nematic liquid crystal rod-like molecules is able to change orientation by applying an external stimulus. This property jointly with the processability of thermoplastic polymers, make these PDLC blends innovative materials, which can be used in different field of applications such as optical switches (light shutters), smart windows and reflective displays, among others [36-40].

The enhancement of the PDLC blend properties in comparison to the properties of the polymer blends is related to the fact that PDLC blends present, on the one hand, some degree of long-range order and, on the other hand, some degree of the mobility. Consequently, the properties such as chemical stability, lower flammability and better processability can be achieved [71-73]. These properties are closely related to the molecular structure of the polymeric chain, which contains rigid liquid crystal phases or mesogens that can be placed in the main chain, in the side chains or in both allowing to the polymer to be oriented in a similar way to neat liquid crystals [60,74,75].

The key point to achieve PDLC blends with tailored properties is the control of the miscibility as a function of the temperature between selected thermoplastic polymers and nematic liquid crystals. The fast cooling rate led to PDLC blends with smaller nematic domains with a narrow size distribution. On the contrary, the slow cooling rate led to the coexistence of very large and small nematic domains [76-80].

PDLC blends are based on NLC droplets with different configurations and orientations homogeneously dispersed in a solid thermoplastic polymer matrix. These small, a few microns in size, droplets are responsible of the respond of the PDLC blends to the external stimulus [48-50]. The NLC molecules are able to change their orientation by applying an external electric field or a gradient of temperature as shown in Figure 1.6.

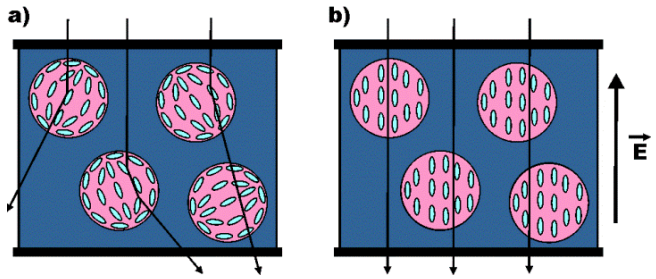

Figure 1.6. Arrangement of the nematic liquid crystal molecules in a PDLC material, a) light scattered OFF state and b) light transmitted ON state.

The arrangement of the NLC molecules as a function of external stimulus provokes a variation on the intensity of transmitted light. When an external stimulus is applied, the NLC droplets are oriented and the PDLC blend switches from opaque to transparent state. Consequently, the optical properties of the PDLC blends are governed by nematic liquid crystal phase, able to maintain its properties in design materials [10,16-18].

The optical anisotropy of the PDLC blends is closely related to the different values of the NLC and polymer matrix refractive indices along the optical director axis. That means that they can be optically switched from opaque state or highly scattering state (OFF-state), if the director axis is nonaligned to transparent state (ON-state), if the director axis is aligned due to mismatching and matching of the NLC and polymer refractive index [8,11,16,31,33,34,81-85].

1.2.1. PDLCs based on block copolymers

The influence of temperature on the properties of both, NLCs and thermoplastic polymers, makes PDLC blends excellent materials for potential LC applications. The main drawback is the weldline strength between different phases [53,54,58,59]. As explained above, the employment of different methods for predicting the miscibility in blends, is an important area in Polymer Blend Technology [72,86-88]. One of the possible ways to control and improve the miscibility of the polymer blend components is the addition of the block copolymers.

Block copolymers are able to reduce the interfacial tension between components and allow controlling the phase separation and consequently, promote higher miscibility between components [89-92].

The ability of the block copolymers to self-assembly and as consequence to control their morphologies at nanoscale, offers new possibilities of application, especially in the field of the miniaturization of opto-eletronic and magnetic devices.

Block copolymers are macromolecules integrated by two or more groups of monomers covalently linked in the same polymer chain. The different ways to connect these blocks led to diverse structures such as diblock AB, triblock ABC or star copolymers.

The most interesting property of the block copolymers is their ability to self-assembly leading to different structures organized at the nanoscale [93,94].

The different chemical composition of the blocks and its covalent union, led to

well-defined structures which morphology is governed by the Flory-Huggins phase diagram. As can be seen in Figure 1.7, block copolymers can form different morphologies at nanoscale such as body centered cubic (BCC), hexagonal (HEX), gyroid (GYD) and lamellar (LAM) and disordered structure (DIS) [95-98].

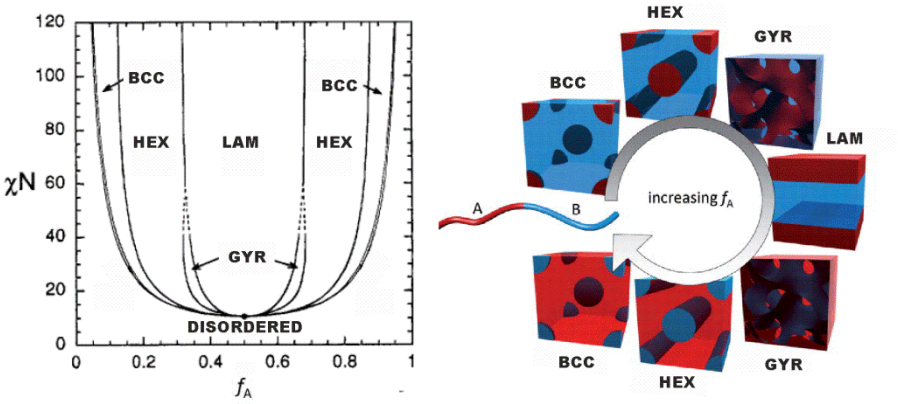

Figure 1.7. Theoretical phase diagram of an AB diblock copolymer.

The microphase separation in block copolymers can be controlled by the Flory-Huggins interaction parameter (χ) between monomers, which form different blocks and the number of polymer repeating units or degree of polymerization (N). This χ is related to the chemical composition of the blocks and the length of the polymer.

Block copolymers integrated by two monomers display different miscibility with respect to the NLC. Generally, one of the blocks is miscible or partially miscible with the NLC, consequently, NLC can be positioned in one block of the block copolymer. Moreover, block copolymers can self-assemble offering nanostructured templates for dispersion of NLC droplets, leading to PDLC materials with electro-optic properties [81-83,99,100].

At the present time, only a few works have reported about PDLC blends based on block copolymers and NLC. Kato et al. [71] have employed block copolymers to self-assembly phase segregated liquid crystal structures.

On the other hand, Tercjak et al. [81-85,99] studied the thermodynamic phase behavior of PDLC blends based on poly(styrene-b-ethylene oxide) PS-b-PEO block copolymer and low-molecular weight 4´-(hexyloxy)-4-biphenyl-carbonitrile (HOBC) nematic liquid crystals.

Additionally, Valenti et al. [100] fabricated PDLC films based on styrene-diene block copolymers and the nematic mixture E7 in order to study the miscibility between components and the influence of several parameters on the morphology of the PDLC blends.

1.3. Thermosetting systems

Thermosetting materials are constituted by polymers linked by chemical bonds which are responsible to generate a highly crosslinked polymer structure (Figure 1.8).

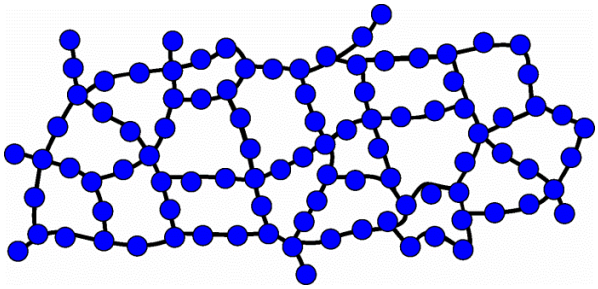

Figure 1.8. Structure of a thermosetting systems.

This structure of crosslinked polymers is responsible for good mechanical properties, an excellent chemical resistance and a high thermal stability among others. However, their main disadvantage is their brittleness and their poor elasticity [101-104].

Epoxy resins are widely employed and investigated thermosetting systems [105,106] and they present an epoxide functional groups in the polymer chain, which are highly reactive due to its structural stress (Figure 1.9).

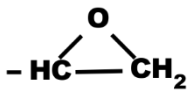

Figure 1.9. Epoxide reactive functional group.

This epoxide group reacts with the functional groups of the same epoxy resin or with the functional groups of a curing agent, generally amine groups, generating the crosslinking of the epoxy resins via bridging reactions [105-109]. In this reaction the network is integrated by epoxy monomers and a curing agent obtaining a material whose properties are function of the thermosetting system formulations [110-112].

The epoxy curing reaction can be divided in two steps. Firstly, a polymerization reaction takes place. This polymerization reaction is based on the reaction of the epoxy group with the functional groups of curing agent leading to fast increase of the molecular weight until all monomers are connected by at least one bond results in the polymer network and reaches the gel point. After the first reaction step, the amount of free monomers significantly decreases and as a consequence, the movement of the polymer chains is reduced. If the molecular weight of the network overcomes the thermodynamically stable molecular weight, the system vitrificates generating a brittle

material.

In order to decrease the brittleness and increase the toughness of this kind of materials, epoxy based thermosetting systems are usually modified with organic components such as thermoplastic homopolymers or block copolymers [104,113-122], or with inorganic nanoparticles [103,123-127].

1.3.1. Thermosetting systems modified with block copolymers

The interest in the use of block copolymers lies in its self-assembly capability which allows obtaining different nanostructures as a function of the composition and the molecular weight as was mentioned before. Moreover, the addition of the block copolymers improves the toughness of the thermosetting systems leading to higher range of their applications [101,122,126].

With the aim of fabricating nanostructured epoxy based thermosetting materials, two different methods are employed. One of the methods is based on the use of amphiphilic block copolymers, which consist of one miscible block and another immiscible block with the epoxy resin [104,113,117-122,128-135]. The second way proposes a chemical functionalization of one immiscible block of the block copolymer to become this block miscible with the epoxy resin and to be able to nanostructured the epoxy resin [114,115,116,124].

The most widely employed amphiphilic block copolymers contain PEO, PCL and PMMA blocks as miscible blocks with epoxy resin [119,131,136-140].

The self-assembly of the block copolymer can take place before or during the curing reaction. On the one hand, when the self-assembly occurs before curing, the epoxy resin acts as solvent only for one of the block and a microphase separation occurs in block copolymer/epoxy resin mixture priori to polymerization reaction. Thus, block copolymer self-assembled before curing reaction [113]. On the other hand, when the self-assembly takes place during network formation, by a reaction induced phase separation (RIPS) [140], the immiscible block is separated from the thermosetting matrix during curing reaction.

As mentioned above, the toughness can be improved modifying the epoxy based thermosetting systems with block copolymers. The one of the block of block copolymers is miscible with the epoxy resin and acts as plasticizer, provoking a considerable reduction in the glass transition temperature (T_g) of the system and improving the toughness [141,142]. The drawback of this modification is related to the

simultaneous decrease of the Young´s modulus due to plasticization effect. This disadvantage can be governed controlling both the formulation of block copolymer modified thermosetting systems and the final morphology of modified thermosetting systems.

On the other hand, the addition of the inorganic nanoparticles to the block copolymer modified thermosetting systems is also an alternative method to increase the toughness without lose the Young´s modulus.

1.3.2. Thermosetting systems modified with inorganic nanoparticles

The modification of epoxy based thermosetting systems with inorganic nanoparticles can increase the toughness without affecting the high glass transition temperature of the epoxy based thermosetting matrix. This is a desirable property for many applications of these kind of materials [128-131].

Moreover, playing with the concentration, size or type of nanoparticles, thermosetting systems with combined optical, mechanical, magnetic and opto-electronic properties of incorporated inorganic nanoparticles can be achieved [102,103,123,125,126].

Inorganic nanoparticles can be synthesized by different methods. The sol-gel technique is an useful method for the synthesis and incorporation of inorganic nanoparticles into epoxy resin. This wet-chemical synthesis involves hydrolysis and condensation reactions of metal precursors leading to the formation of an oxide network [143].

Different inorganic nanoparticles such as Al_2O_3, SiO_2 and TiO_2 nanoparticles, among others were used to modify epoxy based thermosetting systems [144-148].

The main drawback of the use of inorganic nanoparticles is related to the difficulty to reach a good dispersion. A poor dispersion produces aggregates, which are responsible for the heterogeneous properties of the thermosetting systems. The achievement of a homogeneous dispersion of inorganic nanoparticles in thermosetting matrix is a crucial point to control the final properties of designed thermosetting systems [102,123,125-127,130].

In many occasions, the modification of the thermosetting systems with inorganic nanoparticles does not result in an enhancement of the final properties. Thus, in order to overcome this disadvantage, block copolymers are employed to improve the dispersion of the inorganic nanoparticles and consequently the final properties.

1.3.3. Nanostructured thermosetting systems modified with block copolymers and inorganic nanoparticles

The use of both the block copolymers and the inorganic nanoparticles is an effective pathway to achieve epoxy based thermosetting systems with synergistic and desired properties [102,125,130,144-147].

On the one hand, block copolymers offer the opportunity to create nanostructured epoxy based thermosetting systems and, on the other hand, inorganic nanoparticles provide the unique properties related to their own properties such as optical, electrical and magnetic one [149,150].

In this kind of epoxy based thermosetting systems, block copolymers act as nanostructuration agent and as surfactant for the dispersion of inorganic nanoparticles.

Nowadays, in this research field only a few works have been reported. Tercjak and co-workers [125,130,144] have investigated epoxy based thermosetting systems modified with block copolymers as well as with TiO_2 inorganic nanoparticles and liquid crystals. Moreover, they investigated the transparency in the long scale microphase separation threshold. Ocando et al. [145] analyzed the effect of the addition of SBS and Al_2O_3 nanoparticles on the dispersion and final mechanical properties of thermosetting systems. Gutierrez et al. [102,146,147] studied the morphological and optical properties of PS-b-PEO block copolymer nanostructured thermosetting systems modified with sol-gel synthesized TiO_2 nanoparticles.

Taking all the above into account, epoxy based thermosetting systems modified with both, amphiphilic block copolymers and inorganic nanoparticles are interesting to develop advanced materials with unique tunable properties, which can find applications in many fields of Polymer and Material Science.

1.4. References

[1] Chandrasekhar S. Liquid crystals. Cambridge University Press. Cambridge (UK), 1992.

[2] de Gennes PG, Prost J. The physics of liquid crystals. Oxford University Press. Oxford (UK), 1995.

[3] Kumar S. Liquid crystals. Experimental study of properties and phase transitions. Cambridge University Press. Cambridge (UK), 2001.

[4] Singh S. Phase transitions in liquid crystals. Phys. Rep. 2000;324:107-269.

[5] Singh S. Liquid crystals: Fundamentals. World Scientific Publishing Co Pte Ltd. London (UK), 2002.

[6] Kleman M, Lavrentovich OD. Soft matter physics: An introduction. Springer. New York (USA), 2003.

[7] Andrienko D. Introduction to liquid crystals. International Max Planck Research School. Modelling of soft matter. Bad Marienberg (Germany), 2006.

[8] Collings PJ. Liquid Crystals. Nature´s delicate phase of matter. Second Ed., Princeton University Press. Oxford (UK), 2002.

[9] Khoo IC. Liquid crystals. Second Ed., John Wiley & Sons. New Jersey (USA), 2007.

[10] Sengupta A. Topological microfluidics. Nematic liquid crystals and nematic colloids in microfluidic environment. Doctoral Thesis. University of Göttingen (Germany), 2013.

[11] Ramamoorthy A. Thermotropic liquid crystals. Recent advances. Springer. University of Michigan (USA), 2007.

[12] Liu K, Chen D, Marcozzi A, Zheng L, Su J, Pesce D, Zajaczkowski W, Kolbe A, Pisula W, Müllen K, Clark NA, Herrmann A. Thermotropic liquid crystals from biomacromolecules. PNAS 2014;52:18596-18600.

[13] Villanueva-García M, Gutiérrez-Parra RN, Martínez-Richa A, Roblesa J. Quantitative structure-property relationships to estimate nematic transition temperatures in thermotropic liquid crystals. J. Mol. Struc. Theochem 2005;727:63-69.

[14] Matos MRA, Silva BFB, Marques EF. Chain length mismatch and packing effects on the thermotropic phase behavior of salt-free catanionic surfactants. J. Colloid Interf. Sci. 2013;405:134-144.

[15] Chen GQ, Majumdar A, Wang D, Zhang R. Global existence and regularity of

solutions for active liquid crystals. J. Differ. Equations 2017;263:202-239.

[16] Bata L. Advances in liquid crystal research and applications. First Ed., Akadémiai Kiadó. Budapest (Hungary), 1981.

[17] Oswald P, Pieranski P. Smectic and columnar liquid crystals. Taylor & Francis Group, CRS Press. Florida (USA), 2006.

[18] Bahadur B. Liquid crystals: Applications and uses. Vol. 1, World Scientific Publishing Co Pte Ltd. London (UK), 1990.

[19] Mukherjee PK. Smectic-A-smectic-C-smectic-C* Lifshitz point in mixtures of chiral and achiral smectic liquid crystals. J. Mol. Liq. 2015;204:10-14.

[20] Guillén-González F, Tierra G. Approximation of smectic-A liquid crystals. Comput. Methods Appl. Mech. Engrg. 2015;290:342-361.

[21] Chakraborty A, Chakraborty S, Das MK. Critical behavior at the isotropic to nematic, nematic to smectic-A and smectic-A to smectic-C phase transitions in a pyrimidine liquid crystal compound. Physica B 2015;479:90-95.

[22] Osiecka N, Galewski Z, Juszyńska-Gałązka E, Massalska-Arodź M. Studies of reorganization of the molecules during smectic A-smectic C phase transition using infrared spectroscopy and generalized two-dimensional correlation analysis. J. Mol. Liq. 2016;224:677-683.

[23] Mirantsev LV. Novel possible electro-(magneto-)optic effect in smectic-A liquid crystal cell. Phys. Lett. A 2014;378:86-89.

[24] Poursamad JB, Hallaji T. Freedericksz transition in smectic-A liquid crystals doped by ferroelectric nanoparticles. Physica B 2017;504:112-115.

[25] Wei B, Tan S, Liang T, Cao, Wu Y. Synthesis, structural and electrochemical characterization of benzimidazole compounds exhibiting a smectic C liquid crystal phase. J. Mol. Struc. 2017;1133:392-397.

[26] Wang F, Li K, Song P, Wu X, Chen H, Cao H. The effects of thermally induced diffusion of dye on the broadband reflection performance of cholesteric liquid crystals films. Compos. Part B 2013;46:145-150.

[27] Ogiwara A, Kakiuchida H. Thermally tunable light filter composed of cholesteric liquid crystals with different temperature dependence. Sol. Energ. Mat. Sol. C 2016;157:250-258.

[28] Therézio EM, da Silva SFC, Dalkiranis GG, Filho PA, Santos GC, Ely F, Bechtold IH, Marletta A. Light polarization states of a cholesteric liquid crystal probed with optical ellipsometry. Opt. Mater. 2015;48:7-11.

[29] Meyer RB. Effects of electric and magnetic fields on the structure of cholesteric liquid crystals. Appl. Phys. Lett. 1968;12:281-282.

[30] Lv K, Liu D, Li W, Tian O, Zhou X. Reflection characteristics of cholesteric liquid crystal microcapsules with different geometries. Dyes pigments 2012;94:452-458.

[31] Luckhurst GR, Sluckin TJ. Biaxial nematic liquid crystals. Theory, simulation and experiment. John Wiley& Sons. University of Southampton (UK), 2015.

[32] Rego JA, Harvey JAA, MacKinnon AL, Gatdula E. Asymmetric synthesis of a highly soluble 'trimeric' analogue of the chiral nematic liquid crystal twist agent Merck S1011. Liq. Crist. 2010;37:37-43.

[33] Choi SS, Morris SM, Huck WTS, Coles HJ. The switching properties of chiral nematic liquid crystals using electrically commanded surfaces. Soft Matter 2009;5:354-362.

[34] Imamura K, Yoshida H, Ozaki M. Reversible switching of liquid crystal micro-particles in a nematic liquid crystal. Soft Matter 2016;12:750-755.

[35] Gramsbergen EF, Longa L, de Jeu WH. Landau theory of the nematic-isotropic phase transition. Phys. Lett. 1983;4:195-257.

[36] Yamaguchi R, Takasu T. Hybrid aligned nematic liquid crystal smart glass with asymmetrical daylight controls. J. Soc. Inf. Display 2015;23:365-370.

[37] Hoppe CE, Galante MJ, Oyanguren PA, Williams RJJ. Optical properties of novel thermally switched PDLC films composed of a liquid crystal distributed in a thermoplastic/thermoset polymer blend. Mater. Sci. Eng C 2004;24:591-594.

[38] Parab SS, Malik MK, Deshmukh RR. Dielectric relaxation and electro-optical switching behavior of nematic liquid crystal dispersed in poly(methyl methacrylate). J. Non-Cryst. Solids 2012;358:2713-2722.

[39] Kim Y, Jung D, Jeong S, Kim K, Choi W, Seo Y. Optical properties and optimized conditions for polymer dispersed liquid crystal containing UV curable polymer and nematic liquid crystal. Curr. Appl. Phys. 2015;15:292-297.

[40] Kumar P, Raina KK. Morphological and electro-optical responses of dichroic polymer dispersed liquid crystal films. Curr. Appl. Phys. 2007;7:636-642.

[41] Hallcrest LCR. Handbook of thermochromic liquid crystal technology. Pickwick Lane. Chicago (USA), 2014.

[42] Meier G, Sackmann E, Grabmaier JG. Applications of liquid crystals. Springer. Berlin (Germany), 1975.

[43] Brown GH. Properties and applications of liquid crystals. J. Electron. Mater.

1973;2:403-430.

[44] Li J. Refractive indices of liquid crystals and their applications in display and photonic devices. Thesis doctoral. STARS. University of Central Florida (USA), 2005.

[45] Kwon KJ, Kim MB, Heo C, Kim SG, Back JS, Kim YH. Wide color gamut and high dynamic range displays using RGBW LCDs. Displays 2015;40:9-16.

[46] Yoshimura K, Shimamoto K, Ikeda M, Ichikawa K, Naganawa S. A comparative contrast perception phantom image of brain CT study between high-grade and low-grade liquid crystal displays (LCDs) in electronic medical charts. Phys. Medica 2011;27:109-116.

[47] Gago-Calderón A, Fernández-Ramos J, Gago-Bohórquez A. Visual quality evaluation of large LED displays based on subjective sensory perception. Displays 2013;34:359-370.

[48] Brennesholtz MS, Stupp EH. Projection displays. Second Ed., John Wiley & Sons. West Sussex (UK), 2008.

[49] Drzaic PS. Liquid crystal dispersions. Vol. 1, World Scientific Publishing Co Pte Ltd. London (UK), 1995.

[50] Coates D. Liquid crystal polymers: Synthesis, properties and applications. Rapra Technology Ltd. Shropshire (UK), 2000.

[51] Parameswaranpillai J, Thomas S, Grohens Y. Characterization of polymer blends: Miscibility, morphology, and interfaces. First Ed., Wiley-VCH. Weinheim (Germany), 2015.

[52] Bergbreiter DE, Martin CR. Control of phase structure in polymer blends, in functional polymers. Plenum Press. New York (USA), 1989.

[53] Isayeb AI. Polymer blend compounding and processing. Encyclopedia of polymer blends. Vol.2, Wiley-VCH. Weinheim (Germany), 2011.

[54] Ciardelli F, Penczek S. Modification and blending of synthetic and natural macromolecules. Nato Science Series. Kluwer Academic Publishers. Dordrecht (The Netherlands), 2004.

[55] Higgins JS, Lipson JG, White RP. A simple approach to polymer mixture miscibility. Phil. Trans. T. Soc. A 2010;368:1009-1025.

[56] Koningsveld R, Stockmayer WH, Nies E. Polymer phase diagrams: A text book. Oxford University Press. Oxford (UK), 2001.

[57] Flory PJ. Principles of polymer chemistry. Cornell University Press. New York (UK), 1953.

[58] Utracki LA, Wilkie CA. Polymer blends handbook. Second Ed., Springer. Milwaukee (USA), 2014.

[59] Mark EJ. Thermodynamics of polymer blends. Physical properties of polymers handbook. Second Ed., Springer. Ohio (USA), 2007.

[60] Thomas S, Shanks R, Sarathchandran C. Nanostructured Polymer Blends. Elsevier. Waltham (USA), 2014.

[61] Robeson LM. Polymer Blends: A comprehensive Review. Hanser-Garden Inc. Cincinnati (USA), 2007.

[62] Vasile C, Kulshreshtha AK. Handbook of polymer blends and composites. Vol. 3B, Rapra Technology Ltd. Shawbury (UK), 2003.

[63] Brostow W, Chiu R, Kalogeras IM, Vassilikou-Dova A. Prediction of glass transition temperatures: Binary blends and copolymers. Mater. Lett. 2008;62:3152-3155.

[64] Kuo SW, Kao HC, Chang FC. Thermal behavior and specific interaction in high glass transition temperature PMMA copolymer. Polymer 2003;44:6873-6882.

[65] Zhang G, Zhang J, Wang S, Shen D. Miscibility and phase structure of binary blends of polylactide and poly(methyl methacrylate). J. Polym. Sci. Pol. Phys. 2002;41:23-30.

[66] Yu L, Dean K, Li L. Polymer blends and composites from renewable resources. Prog. Polym. Sci. 2006;31:576-602.

[67] Mano JF, Koniarova D, Reis RL. Thermal properties of thermoplastic starch/synthetic polymer blends with potential biomedical applicability. J. Mater. Sci-Mater. M 2003;14:127-135.

[68] Mannan HA, Mukhtar H, Nasir R, Mohshim DF, Mushtaq A. Recent applications of polymer blends in gas separation membranes. Chem. Eng. Technol. 2013;36:1838-1846.

[69] McNeill CR, Greenham NC. Conjugated-polymer blends for optoeletronics. Adv. Mater. 2009;21:3848-3850.

[70] Narkis M, Srivastava S, Tchoudakov R, Breuer O. Sensors for liquids based on conductive immiscible polymer blends. Synthetic Met. 2000;113:29-34.

[71] Kato T. Self-assembly of phase-segregated liquid crystal structures. Science 2002;295:2414-2418.

[72] Chung TS. Thermotropic liquid crystal polymers. Thin-film polymerization, characterization, blends and applications. Technomic Publishing Co Inc. Pennsylvania

(USA), 2001.

[73] Coates D. Liquid crystal polymers. Rapra Technology Ltd. Shropshire (UK), 2000.

[74] Verploegen E, Zhang T, Jung YS, Ross C, Hammond PT. Controlling the morphology of side chain liquid crystalline block copolymer thin films through variations in liquid crystalline content. Nano Lett. 2008;10:3434-3440.

[75] Wei R, Zhou L, He Y, Wang X, Keller P. Effect of molecular parameters on thermomechanical behaviour of side-on nematic liquid crystal elastomers. Polymer 2013;54:5321-5329.

[76] Simoni F. Nonlinear optical properties of liquid crystals and polymer dispersed liquid crystals. World Scientific Publishing Co Pte Ltd. London (UK), 1997.

[77] Drzaic PS. Liquid crystals dispersions. World Scientific Publishing Co Pte Ltd. London (UK), 1995.

[78] Coates D. Polymer dispersed liquid crystals. J. Mater. Chem. 1995;5:2063-2072.

[79] Drzaic PS. Polymer dispersed nematic liquid crystal for large area displays and light valves. J. Appl. Phys. 1986;60:2142-2148.

[80] Gill N, Pojman JA,Willis J, Whitehead Jr JB. Polymer-dispersed liquid-crystal materials fabricated with frontal polymerization. J. Polym. Sci. Pol. Chem. 2003;41:204-212.

[81] Tercjak A, Gutierrez J, Ocando CJ, Peponi L, Mondragon I. Thermoresponsive inorganic/organic hybrids based on conductive TiO_2 nanoparticles embedded in poly(styrene-b-ethylene oxide) block copolymer dispersed liquid crystals. Acta Mater. 2009;57:4624-4631.

[82] Tercjak A, Serrano E, Garcia I, Mondragon I. Thermoresponsive meso/nanostructured thermosetting materials based on PS-b-PEO block copolymer-dispersed liquid crystal: Curing behavior and morphological variation. Acta Mater. 2008;56:5112-5122.

[83] Tercjak A, Serrano E, Mondragon I. Multifunctional thermally reversible nanostructured thermosetting materials based on block copolymers dispersed liquid crystal. Macromol. Rapid. Comm. 2007;28:937-941.

[84] Ahmad F, Jamil M, Lee, JW, Ri YH, Jeon YJ. Characteristics of di- and tri-block copolymers: polymer disperse liquid crystal display. J. Mod. Optic. 2014;61:1027-1032.

[85] Hoppe CE, Galante MJ, Oyanguren PA, Williams RJJ. Polymer-dispersed liquid crystals based on polystyrene and EBBA: analysis of phase diagrams and morphologies generated. Macromol. Chem. Phys. 2003;204:928-935.

[86] Hempel P. Constitutive modeling of amorphous thermoplastic polymers with special emphasis on manufacturing processes. Karlsruher Institut für Technologie Scientific Publishing. Karlsruher (Germany), 2016.

[87] Cogswell FN. Thermoplastic aromatic polymer composites: A study of the structure, processing and properties of carbon fibre reinforced polyetheretherketone and related materials. Butterworth Heinemann. London (UK), 1992.

[88] Advani SG, Hisiao KT. Manufacturing techniques for polymer matrix composites (PMCs). Woodhead Publishing. Philadelphia (USA), 2012.

[89] Eastwood E, Viswanathan S, O´Brien CP, Kumar D, Dadmun MD. Methods to improve the properties of polymer mixtures: optimizing intermolecular interactions and compatibilization. Polymer 2005;46:3957-3970.

[90] Zhu S, Liu Y, Rafailovich MH, Sokolov J, Gersappe D, Winesett DA, Ade H. Confinement-induced miscibility in polymer blends. Nature 1999;400:49-51.

[91] Bai Z, Guo H. Interfacial properties and phase transitions in ternary symmetric homopolymer-copolymer blends: A dissipative particle dynamics study. Polymer 2013;54:2146-57.

[92] Mucha M. Polymer as an important component of blends and composites with liquid crystals. Prog. Polym. Sci. 2003:28;837-73.

[93] Abetz V. Block copolymers I. Springer. Berlin (Germany), 2005.

[94] Hadjichristidis N, Pipas S, Floudas GA. Block copolymers. Synthetic strategies, physical properties and applications. John Wiley & Sons. Canada (USA), 2003.

[95] Matsen MW, Bates FS. Unifying weak and strong segregation block copolymer theories. Macromolecules 1996;29:1091-1098.

[96] Botiz I, Darling B. Optoelectronics using block copolymers. Mater. Today 2010;13:42-51.

[97] Hu H, Goponadhant M, Osuji CO. Directed self-assembly of block copolymers: a tutorial review of strategies for enabling nanotechnology with soft matter. Soft Matter 2014;10:3867-3889.

[98] Mai Y, Eisenberg A. Self-assembly of block copolymers. Chem. Soc. Rev. 2012;41:5969-59-85.

[99] Tercjak A, Serrano E, Larrañaga M, Mondragon I. Polymer dispersed liquid crystals based on poly(styrene-b-ethylene oxide), poly(bisphenol a carbonate) or poly(methylphenylsiloxane), and 4´-(hexyloxy) 4-biphenyl-carbonitrile: Analysis of phase diagrams and morphologies generated. J. Appl. Polym. Sci. 2008;108:1116-1125.

[100] Valenti B, Turturro A, Losio S, Falqui L, Costa G, Cavazza B, Castellano M. Styrene-diene block copolymers as embedding matrices for polymer-dispersed liquid crystal films. Polymer 2001;42:2427-2438.

[101] Johnsen BB, Kinloch AJ, Mohammed RD, Taylor AC. Toughening mechanisms of nanoparticle-modified epoxy. Polymer 2007;48:530-541.

[102] Gutierrez J, Mondragon I, Tercjak A. Morphological and optical behavior of thermoset matrix composites varying both polystyrene-block-poly(ethylene oxide) and TiO_2 nanoparticle content. Polymer 2011;52:5699-5707.

[103] Hsieh TH, Kinloch AJ, Masania K, Taylor AC, Sprenger S. The mechanisms and mechanics of the toughening of epoxy polymers modified with silica nanoparticles. Polymer 2010;51:6284-6294.

[104] Cano L, Builes DH, Tercjak A. Morphological and mechanical study of nanostructured epoxy systems modified with amphiphilic poly(ethylene oxide-b-propylene oxide-b-ethylene oxide) triblock copolymer. Polymer 2014;55:738-745.

[105] Ratna D. Handbook of thermoset resins, iSmithers-A Smithers Group Company. Shrewsbury (UK), 2009.

[106] Jin FL, Li X, Park SJ. Synthesis and application of epoxy resins: A review. J. Ind. Eng. Chem. 2015;29:1-11.

[107] Bilyeu B, Brostow W, Menard KP. Epoxy thermosets and their applications I: Chemical structures and applications. J. Mater. Educ. 1999;21:281-286.

[108] Bonnet A, Pascault JP, Sautereau H, Taha M. Epoxy-diamine thermoset/thermoplastic blends. 1. Rates of reactions before and after Phase Separation. Macromolecules 1999; 32, 8517-8523.

[109] Nikolic G, Zlatkovic S, Cakic M, Cakic S, Lacnjevac C, Rajic Z. Fast Fourier transform IR characterization of epoxy GY systems crosslinked with aliphatic and cycloaliphatic EH polyamine adducts. Sensors 2010;10:684-696.

[110] Park SJ, Jeong HJ, Nah C. A study of oxyfluorination of multi-walled carbon nanotubes on mechanical interfacial properties of epoxy matrix nanocomposites. Mater. Sci. Eng. A 2004;385:13-16.

[111] Park SJ, Jin FL, Lee JR, Shin JS. Cationic polymerization and physicochemical properties of a biobased epoxy resin initiated by thermally latent catalysts. Eur. Polym. J. 2005;41:231-237.

[112] Jeon HR, Park JH, Shon MY. Corrosion protection by epoxy coating containing multi-walled carbon nanotubes. J. Ind. Eng. Chem. 2013;19:849-853.

[113] Hillmyer MA, Lipic PM, Hajduk DA, Almdal K, Bates FS. Self-assembly and polymerization of epoxy resin-amphiphilic block copolymer nanocomposites. J. Am. Chem. Soc. 1997;119:2749-2750.

[114] Serrano E, Martin MD, Tercjak A, Pomposo JA, Mecerreyes D, Mondragon I. Nanostructured thermosetting systems from epoxidized styrene butadiene block copolymers. Macromol. Rapid Commun. 2005;26:982-985.

[115] Serrano E, Tercjak A, Ocando C, Larrañaga M, Parellada MD, Corona-Galván S, Mecerreyes D, Zafeiropoulos NE, Stamm M, Mondragon I. Curing behavior and final properties of nanostructured thermosetting systems modified with epoxidized styrene-butadiene linear diblock copolymers. Macromol. Chem. Phys. 2007;208:2281-2292.

[116] Mijovic J, Shen M, Sy JW. Dynamics and morphology in nanostructured thermoset network/block copolymer blends during network formation. Macromolecules 2000;33:5235-5244.

[117] Thio YS, Wu J, Bates SF. Epoxy toughening using low molecular weight poly(hexylene oxide)-poly(ethylene oxide) diblock copolymers. Macromolecules 2006;39:7187-7189.

[118] Lipic PM, Bates FS, Hillmyer MA. Nanostructured thermosets from self-assembled amphiphilic block copolymer/epoxy resin mixtures. J. Am. Chem. Soc. 1998;12:8963-8970.

[119] Ocando C, Serrano E, Tercjak A, Peña C, Kortaberria G, Calberg C, Grignard B, Jerome R, Carrasco PM, Mecerreyes D, Mondragon I. Structure and properties of a semifluorinated diblock copolymer modified epoxy blend. Macromolecules 2007;40:4068-4074.

[120] Liu JD, Thompson ZJ, Sue HJ, Bates FS, Hillmyer MA, Dettloff M, Jacob G, Verghese N, Pham H. Toughening of epoxies with block copolymer micelles of wormlike morphology. Macromolecules 2010;43:7238-7243.

[121] Tercjak A, Larrañaga M, Martin MD, Mondragon I. Thermally reversible nanostructured thermosetting blends modified with poly(ethylene-b-ethylene oxide) diblock copolymer. J. Therm. Anal. Calorim. 2006;86:663-667.

[122] Pérez-Ruiz L, Royston GJ, Fairclough JPA, Ryan AJ. Toughening by nanostructure. Polymer 2008;49:4475-4488.

[123] Chau Hang JL, Liu HW, Su WF. Fabrication of hybrid surface-modified titania-epoxy nanocomposite films. J. Phys. Chem. Solids 2009;70:1385-1389.

[124] Ocando C, Tercjak A, Martín MD, Ramos JA, Campo M, Mondragon I.

Morphology development in thermosetting mixtures through the variation on chemical functionalization degree of poly(styrene-b-butadiene) diblock copolymer modifiers. Thermomechanical properties. Macromolecules 2009;45:6215-6224.

[125] Tercjak A, Gutierrez J, Mondragon I. Conductive properties of inorganic/organic nanostructured systems based on block copolymers. Mater. Sci. Forum 2012;714:153-158.

[126] Carolan D, Ivankovic A, Kinloch AJ, Sprenger S, Taylor AC. Toughening of epoxy-based hybrid nanocomposites. Polymer 2016;97:179-190.

[127] Kobayashi M, Saito H, Boury B, Matsukawa K, Sugahara Y. Epoxy-based hybrids using TiO_2 nanoparticles prepared via a non-hydrolytic sol-gel route. Appl. Organomet. Chem. 2013;27:673-677.

[128] Zhu L, Zhang C, Han J, Zheng S, Li X. Formation of nanophases in epoxy thermosets containing an organic-inorganic macrocyclic molecular brush with poly(ε-caprolactone)-block-polystyrene side chains. Soft Matter 2012;8:7062-7072.

[129] Maiez-Tribut S, Pascault JP, Soule ER, Borrajo J, Williams RJJ. Nanostructured epoxies based on the self-assembly of block copolymers: A new miscible block that can be tailored to different epoxy formulations. Macromolecules 2007;40:1268-1273.

[130] Tercjak A, Gutierrez J, Martin MD, Mondragon I. Transparent titanium dioxide/block copolymer modified epoxy-based systems in the long scale microphase separation threshold. Eur. Polym. J. 2012;48:16-25.

[131] Meng F, Zheng S, Li H, Liang Q, Liu T. Formation of ordered nanostructures in epoxy thermosets: A mechanism of reaction-induced microphase separation. Macromolecules 2006;39:5072-5080.

[132] Guo Q, Thomann R, Gronski W. Nanostructures, semicrystalline morphology, and nanoscale confinement effect on the crystallization kinetics in self-organized block copolymer/thermoset blends. Macromolecules 2003;36:3635-3645.

[133] Guo Q, Liu J, Chen L, Wang K. Nanostructures and nanoporosity in thermoset epoxy blends with an amphiphilic polyisoprene-block-poly (4-vinyl pyridine) reactive diblock copolymer. Polymer 2008;49:1737-1742.

[134] Yi F, Zheng S. Nanostructures and surface hydrophobicity of self-assembled thermosets involving epoxy resin and poly(2,2,2-trifluoroethyl acrylate)-block-poly(ethylene oxide) amphiphilic diblock copolymer. J. Phys. Chem. B 2009;113:1857-1868.

[135] Sun P, Dang Q, Li B, Chen T, Wang Y, Lin H, Jin Q, Ding D. Mobility,

miscibility, and microdomain structure in nanostructured thermoset blends of epoxy resin and amphiphilic poly(ethylene oxide)-block-poly(propylene oxide)-block-poly(ethylene oxide) triblock copolymers characterized by solid-state NMR. Macromolecules 2005;38:5654-5667.

[136] Larrañaga M, Martin MD, Gabilondo N, Kortaberria G, Eceiza A, Riccardi CC, Mondragon I. Toward microphase separation in epoxy systems containing PEO-PPO-PEO block copolymers by controlling cure conditions and molar ratios between blocks. Colloid Polym. Sci. 2006;284:1403-1410.

[137] Meng F, Zheng S, Liu T. Epoxy resin containing poly(ethylene oxide)-block-poly(ε-caprolactone) diblock copolymer: Effect of curing agents on nanostructures. Polymer 2006;47:7590-7600.

[138] Blanco M, Lopez M, Kortaberria G, Mondragon I. Toward microphase separation in epoxy systems containing PEO-PPO-PEO block copolymers by controlling: Effect of copolymer content on nanostructures. Polym. Int. 2009;59:523-528.

[139] Grubbs RB, Dean JM, Broz ME, Bates FS. Reactive block copolymers for modification of thermosetting epoxy. Macromolecules 2000;33:9522-9534.

[140] Rotrekl J, Sikora A, Kaprálková L, Dybal J, Kelnar I. Effect of an organoclay on the reaction-induced phase-separation in a dynamically asymmetric epoxy/PCL system. Express Polym. Lett. 2013;12:1012-1019.

[141] Nambiar R, Blum F. Segmental dynamics of bulk poly(vinyl acetate)-d_3 by solid-state ^{2}H NMR: Effect of small molecule plasticizer. Macromolecules 2008;41:9837-9845.

[142] Immergur EH, Mark HF. Principles of plasticization. Advances in chemistry. American Chemical Society. Washington DC (USA) 1965.

[143] Rao CNR, Ramakrishna HSS, Voggu R, Govindaraj A. Recent progress in the synthesis of inorganic nanoparticles. Dalton Trans. 2012;41:5089-5120.

[144] Tercjak A, Gutierrez J, Peponi L, Rueda L, Mondragon I. Arrangement of conductive TiO_2 nanoparticles in hybrid inorganic/organic thermosetting materials using liquid crystal. Macromolecules 2009;42:3386-3390.

[145] Ocando C, Tercjak A, Mondragon I. Nanostructured systems based on SBS epoxidized triblock copolymers and well-dispersed alumina/epoxy matrix composites. Compos. Sci. Technol. 2010;70:1106-1112.

[146] Gutierrez J, Tercjak A, Mondragon I. Transparent nanostructured thermoset composites containing well-dispersed TiO_2 nanoparticles. J. Phys. Chem. C

2010;114:22424-22430.

[147] Gutierrez J, Mondragon I, Tercjak A. Multifunctional Nanostructured Composites Based on TiO_2 Nanoparticles. Macromol. Symp. 2012;321/322:99-104.

[148] Keller A, Masania K, Taylor AC, Dransfeld C. Fast-curing epoxy polymers with silica nanoparticles: properties and rheo-kinetic modelling. J. Matter. Sci. 2016;51:236-251.

[149] Li M, Ober CK. Block copolymer patterns and templates. Mater. Today 2006;9-30-39.

[150] Hampley IW. Ordering in thin films of block copolymers: Fundamentals to potential application. Prog. Polym. Sci. 2009;34:1161-1210.

2 Materials and characterization techniques

2. Materials and characterization techniques

The materials and the characterization techniques employed along this investigation work will be described in this Chapter. The experimental procedures as well as characterization techniques conditions will be detailed in each Chapter.

2.1. Materials

2.1.1. Liquid crystals

Two different nematic liquid crystals 4'-(hexyloxy)-4-biphenylcarbonitrile (HOBC) with 96 % purity and N-(4-ethoxybenzylidene)-4-butylaniline (EBBA) with 98 % purity were purchased from Sigma-Aldrich and were used as received.

2.1.2. Block copolymers

Two different poly(ethylene-b-ethylene oxide) diblock copolymers (PE-b-PEO) one with an average molecular weight (M_n) of 920 g mol^{-1} and 50 wt % of PEO block content and the other one with an average molecular weight of 2250 g mol^{-1} and 80 wt % of PEO block content, were provided by Sigma-Aldrich. These block copolymers were used without purification.

2.1.3. Homopolymers

Polyethylene oxide homopolymer (PEO) with an average molecular weight equal to 950-1050 g mol^{-1}, similar to this block in the PE-b-PEO block copolymer, was supplied by Sigma-Aldrich.

Polylactic acid homopolymer (PLA) 3051D with a molecular weight of 93500 g mol^{-1} was purchased from Natureworks and was used as received.

2.1.4. Epoxy resin

Diglycidyl ether of bisphenol A (DGEBA) epoxy resin monomer was provided by Dow Chemical Company with an epoxy equivalent weight between 176 and 185 g/eq (trade name DER 330).

This epoxy resin was cured with a stoichiometric amount of the aromatic amine curing agent 4,4’-methylene bis(3-chloro-2,6-diethylaniline) (MCDEA) kindly supplied by Lonza.

The chemical structures of all materials used in this investigation work are presented in Table 2.1.

Table 2.1. Chemical structure of the PE-b-PEO block copolymer, HOBC and EBBA nematic liquid crystals, PEO and PLA homopolymers, DGEBA epoxy resin monomer and MCDEA curing agent.

Materials	Chemical structure
Poly(ethylene-b-ethylene oxide) block copolymer (PE-b-PEO)	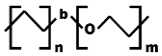
4'-(hexyloxy)-4-biphenylcarbonitrile (HOBC)	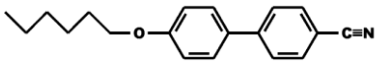
N-(4-ethoxybenzylidene)-4-butylaniline (EBBA)	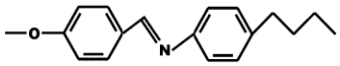
Polyethylene oxide (PEO)	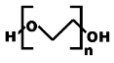
Polylactic acid (PLA)	
Diglycidyl ether of bisphenol A (DGEBA)	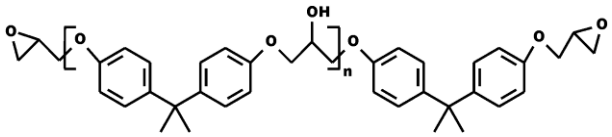
4,4'-methylene-bis(3-chloro-2,6-diethylaniline) (MCDEA)	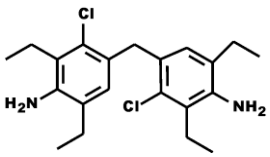

2.2. Electrospinning technique

Electrospinning is the preparation technique that allows, through axial stretching of the viscoelastic solutions, the fabrication of micro and nanofibers from polymeric materials. These fiber sizes permit the discovery of unique features, such as high surface

area to volume and large length to diameter ratios [1].

Firstly, in the electrospinning process, a polymer solution is pushed by a pump through a capillary up to a needle. Then, a strong electric field is applied between the needle and the collector, which provokes the stretching of this solution and the solvent evaporation allowing the fabrication of polymeric fibers [1-4].

The most recent research development in the relation to this technique is focused on the fabrication of hybrid electrospun nanofibers, for example, by means of a coaxial electrospinning technique. Co-electrospinning is a modification of the conventional electrospinning technique, based on two concentric needles. This technique is able to simultaneously electrospin different polymeric materials with the aim of the fabrication of core-shell structure nanofibers [2,5-7].

In our case, during the electrospinning process, the block copolymer solution was pushed using a pump through a capillary up to the inner needle of the concentric needle, while solvent flowed through the outer one. For the preparation of hybrid electrospun fibers, the EBBA liquid crystal solution was used instead of the solvent. Figure 2.1 shows co-electrospinning employed in this research work.

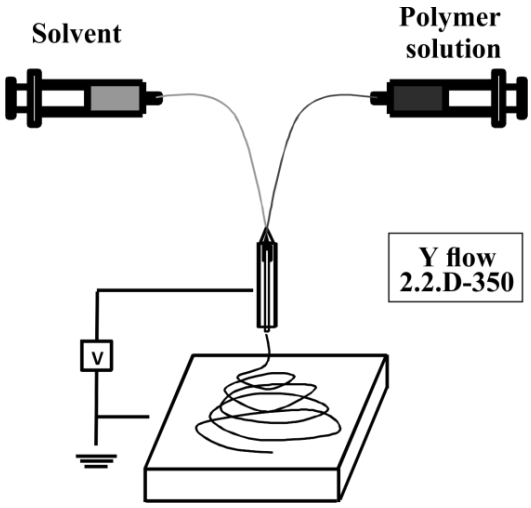

Figure 2.1. Co-electrospinning system.

The main difficulty of this technique lies in the number of parameters that are required to control the final properties of the fabricated fibers. The parameters involved in the generation of these fibers are the concentration of the polymer solution, surface tension, solution conductivity, voltage, outflow, distance needle-collector and relative humidity, among others [3,5].

The low production rate and the solvents used are the most important problems in the electrospinning process since their can limited the possible application leading to

significant safety problem during fabrication due to their flammability, toxicity or carcinogenic character. Moreover, another handicaps related to the solvents used can be also cost and recovery [6-8].

Table 2.2 summarizes the most important parameters that take part in the electrospinning process and their influence on the final properties of the designed fibers. This technique allows to collect continuous single fibers with regular and controllable diameters and defect free surface by playing with the electrospinning parameters.

Table 2.2. The effect of the electrospinning parameters on the fibers formation.

Parameter	High values	Low values
Concentration of the polymer solution	Hinders the passage of the solution through the capillary	Fibers breakage, droplet formation
Surface tension	Defects (beads) in fibers	Smooth fibers
Solution conductivity	Thin fibers	Thick fibers
Voltage	Thick fibers, the appearance of beads	The solution does not reach the collector
Outflow	Thick fibers, beads with larger sizes	Fibers without defects
Distance needle-collector	Thin fibers and appearance of beads (the fibers may break due to its own weight)	Appearance of beads
Relative humidity	Appearance of pores	No effect

2.3. Characterization techniques

2.3.1. Physico-chemical characterization

2.3.1.1. Fourier transform infrared spectroscopy (FTIR)

FTIR is an analytical technique employed to identify organic and in some cases inorganic materials through the infrared absorption as a function of the wavelength [9].

The irradiated materials excite its molecules into a higher vibrational state. The absorbed radiation is related to the chemical bonds and functional groups present in investigated materials. The wavelength, between 4000 and 600 cm^{-1}, absorbed by materials is characteristic and unique for their molecular structure and is a function of the energy difference between the excited and rested vibrational states. Consequently,

this technique is employed for the recognition of organic molecular groups, side chains and network formations such as curing reaction studied in this research work [10].The FTIR spectrometer modulates the wavelength employing an interferometer in a broadband infrared source and the intensity of transmitted or reflected light as a function of its wavelength is measured by a detector. The signal obtained is analyzed with a computer using Fourier transforms to obtain the absorption spectrum.

Attenuated total reflectance (ATR) is a complementary accessory of the FTIR spectrometer. ATR measure the changes in the internally reflected infrared beam in contact with investigated material. The infrared beam is conducted to an optically dense crystal with a high refractive index in a defined angle. This internal reflectance generates an evanescent wave that extends to investigated material. The wave is attenuated in the regions of the infrared spectrum in which investigated material absorbs energy. The attenuated beam returns and passes through the ATR crystal leading to the infrared spectrometer. Then, the detector records the attenuated infrared beam as a signal, which can be used to generate an infrared spectrum [10].

2.3.1.2. Photoluminescence spectroscopy (PL)

PL is a non-destructive method based on the detection of absorption of light of different investigated materials, which provoke an excess energy which is dissipated by photoexcitation process [11]. After excitation, electrons within the material move into permissible excited states, generating several relaxation processes due to return to their equilibrium states. The excess of energy is released and may include the emission of light due to a radiative process, however non-radiative process can be also take place.

The photoluminescence process at a certain energy can be viewed as indication that excitation populated an excited state associated with this transition energy as shown in Figure 2.2.

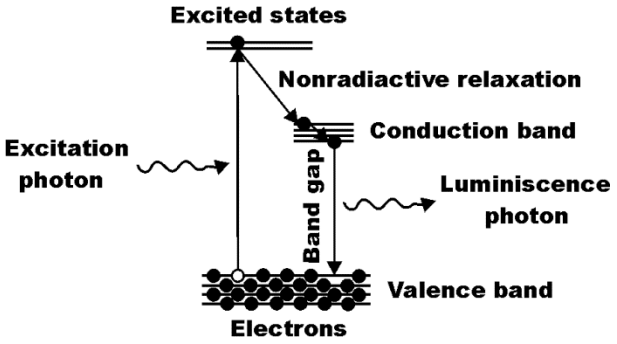

Figure 2.2. Photoluminescence process initiated by an excited electron when an excitation photon is applied.

The difference in energy levels between the two electron states involved in the transition between the excited state and the equilibrium state is related to the energy of the emitted light.

2.3.1.3. Ultraviolet-visible spectroscopy (UV-vis)

Absorbance spectroscopy measure the amount of light absorbed or transmitted by an investigated material as a function of the wavelength. In the region of the electromagnetic spectrum, atoms and molecules undergo electronic transitions.

In conventional spectrometers a visible-UV monochromatic light beam passes through a investigated material which is held in a small section cell.

Ultraviolet-visible radiation with a determinate frequency and intensity passed through the investigated material and a reference cell, which contains only the solvent. The intensity of this light beam is measured by electronic detectors and compared to the intensity of the light, which passed through the reference cell.

An absorption spectrum shows a number of absorption bands corresponding to structural groups within the molecule, since different molecules absorb radiation of different wavelengths.

When an atom or molecule absorbs energy, electrons are promoted from their ground state to an excited state hence, the absorption of UV or visible radiation corresponds to the excitation of outer electrons.

The spectrometer usually displays absorbance on the vertical axis versus wavelength or transmittance versus wavelength, being the transmittance related with the light that passes through the investigated material in comparison to the light that has not. The most investigated materials have characteristic absorbance spectra and can be identified [12].

2.3.2. Thermal characterization

2.3.2.1. Differential scanning calorimetry (DSC)

DSC is a thermo-analytical technique based on the compensation of differences in heat required to increase the temperature of both an investigated material and the reference as a function of temperature or time with control heating or cooling rate [13].

Both the investigated material and reference are maintained at the same temperature throughout the experiment. In general, in a DSC analysis, the temperature

program is designed such that the investigated material holder temperature increases linearly as a function of temperature or time. The reference sample has a well-defined heat capacity over the temperatures range.

While the investigated material suffers a physical transformation such as first and second-order phase transitions or chemical reaction (reaction kinetics, curing reactions and other) the difference in heat flow between the investigated material and reference sample are compensated by DSC. Thus, during endothermic process DSC equipment provide heat to allow the fusion of the investigated material, and during an exothermic process, the investigated material releases heat which is absorbed by DSC equipment.

The difference in heat flow between the investigated material and reference sample is compensated by DSC equipment which absorbs or release heat during phase transitions, which take place in the investigated material. The main application of DSC is in studying phase transitions, such as melting, glass transitions, or ever in studying polymer curing.

2.3.2.2. Thermal gravimetric analysis (TGA)

TGA is a method of thermal analysis in which physical and chemical changes in the investigated materials are detected by means of the weight loss as a function of temperature, with determined heating rate or as a function of time with constant temperature [14].

This technique can provide information about physical phenomena, such as phase transitions, including vaporization, sublimation, absorption, adsorption and desorption as well as information about chemical phenomena including chemisorptions, desolvation, especially dehydration, decomposition, and solid-gas reactions.

TGA is generally used to analyze materials that exhibit either mass loss or gain due to decomposition, oxidation, or loss of volatiles, such as moisture or CO_2 by combustion. The characterization of materials through analysis of defined decomposition patterns, degradation mechanisms and reaction kinetics, is necessary to determine the organic and inorganic content in the investigated material, which may be useful for corroborating the predicted structures or simply used as a chemical analysis.

It is an especially useful technique for the study of polymeric materials, including thermoplastics, thermosets, elastomers, composites, plastic films, fibers, coatings and paints.

2.3.3. Morphological characterization

2.3.3.1. Atomic force microscopy (AFM)

AFM technique measures the local properties of the investigated material with high resolution providing material surface information at the nanometric scale. This technique employs a very sharp tip (generally 4-6 μm tall with 15-40 nm end radius) to scan the investigated material surface. The force along the investigated material surface is carefully maintained at a set level [15,16]. AFMs can generally measure the vertical and lateral deflections of the cantilever employing the optical lever to acquire the high image resolution. The optical lever operates by reflecting a laser beam off the cantilever and the reflected laser beam strikes a position-sensitive photo-detector, as shown in Figure 2.3.

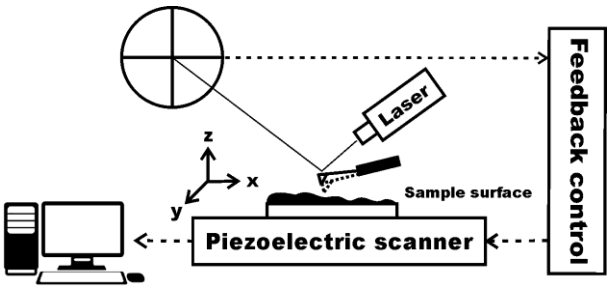

Figure 2.3. Schematic illustration of the AFM tapping mode operation.

A piezoelectric material, which can move the probe very precisely in the x, y, and z, position the tip with high resolution. In the presence of a voltage gradient, piezoelectric materials expand or contract. During the scanning, the z-piezo moves up and down to maintain constant the set point deflection signal. The distance between the tip and investigated material surface, provides the topography information. The height provides the topography of the investigated material and phase image the material properties like elasticity and adhesion. Both images are collected simultaneously [17].

The AFM measures and regulates the force on the investigated material allowing acquisition of images at very low forces.

2.3.3.2. Optical microscopy (OM)

The OM employs a microscope which uses visible light as light source and a system of lenses for magnification the image of the investigated materials.

Basic optical microscopes can be very simple using only a lens although there

are many complex designs which aim to improve resolution and the investigated material contrast. Optical microscope generates micrographs which can be captured by normal light sensitive cameras.

Currently digital microscopes are available which show the resulting image directly on a computer screen without the need for eyepieces. When a material is analyzed by optical microscopy, it uses a close lens (the objective lens) which generates a real image inside the microscope. A second lens or group of lenses (the eyepiece) magnifies the image obtaining an enlarged inverted virtual image of the object. Common compound microscopes often feature exchangeable objective lenses, allowing the user to quickly adjust the magnification [18]. Moreover, a compound microscope also enables more advanced illumination setups, such as phase contrast.

2.3.3.3. Scanning electron microscopy (SEM)

SEM is a technique employed to obtain high-resolution images of the investigated materials. A focused beam of electrons scans an investigated material to produce images of its surface.

The surface topography of the investigated materials and their composition are obtained due to the interaction between the beam of electron and the atoms of the investigated materials.

The electrons of the beam, created by a thermal emission source (a heated tungsten filament or a field emission cathode) generate energy between from 100 eV to 30 keV depending on the evaluation objectives. A series of electromagnetic lenses focus the electrons into a small beam onto the investigated material surface. This causes the release of secondary emitted electrons and other types of radiations such as backscattered electrons, diffracted backscattered electrons, photons, visible light and heat from the investigate material.

The shape and the chemical composition of the investigated material is related to the intensity of the secondary electrons, which are collected by a detector, generating electronic signals. These signals are displayed as brightness on a display monitor and/or in a digital image file, which is recorded by capturing it from the cathode ray tube [19].

The external morphology, chemical composition and crystalline structure and orientation of the investigated material are achieved through the signals that derive from electron- investigated material interactions.

2.3.4. Surface characterization

2.3.4.1. Water contact angle

The contact angle is the angle generated between a liquid, water in this case, and a solid surface. It is related to the solid surface and water properties, to the interaction and repulsion forces between water and solid surface and to the three phase interface properties, gas, liquid and solid. Those interactions are described by intermolecular forces such as cohesion and adhesion forces [20]. This contact angle can be measured directly from the angle formed at the contact between the water drop and the flat surface as shown in Figure 2.4.

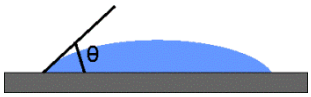

Figure 2.4. Water contact angle formed at the contact between the water drop and the solid surface.

The contact angle quantifies the wettability of a solid surface. If the liquid molecules are strongly attracted to the solid molecules, cohesive forces are weaker than adhesive forces then the liquid drop will completely spread out on the solid surface. In this case the contact angle is equal to 0°.

Generally, when the water contact angle is smaller than 90°, the solid surface is considered hydrophilic and when is larger than 90°, the solid surface is considered hydrophobic [21].

In order to control the wetting contact angle, different procedures, such as deposition or incorporation of various organic and inorganic molecules onto the surface of the investigated material, are carry out. The contact angle of the surface can be tuned with the proper selection of the organic molecules with varying molecular structures and amounts of hydrocarbon terminations.

2.4. References

[1] Li D, Xia L. Electrospinning of nanofibres: Reinventing the wheel? Adv. Mater. 2004;16:1151-1170.

[2] Greiner A, Wendorff JH. Electrospinning: A fascinating method for the preparation of ultrathin fibers. Angew. Chem. Int. Edit. 2007;46:5670-5703.

[3] Burger C, Hsiao BS, Chu B. Nanofibrous materials and their applications. Annu. Rev. Mater. Res. 2006;36:333-368.

[4] Richard-Lacroix M, Pellerin C. Molecular orientation in electrospun fibers: From mats to single fibers. Macromolecules 2013;46:9473-9493.

[5] Ko FK, Wan Y. Nanofiber technology. Introduction to nanofiber materials. Cambridge University Press. Cambridge (UK), 2014.

[6] Chen X, Dong B, Wang B, Shah R, Li CY. Crystalline block copolymer decorated, hierarchically ordered polymer nanofibres. Macromolecules 2010;43:9918-9927.

[7] Cho SJ, Jung SM, Kang M, Shin HS, Youk JM. Preparation of hydrophilic PCL nanofiber scaffolds via electrospinning of PCL/PVP-b-PCL block copolymers for enhanced cell biocompatibility. Polymer 2015;69:95-102.

[8] Schiffman JD, Schauer CL. A review: Electrospinning of biopolymer nanofibers and their applications. Polym. Rev. 2008;48:317-352.

[9] Griffiths P, de Hasseth JA. Fourier transform infrared spectrometry. Second Ed., Wiley-Blackwell. New Jersey (USA), 2007.

[10] Alpert NL, Keiser WE, Szymanski HA. IR theory and practice of infrared spectroscopy. Plenum Press. New York (USA), 2012.

[11] McNaught AD, Wilkinson A. Compendium of chemical terminology. Second Ed., Blackwell Scientific Publications. Oxford (UK), 1997.

[12] Kumar CSSR. UV-vis and photoluminiscence spectroscopy for nanomaterials characterization. Springer. London (UK), 2013.

[13] Höhne GWH, Hemminger WF, Flammersheim HJ. Differential scanning calorimetry. Springer. Berlin (Germany), 2003.

[14] Coats AW, Redfern JP. Thermogravimetric analysis: A review. Analyst 1963;88:906-924.

[15] Dimension Icon AFM manual from Bruker Corporation. 2010.

[16] Butt HJ, Cappella B, Kappl M. Force measurements with the atomic force microscope: Technique, interpretation and applications. Surf. Sci. Rep. 2005;59:1-152.

[17] García R, Pérez R. Dynamic atomic force microscopy methods. Surf. Sci. Rep. 2002;47:197-301.

[18] Watt IM. The principles and practice of electron microscopy. Second Ed., Cambridge University Press. Cambridge (UK), 1997.

[19] Clarke AR, Eberhardt CN. Microscopy techniques for materials science. Woodhead Publishing Limited. Cambridge (UK), 2002.

[20] Zisman WA, Fowkes F. Contact angle, wettability and adhesion. American Chemical Society. Los Angeles (USA), 1964.

[21] Förch R, Schönherr H, Tobias A, Jenkins A. Surface design: Applications in bioscience and nanotechnology. Wiley-VCH. Weinheim (Germany), 2009.

3 PE-b-PEO block copolymer dispersed liquid crystal blends

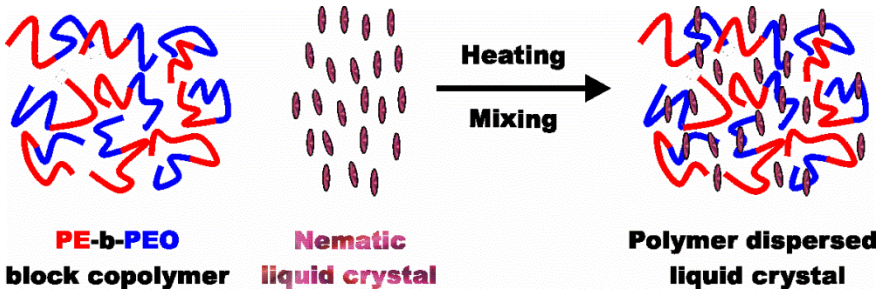

3. PE-b-PEO block copolymer dispersed liquid crystal blends

In this Chapter, different block copolymer dispersed liquid crystal (PDLC) blends based on PE-b-PEO block copolymer and modified with two different low molecular weight nematic liquid crystals, HOBC and EBBA, will be fabricated and characterized. The miscibility between each block of the PE-b-PEO block copolymer and each nematic liquid crystal and the thermal stability of the PE-b-PEO/HOBC and PE-b-PEO/EBBA blends will be addressed. The morphology of the fabricated PE-b-PEO/HOBC and PE-b-PEO/EBBA blends will be visualized using OM.

3.1. Introduction

As was explained in the Chapter 1, Polymer Blend Technology is one of the main areas of research and development in Polymer and Material Science since offers opportunities to create novel materials with tailored properties [1-8]. In order to control and improve the miscibility in polymer blends, the addition of block copolymers, which are able to reduce the interfacial tension between components and allows controlling the phase separation and consequently promoting higher miscibility between components, are employed [1,9-23].

In the last decade, PDLC blends were investigated due to their wide range of applications in the field of thermal and electro-optical devices such as optical switches (light shutters), smart windows, reflective displays and others [24-32].

Nematic liquid crystals (NLC) with their optical anisotropy and dielectric properties allow to design PDLC materials, which can switch from a state of high dispersion of light (OFF state) to a transparent state (ON state) by applying an external field such as thermal gradient, electrical voltage or magnetic field [20,24-35].

As it is well known, block copolymers consist of two or more covalently linked polymers, which can self-assemble offering nanostructured templates for dispersion of NLCs. Consequently, NLCs can be positioned in one block of the block copolymer leading to PDLC materials with tunable properties.

The main objective of this Chapter was the fabrication and characterization of PDLC blends based on PE-b-PEO block copolymer and two different low molecular weight nematic liquid crystals, HOBC and EBBA, in order to check the nematic character of the investigated PDLC blends.

3.2. Materials and characterization techniques

3.2.1. Materials

In this Chapter the HOBC and EBBA nematic liquid crystals and the PE-b-PEO diblock copolymer with an average molecular weight of 920 g mol^{-1} and 50 wt % of PEO block content, were employed in order to fabricate PDLC blends (for more details see the Chapter 2).

Additionally, the PEO homopolymer with a molecular weight similar to this block in the PE-b-PEO block copolymer, as was specified in the Chapter 2, was also used with the aim to better understand the miscibility of each block of the PE-b-PEO block copolymer with each NLC.

3.2.2. Sample preparation

The PE-b-PEO block copolymer dispersed liquid crystal blends were prepared by melting different weight percentages of the PE-b-PEO block copolymer (25, 50 and 75 wt %) with the HOBC and EBBA nematic liquid crystals. These PDLC blends were denominated 25PE-b-PEO/LC, 50PE-b-PEO/LC and 75PE-b-PEO/LC, being LC equal to HOBC or EBBA nematic liquid crystal.

For comparison, the PEO homopolymer was used to prepare PDLC blends with the same weight percentages as in blends based on PE-b-PEO block copolymer (25, 50 and 75 wt %) denominated as 25PEO/LC, 50PEO/LC and 75PEO/LC being LC equal to HOBC or EBBA nematic liquid crystal.

All mixtures of the PDLC blends were melted keeping them in an oven at 100 ºC during 1 h and stirred manually to promote their mixing.

3.2.3. Characterization techniques

3.2.3.1. Fourier transform infrared spectroscopy

FTIR was performed using a Nicolet Nexus 670 spectrometer equipped with a single horizontal Golden Gate cell (ATR). Spectra were recorded in the range from 600 to 4000 cm^{-1}, with 2 cm^{-1} resolution and an accumulation of 20 scans.

3.2.3.2. Thermogravimetric analysis

TGA was performed with a TGA/SDTA-851^{e} equipment under nitrogen

atmosphere in the temperature range from 25 to 700 ºC at a heating rate of 10 ºC min^{-1}.

3.2.3.3. Differential scanning calorimetry

DSC measurements of the investigated PE-b-PEO block copolymers or PEO homopolymer dispersed liquid crystal blends were performed using a Mettler Toledo DSC 822^e differential scanning calorimeter. Indium (T_m = 157 ºC, ΔH_m = 29 J g^{-1}) and zinc (T_m = 420 ºC, ΔH_m = 108 J g^{-1}) were used for DSC calibration. The PE-b-PEO block copolymer, PEO homopolymer, HOBC and EBBA nematic liquid crystals as well as the investigated PDLC blends were encapsulated in aluminium pans weight. All investigated materials were around 6 mg and measured under nitrogen atmosphere at a flow of 25 mL min^{-1}.

To avoid the thermal history, all investigated materials were first heated from 25 to 150 ºC at 5 ºC min^{-1}, then the samples were cooled to -25 ºC at 5 ºC min^{-1} and after the crystallization process, the melting was performed heating the investigated materials up to 150 ºC at a heating rate of 5 ºC min^{-1}. The melting temperature, T_m, was regarded as corresponding to the maximum of the endothermic peak detected during the heating scan. The crystallization temperature, T_c, corresponded to the minimum of the exothermic peak obtained during the cooling process.

In order to estimate the miscibility between the components of the investigated PDLC blends the changes of the crystallization degree (X_c) were calculated using the following equation [1-3]:

$$X_c = \frac{\Delta Hex}{\omega \Delta H100\%} \text{ x } 100$$

where ω was the weight fraction of the component of the PDLC blends for which the degree of crystallization was calculated and $\Delta H_{100\%}$ was the theoretical melting enthalpy of investigated material in 100 % crystalline state.

The experimental enthalpy of the melting transition, ΔH_{ex}, was calculated from the area of the endotherm peak during heating.

The enthalpies of the NLCs in 100 % crystalline state were calculated considering the purity of nematic liquid crystals given by Sigma Aldrich and the melting enthalpy of each nematic liquid crystal obtained experimentally by DSC measurement, being $\Delta H_{100\%}$ equal to 115.9 J g^{-1} and 47.5 J g^{-1} for the HOBC and EBBA nematic liquid crystals, respectively.

3.2.3.4. Optical microscopy

OM measurements were carried out using a Nikon Eclipse E600W microscope equipped with a hot stage Mettler FP 82 HT. Micrographs were captured with a Color View 12 camera with Analysis Auto 3.2 software (Soft Imaging System GmbH) the nematic liquid crystal droplets size was analyzed using the same software.

In order to visualized the nematic liquid crystal character of the PDLC blends, the same quantity of each investigated blend was placed between two microscopy glasses and kept 10 min at 120 ºC to avoid thermal history and then quenched with the highest controlled speed of hot stage Mettler FP 82 HT (40 ºC min^{-1}) to room temperature.

The morphology generated after this treatment was observed using OM with crossed polarizers at room temperature before any crystallization took place (5 min for every investigated samples). This procedure allowed to visualize the presence of the mesostable nematic morphology of the HOBC and EBBA liquid crystal phases in investigated PDLC blends.

3.3. Results and discussion

3.3.1. FTIR of the PDLCs

ATR-FTIR spectra of the PDLC blends based on PE-b-PEO block copolymer and HOBC or EBBA nematic liquid crystals are shown in Figures 3.1a and 3.1b. For comparison, the ATR-FTIR spectra of neat PE-b-PEO block copolymer, HOBC and EBBA nematic liquid crystals were also plotted.

The main groups detected in ATR-FTIR spectrum for the HOBC nematic liquid crystal are vibrations at 2800-3000 cm^{-1} attributed to the CH_2 and CH_3 groups and at 2210-2260 cm^{-1} related to the CN group. Additionally, strong vibration at 1625 cm^{-1} and 800-860 cm^{-1} corresponding to the C_6H_4 group are also visible. Similar to the HOBC nematic liquid crystal, ATR-FTIR spectrum of the EBBA nematic liquid crystal showed characteristic vibrations at 2800-3000 cm^{-1} and 1615-1700 cm^{-1} related to the CH_2 and CH_3 groups and C=N group, respectively. The C_6H_4 group was also detected as vibration at 1625 and 800-860 cm^{-1}. Simultaneously, ATR-FTIR spectrum of the PE-b-PEO block copolymer exhibits vibrations at 2800-3000 and 1120 cm^{-1} attributed to the CH_2CH_3 and -O- ether groups, respectively.

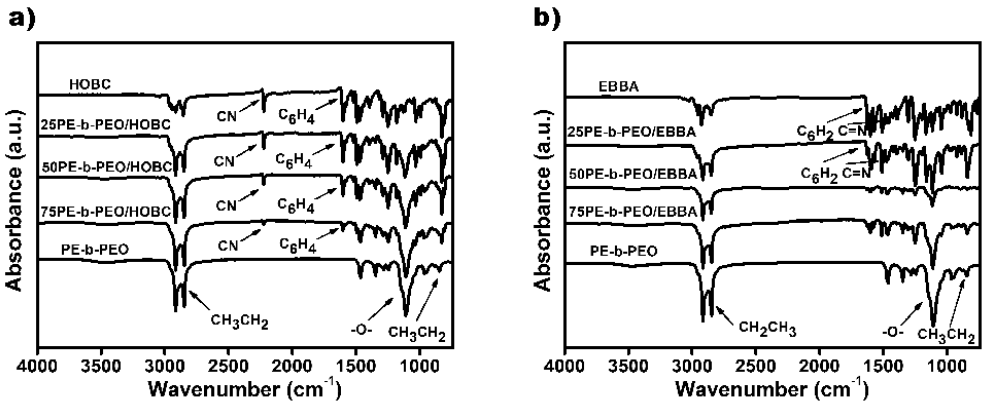

Figure 3.1. ATR-FTIR spectra of the a) PE-b-PEO/HOBC and b) PE-b-PEO/EBBA blends with different PE-b-PEO block copolymer content. For comparison, the ATR-FTIR spectra of neat components were also plotted.

As can be clearly identified from the comparison between ATR-FTIR spectra of the PE-b-PEO/HOBC blends and ATR-FTIR spectrum of the HOBC nematic liquid crystal, the intensity of the vibrations at 2210-2260 cm^{-1} related to the CN group characteristic for the HOBC nematic liquid crystal decreased with the increase of the PE-b-PEO block copolymer content in the PDLC blends. This fact is related to the decrease of the HOBC nematic liquid crystal content in the PE-b-PEO/HOBC blends.

Simultaneously, the increase of the intensity of vibration of the CH_2 and CH_3 groups at 2800-3000 cm^{-1} is related to the fact that these groups are present in both, the PE-b-PEO block copolymer and the HOBC nematic liquid crystal. The intensity of the signals corresponds to each groups changed, the vibrations signal appeared at the same wavelength, indicating lack of chemical interaction between components of the PDLC blends.

Similar to the PE-b-PEO/HOBC blends in the case of the PE-b-PEO/EBBA blends, the intensity of the C=N group at 1615-1700 cm^{-1} characteristic for the EBBA nematic liquid crystal decreased with the increase of the PE-b-PEO block copolymer.

The same tendency is also shown for the C_6H_4 group at 1625 cm^{-1} and 800-860 cm^{-1}. Additionally, the intensity of vibration at 2800-3000 cm^{-1} corresponding to the CH_2 and CH_3 groups increased with the increase of the PE-b-PEO block copolymer content. Similar phenomenon is shown for the signal related to the -O- group.

Neither the PE-b-PEO/HOBC nor PE-b-PEO/EBBA blends showed shifts in the signals related to both, the PE-b-PEO block copolymer and the HOBC or EBBA nematic liquid crystals. This indicated the lack of chemical interactions between components of the PDLC blends.

3.3.2. Thermal stability of the PDLC blends by TGA

The thermal stability of the PE-b-PEO/HOBC and PE-b-PEO/EBBA blends was studied by TGA. Obtained thermogravimetric and differential thermogravimetric curves are shown in Figure 3.2. Thermogravimetric and differential thermogravimetric curves of neat components were also plotted for a better understanding thermal stability of investigated PDLC blends.

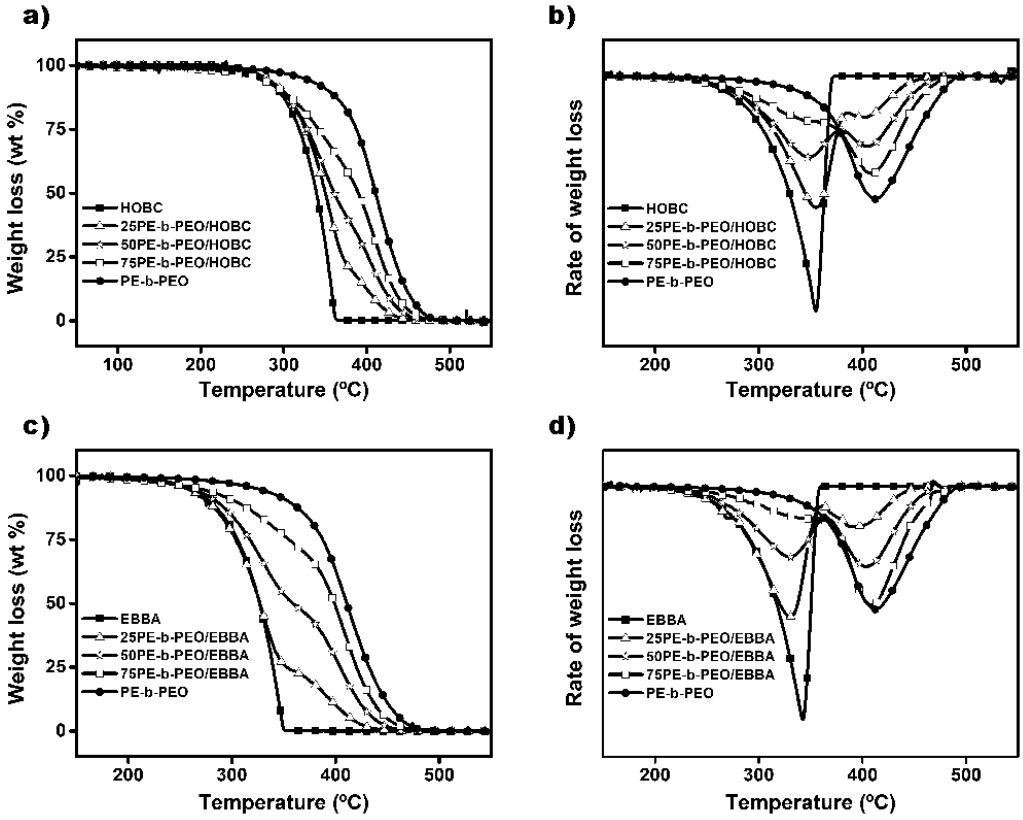

Figure 3.2. a) Thermogravimetric and b) differential thermogravimetric curves of the PE-b-PEO/HOBC blends, and c) thermogravimetric and d) differential thermogravimetric curves of the PE-b-PEO/EBBA blends. For comparison the thermogravimetric and differential thermogravimetric curves of neat components were also plotted.

As shown in Figure 3.2, the stabilization temperature of the PE-b-PEO block copolymer is higher than the stabilization temperature of both, the HOBC and EBBA nematic liquid crystals being the stabilization temperature of the HOBC nematic liquid crystal slightly higher than the stabilization temperature of the EBBA nematic liquid crystal.

In more details, the degradation process of the PE-b-PEO block copolymer followed one step degradation and started at around 412 °C. Similarly, the degradation process of both, the HOBC and EBBA nematic liquid crystals consisted of one step with

the stabilization temperature at around 325 and 310 ºC for the HOBC and EBBA nematic liquid crystals, respectively.

As expected, the PE-b-PEO/HOBC blends followed two steps degradation process. The first step was related to the degradation of the HOBC nematic liquid crystal and the second step can be ascribed to the degradation process of the PE-b-PEO block copolymer. The stabilization temperatures for both steps merged between the stabilization temperatures of the PE-b-PEO block copolymer and the HOBC nematic liquid crystal.

Moreover, the stabilization temperatures increased with the increase of the PE-b-PEO block copolymer content. This fact can be related to the interaction between the components, which is in good agreement with the DSC results described below in this Chapter. Thus, the increase of the PE-b-PEO block copolymer content had strong effect on the degradation of the HOBC nematic liquid crystals and vice versa confirming interaction between components [34].

As can be easily deduced from the comparison of the thermogravimetric curves of the PDLC blends based on the HOBC and EBBA nematic liquid crystals, the degradation process of the PE-b-PEO/EBBA blends is similar to the degradation process of the PE-b-PEO/HOBC blends. Thus, the degradation process of these PDLC blends followed two steps, the first step being related to the degradation process of the EBBA nematic liquid crystal and the second one related to the PE-b-PEO block copolymer. The stabilization temperatures of the PE-b-PEO/EBBA blends depend strongly on the PE-b-PEO block copolymer content suggesting the possible interaction between the PE block of the PE-b-PEO block copolymer and the EBBA nematic liquid crystal.

3.3.3. Thermal behavior of the PDLC blends by DSC

DSC thermograms of the heating and cooling processes of the PE-b-PEO block copolymer and the HOBC and EBBA nematic liquid crystals and their PDLC blends are shown in Figure 3.3.

As expected, the T_m of the PE block of the PE-b-PEO block copolymer was 88 ºC and the T_c was 85 ºC. Under the same DSC measurement conditions, the T_m of the PEO block of the block copolymer was detected at 37 ºC and the T_c at -4 °C. These results confirmed the semicrystalline character of both blocks of the PE-b-PEO block copolymer. The T_m of the HOBC nematic liquid crystal appeared at 58 ºC and its T_c at

22 ºC whereas the T_m of the EBBA nematic liquid crystal was 36 ºC and its T_c 5 ºC.

Additionally, the nematic character of employed liquid crystals was also analyzed using DSC measurement. The nematic-isotropic transition was detected at 77 ºC for the HOBC nematic liquid crystal and at 76 ºC for the EBBA nematic liquid crystal. As it is well known, the nematic-isotropic transition of liquid crystals is a reversible process and can be easily distinguished also during cooling process at around 76 ºC for both liquid crystals.

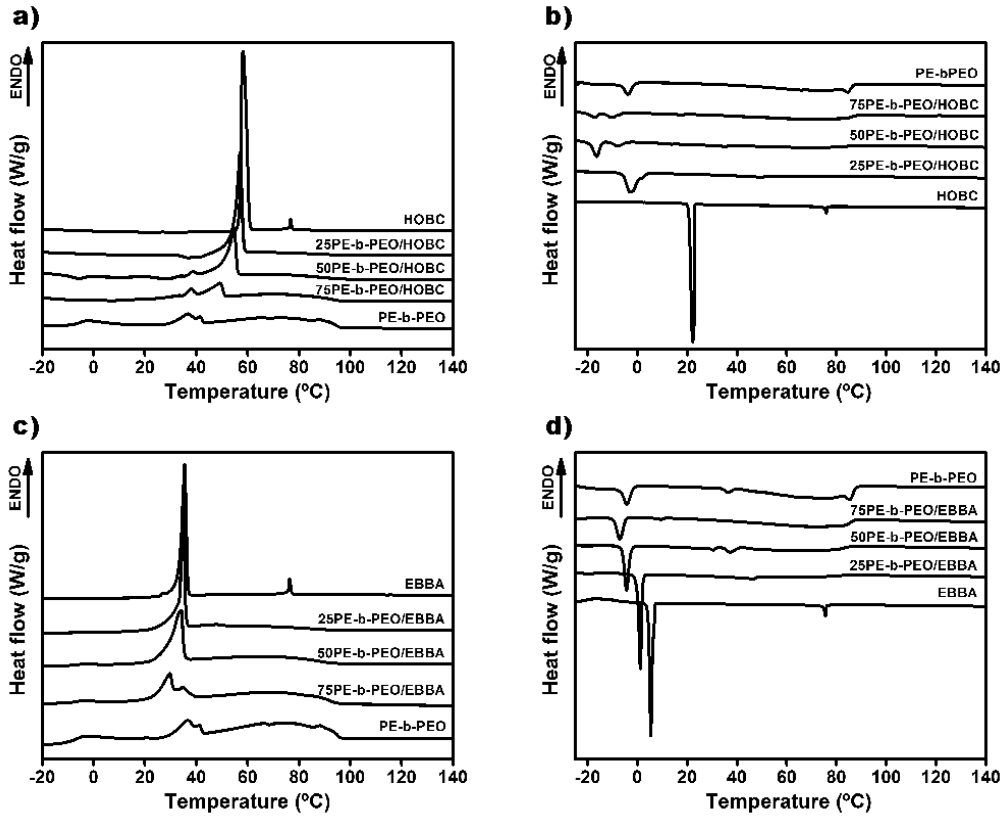

Figure 3.3. DSC thermograms of the PDLC blends based on the PE-b-PEO block copolymer and the HOBC (a, b) and EBBA (c, d) nematic liquid crystals during heating and cooling processes. For comparison the DSC thermograms of neat components were also plotted.

As clearly observed in Figure 3.3a, the addition of the PE-b-PEO block copolymer led to notable decrease of the T_m of the HOBC nematic liquid crystal in the PE-b-PEO/HOBC blends. The T_m of the HOBC liquid crystal phase decreased 1 ºC with the addition of 25 wt % of PE-b-PEO block copolymer and 9 ºC when 75 wt % of PE-b-PEO block copolymer was added to the PE-b-PEO/HOBC blend if compare to the T_m of neat HOBC nematic liquid crystal. This phenomenon can be related with the partial miscibility between the HOBC liquid crystal rich phase and one of the blocks of the PE-b-PEO block copolymer rich phase. Especially, taken into account that X_c decreased

with the increase of the PE-b-PEO block copolymer, being 94 % for the 25PE-b-PEO/HOBC blend, 84 % for the 50PE-b-PEO/HOBC blend and 52 % for the 75PE-b-PEO/HOBC blend as shown in Table 3.1.

Table 3.1. Degree of crystallization of the HOBC liquid crystal phase in the PE-b-PEO/HOBC blends.

% PE-b-PEO	0	25	50	75	100
% X_c HOBC	100	94	84	52	-

Both, the crystallization degree tendency to decrease and the diminution of the T_m of the HOBC liquid crystal phase with the increase of the PE-b-PEO block copolymer content indicated that the HOBC liquid crystal phase can crystalize within the PE-b-PEO block copolymer.

The T_m of the PEO block of the PE-b-PEO block copolymer in the PE-b-PEO/HOBC blends increased slightly with the increase of the HOBC nematic liquid crystal content, being 3 ºC higher for the 25PE-b-PEO/HOBC blend if compared with the T_m of the PE-b-PEO block copolymer.

The T_m of the PE block phase in the PE-b-PEO/HOBC blends was not clearly detected. However, the general tendency indicates that the onset corresponding to the PE block melting transition in the PE-b-PEO/HOBC blends remained in the same position as in the PE block phase in the PE-b-PEO block copolymer indicating lack of miscibility between the PE block and the HOBC liquid crystal phase in these polymer blends.

Similar tendencies were observed for the PE-b-PEO/EBBA blends (Figure 3.3c). The increase of the PE-b-PEO block copolymer content led to a decrease of the T_m of the EBBA liquid crystal phase in the PE-b-PEO/EBBA blends. Similar to the T_m corresponding to the HOBC liquid crystal phase in the PE-b-PEO/HOBC blends, the T_m of the EBBA liquid crystal phase decreased 1 and 6 ºC if compared to the T_m of neat EBBA liquid crystal when 25 and 75 wt % of PE-b-PEO block copolymer were added to the PE-b-PEO/EBBA blends.

The T_m of the PEO block of the PE-b-PEO block copolymer in the PE-b-PEO/EBBA blends, decreased slightly with the increase of the EBBA liquid crystal content, being 2 ºC lower for the 75PE-b-PEO/EBBA blend if compared with the T_m of the PEO block of the PE-b-PEO block copolymer, in contrast with the PE-b-PEO/HOBC blends.

Under the same DSC measurement conditions, the T_m of the PE block phase of the PE-b-PEO/EBBA blends was not clearly detected similar to the T_m of the PE block phase in the PE-b-PEO/HOBC blends. The onset of the melting transition of the PE block phase in the PE-b-PEO/EBBA blends decreased slightly with the increase of the PE-b-PEO block copolymer in these PDLC blends.

The thermal behavior of the PE-b-PEO/HOBC and PE-b-PEO/EBBA blends is in good agreement with the miscibility prediction between the PE-b-PEO block copolymer and the HOBC and EBBA nematic liquid crystals calculated using solubility parameters of each component of the investigated PDLC blends. According to the Hoftyzer, Van Krevelen and Jones methods [36,37], the miscibility between the components of the polymeric blends can be predicted by estimation of the solubility parameters. From these calculations, the values of the solubility parameters of each block of the PE-b-PEO block copolymer were 16.41 $(J\ cm^{-3})^{1/2}$ and 21.28 $(J\ cm^{-3})^{1/2}$ for the PE and PEO blocks, respectively. In the case of the HOBC nematic liquid crystal, the solubility parameter was 19.44 $(J\ cm^{-3})^{1/2}$ and for the EBBA nematic liquid crystal was 16.89 $(J\ cm^{-3})^{1/2}$. Based on this prediction and as also confirmed by the DSC results, the PE block of the PE-b-PEO block copolymer showed higher miscibility with the EBBA nematic liquid crystal and the PEO block of the PE-b-PEO block copolymer presented higher miscibility with the HOBC nematic liquid crystal as schematically represented in Scheme 3.1.

Scheme 3.1. Miscibility between the PE-b-PEO block copolymer and the HOBC and EBBA nematic liquid crystals.

Moreover, the miscibility predicted employing the solubility parameters was also supported by the DSC results obtained for the PDLC blends of the PEO homopolymer and the HOBC or EBBA nematic liquid crystals.

Figure 3.4 shows the DSC thermograms of the PDLC blends of the PEO homopolymer and the HOBC or EBBA nematic liquid crystals. As shown in Figure 3.4a, the addition of the PEO homopolymer to the PEO/HOBC blends led to an insignificant decrease of the T_m of the HOBC liquid crystal rich phase in the PEO/HOBC blends. The T_m of the HOBC liquid crystal rich phase decreased only 1 ºC for the 75PEO/HOBC blend if compared to the T_m of the HOBC nematic liquid crystal.

Simultaneously, under the same measurement conditions, the T_m of the PEO

homopolymer rich phase in the PEO/HOBC blends was not detected, neither for the 25PEO/HOBC nor for 75PEO/HOBC blends, indicating high miscibility between the PEO homopolymer and the HOBC liquid crystal. Thus, the addition of the PEO homopolymer into the HOBC liquid crystal hindered the crystallization process of the HOBC liquid crystal phase in the investigated PDLC blends. This fact is in good agreement with the miscibility prediction based on the solubility parameters of polymer blend components.

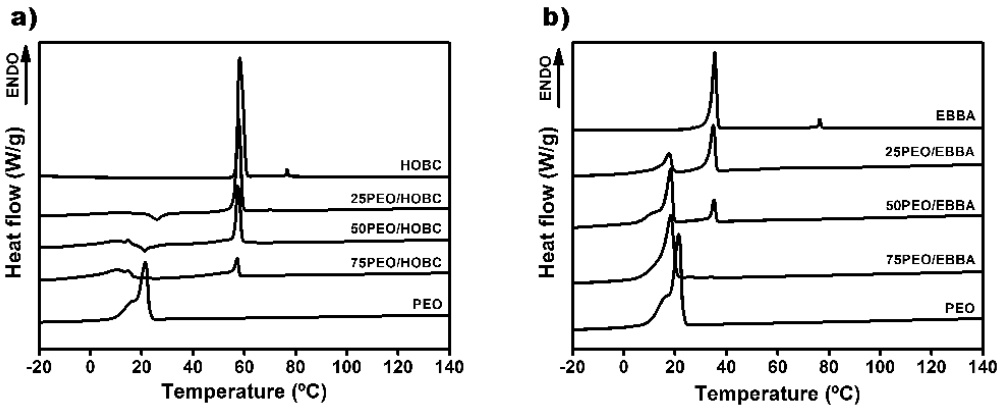

Figure 3.4. DSC thermograms of the a) PEO/HOBC and b) PEO/EBBA blends with different PE-b-PEO block copolymer content during heating process. For comparison, the DSC thermogram of neat PEO homopolymer was also plotted.

On the contrary, as can be observed in Figure 3.4b, the T_m of the PEO homopolymer rich phase in the PEO/EBBA blends was maintained almost in the same temperature with the increase of the EBBA liquid crystal content up to 75 wt % of EBBA liquid crystal suggesting low miscibility between the PEO homopolymer and the EBBA nematic liquid crystal.

However, the crystallization degree of the PEO homopolymer rich phases in the PEO/EBBA blends decreased from 51 % for the PEO homopolymer to 31 % for the 25PEO/EBBA blend (Table 3.2), which indicates some miscibility between components.

Table 3.2. Degree of crystallization of the PEO homopolymer phase in the PEO/EBBA blends.

% PEO	0	25	50	75	100
% X_c PEO	-	31	45	49	51

As it is shown in Figure 3.3b for the PDLC blends based on the HOBC nematic liquid crystal and in Figure 3.3d for the PDLC blends based on the EBBA nematic

liquid crystal, the addition of 25, 50 and 75 wt % of PE-b-PEO block copolymer to the PE-b-PEO/HOBC or PE-b-PEO/EBBA blends had a strong effect on the crystallization process of the HOBC or EBBA liquid crystal phases.

In the case of the PE-b-PEO/HOBC blends, increasing of the PE-b-PEO block copolymer content provoked the decrease of the T_c of the HOBC liquid crystal phase from 22 ºC for neat HOBC nematic liquid crystal to -3 and -17 ºC for the 25PE-b-PEO/HOBC and 75PE-b-PEO/HOBC blends, respectively. Simultaneously, the T_c of the PEO block phase in the PE-b-PEO/HOBC blends decreased with the increase of the HOBC liquid crystal content. Thus, the T_c of the PEO block of the PE-b-PEO block copolymer decreased from -4 ºC for the PE-b-PEO block copolymer to -16 ºC for the 25PE-b-PEO/HOBC blend. Neither for the PEO block phase in the PE-b-PEO/HOBC blends with the PE-b-PEO block copolymer content higher that 25 wt % nor for the PE block in all investigated PE-b-PEO/HOBC blends the T_c were detected.

The strong effect of the addition of the PE-b-PEO block copolymer on the crystallization of the HOBC liquid crystal phase in the PE-b-PEO/HOBC blends once more proved the high miscibility between the PEO block and the HOBC liquid crystal phase.

In the case of the PE-b-PEO/EBBA blends (Figure 3.3d), the addition of 25, 50 and 75 wt % of PE-b-PEO block copolymer had also a strong effect on the crystallization process of the EBBA liquid crystal phase. The increase of the PE-b-PEO block copolymer content provoked a decrease of the T_c related to the EBBA liquid crystal phase, from 5 ºC for neat EBBA nematic liquid crystal to 1 and -4 ºC for the 25PE-b-PEO/EBBA and 50PE-b-PEO/EBBA blends, respectively.

The shift of the T_c of the EBBA liquid crystal phase toward lower temperatures is smaller than for the T_c of the HOBC liquid crystal phase for the same polymer blends compositions. Thus, the addition of the PE-b-PEO block copolymer had stronger effect on crystallization process of the HOBC liquid crystal phase than on the EBBA liquid crystal phase, which once more confirmed that the HOBC liquid crystal phase exhibited higher miscibility with the PE-b-PEO block copolymer than the EBBA liquid crystal phase in the investigated PDLC blends.

Under the same measurement conditions, the T_c of the PEO block phase in the PE-b-PEO/EBBA blends decreased with the increasing of the EBBA liquid crystal content, being -4 ºC for the PE-b-PEO block copolymer and -7 ºC for the 75PE-b-PEO/EBBA blend. Similar to the tendency of the crystallization process of the HOBC

liquid crystals phase, the effect of the addition of the EBBA nematic liquid crystal on the crystallization process of the PEO block of the PE-b-PEO block copolymer proved higher miscibility with the HOBC nematic liquid crystal than with the EBBA nematic liquid crystal (Figure 3.3b and 3.3d).

3.3.4. Droplet-like morphology of the PDLC blends by OM

The morphology of the PE-b-PEO/HOBC and PE-b-PEO/EBBA blends with different PE-b-PEO block copolymer content is shown in Figure 3.5.

In order to avoid the thermal history effect and visualize the liquid crystal character of the investigated PDLC blends, all investigated materials were analyzed after quenching from 120 ºC to the room temperature. OM micrographs were taken before crystallization, which allowed to confirm the presence of the mesostable nematic state of the HOBC and EBBA nematic liquid crystals in the designed PDLC blends [20,28].

As clearly showed in Figure 3.5a, the HOBC nematic liquid crystal possessed typical Schlieren texture characteristic for the nematic liquid crystals.

The addition of 25 wt % of PE-b-PEO block copolymer into the PE-b-PEO/HOBC blends led to coalesced droplets of the HOBC liquid crystal phase clearly observed in Figure 3.5b, while the addition of 50 wt % of PE-b-PEO block copolymer resulted in droplet-like morphology with an average size of the nematic HOBC domains of around 2.5 ± 0.5 μm (Figure 3.5 c).

The incorporation of 75 wt % of PE-b-PEO block copolymer (Figure 3.5d) changed the morphological character of the fabricated blends. Consequently, no coalescence droplets of the HOBC liquid crystal phase were detected for this PDLC blend. In this case, only some small bright spherical crystals of the PE-b-PEO block copolymer appeared on the black amorphous phase similar to the morphology exhibited by neat PE-b-PEO block copolymer (compare Figure 3.5d and 3.5i).

The morphology of neat EBBA nematic liquid crystal was similar to the morphology of neat HOBC nematic liquid crystal (compare Figure 3.5a and 3.5e). The 25PE-b-PEO/EBBA and 50PE-b-PEO/EBBA blends showed droplet-like morphology with the uniform size of the nematic EBBA domains. The average size of these mesostable nematic EBBA liquid crystal phase increase with the increase of the PE-b-PEO block copolymer content being 1.5 ± 0.5 μm (Figure 3.5f) and 3 ± 0.5 μm (Figure 3.5g) for the PE-b-PEO/EBBA blends modified with 25 and 50 wt % of PE-b-PEO

block copolymer content, respectively. The addition of 75 wt % of PE-b-PEO block copolymer into the PE-b-PEO/EBBA blends allowed envisaging that and for this ratio between components designed materials did not show any liquid crystals droplets (Figure 3.5h).

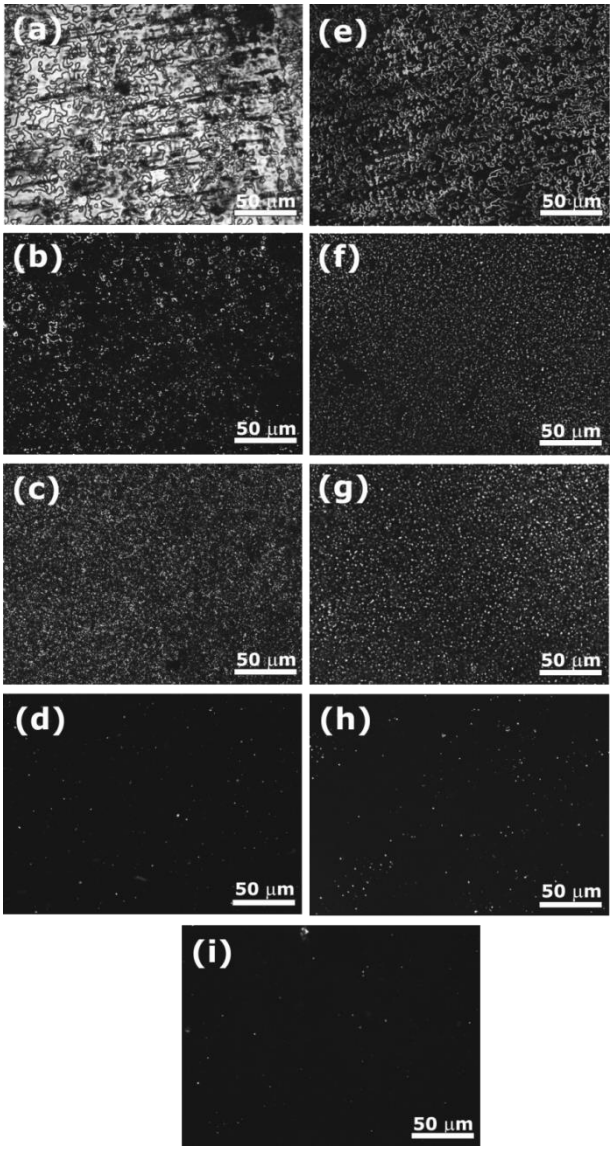

Figure 3.5. OM micrographs of the a) HOBC nematic liquid crystal and its PDLC blends containing b) 25 wt %, c) 50 wt %, d) 75 wt % of PE-b-PEO block copolymer, and e) EBBA nematic liquid crystal and its PDLC blends containing f) 25 wt %, g) 50 wt %, h) 75 wt % of PE-b-PEO block copolymer. For comparison optical micrograph of the i) PE-b-PEO block copolymer was also presented. All OM micrographs were taken between crossed polarizers.

Thus, under thermal treatment conditions, the addition of more than 50 wt % of PE-b-PEO block copolymer prevents the formation of the mesostable nematic state of the EBBA phase domains. On the contrary, small spherical crystals of the PE-b-PEO block copolymer were easily detected confirming that the 75PE-b-PEO/EBBA blends

had the morphology similar to the morphology of neat PE-b-PEO block copolymer (compare Figure 3.5h and 3.5i).

Well-dispersed, uniform in size nematic droplets of the HOBC or EBBA liquid crystal phase in PDLC blends containing up to 50 wt % of PE-b-PEO block copolymer made these PDLC blends potential candidate to be used in electro-optical devices.

3.4. Conclusions

In the investigation work related to this Chapter, PE-b-PEO block copolymer dispersed liquid crystals were fabricated using two different low molecular weight nematic liquid crystals.

The miscibility between the PE-b-PEO block copolymer and the HOBC and EBBA nematic liquid crystals was confirmed by decrease of the T_m of the HOBC and EBBA liquid crystals phases with the increase of the PE-b-PEO block copolymer content as well as the decrease of the crystallization degree of liquid crystal phase in the PDLC blends.

These results are in good agreement with the theoretical prediction based on the solubility parameters calculated for each block of the PE-b-PEO block copolymer and the HOBC and EBBA nematic liquid crystals.

DSC results confirmed that the PEO block of the PE-b-PEO block copolymer showed higher miscibility with the HOBC nematic liquid crystal than with the EBBA nematic liquid crystal as also confirmed by miscibility studied of the PEO/HOBC and PEO/EBBA blends.

As expected, the addition of the PE-b-PEO block copolymer resulted in increase of the thermal stability of the PE-b-PEO/HOBC and PE-b-PEO/HOBC blends corroborated with the partial miscibility between the PDLC blends components.

Thermal treatment performed to visualize liquid crystal character of the PE-b-PEO/HOBC and PE-b-PEO/EBBA blends indicated that the PDLC blends containing 25 and 50 wt % of PE-b-PEO block copolymer exhibited droplets-like morphology with uniform and narrow size distribution of the nematic HOBC or EBBA domains.

3.5. References

[1] Gao C, Zhang S, Li X, Zhu S, Jiang Z. Synthesis of poly(ether ether ketone)-block polyimide copolymer and its compatibilization for poly(etheretherketone)/thermoplastic polyimide blends. Polymer 2014;55:119-125.

[2] Panapitiya NP, Wijenayake SN, Huang Y, Bushdiecker D, Nguyen D, Ratanawanate C, Kalaw GJ, Gilpin CJ, Musselman IH, Balkus Jr KJ, Ferraris JP. Stabilization of immiscible polymer blends using structure directing metal organic frameworks (MOFs). Polymer 2014;55:2028-2034.

[3] Aroguz AZ, Engin HH, Baysal BM. The assessment of miscibility and morphology of poly(ε-caprolactone) and poly(para-chlorostyrene) blends. Eur. Polym. J. 2007;43:403-409.

[4] Masegosa RM, Nava D, Prolonga MG, Salom C. Linear unsaturated polyester + poly(ε-caprolactone) blends: Calorimetric behavior and morphology. Thermochim. Acta 2006;440:93-101.

[5] Rastin H, Jafari SH, Saeb MR, Khonakdar HA, Wagenknecht U, Heinrich G. On the reliability of existing theoretical models in anticipating type of morphology and domain size in HDPE/PA-6/EVOH ternary blends. Eur. Polym. J. 2014;53:1-12.

[6] Khalf AI, Nashar DEE, Maziad NA. Effect of grafting cellulose acetate and methylmethacrylate as compatibilizer onto NBR/SBR blends. Mater. Design. 2010;31:2592-2598.

[7] Mourad AHI. Thermo-mechanical characteristics of thermally aged polyethylene/polypropylene blends. Mater. Design. 2010;31:918-929.

[8] Aouachria K, Belhaneche-Bensemra N. Thermo-oxidative dehydrochlorination of rigid and plasticised poly(vinyl chloride)/poly(methyl methacrylate) blends. Polym. Degrad. Stabil. 2006;91:504-511.

[9] Ravati S, Favis BD. Interfacial coarsening of ternary polymer blends with partial and complete wetting structures. Polymer 2013;54:6739-6751.

[10] Bai Z, Guo H. Interfacial properties and phase transitions in ternary symmetric homopolymer-copolymer blends: A dissipative particle dynamics study. Polymer 2013;54:2146-2157.

[11] Nesterov AE, Lipatov YS, Ignatova TD. Effect of an interface with solid on the component distribution in separated phases of binary polymer mixtures. Eur. Polym. J. 2001;37:281-285.

[12] Lipatov YS, Nesterov AE, Ignatova TD, Nesterov DA. Effect of polymer-filler surface interactions on the phase separation in polymer blends. Polymer 2002;43:875-880.

[13] Bose S, Pramanik N, Das CK, Ranjan A, Saxena AK. Synthesis and effect of polyphosphazenes on the thermal, mechanical and morphological properties of poly(etherimide)/thermotropic liquid crystalline polymer blend. Mater. Design. 2010;31:1148-1155.

[14] Fekete E, Földes E, Pukánszky B. Effect of molecular interactions on the miscibility and structure of polymer blends. Eur. Polym. J. 2005;41:727-736.

[15] Kihara H, Kishi R, Miura T, Kato T, Ichijo H. Phase behavior of liquid-crystalline copolymer/liquid crystal blends. Polymer 2001;42:1177-1182.

[16] Bose S, Cardinaels R, Özdilek C, Leys J, Seo JW, Wübbenhorst M, Moldenaers P. Effect of multiwall carbon nanotubes on the phase separation of concentrated blends of poly[(α-methyl styrene)-co-acrylonitrile] and poly(methyl methacrylate) as studied by melt rheology and conductivity spectroscopy. Eur. Polym. J. 2014;53:253-269.

[17] Müller AJ, Arnal ML, Trujillo M, Lorenzo AT. Super-nucleation in nanocomposites and confinement effects on the crystallizable components within block copolymers, miktoarm star copolymers and nanocomposites. Eur. Polym. J. 2011;47:614-629.

[18] Sinturel C, Vayer M, Erre R, Amenitsch H. Thermal induced mobility of self-assembled platelets of polyethylene-block-poly(ethylene oxide) in liquid precursors of unsaturated polyester thermoset. Eur. Polym. J. 2009;45:2505-2512.

[19] Mucha M. Polymer as an important component of blends and composites with liquid crystals. Prog. Polym. Sci. 2003;28:837-873.

[20] Tercjak A, Serrano E, Larrañaga M, Mondragon I. Polymer dispersed liquid crystals based on poly(styrene-b-ethylene oxide), poly(bisphenol a carbonate) or poly(methylphenylsiloxane), and 4´-(hexyloxy)-4-biphenyl-carbonitrile: Analysis of phase diagrams and morphologies generated. J. Appl. Polym. Sci. 2008;108:1116-1125.

[21] Papalia JM, Marencic AP, Adamson DH, Chaikin PM, Register RA. Thin films of block copolymer-homopolymer blends with a continuously tuneable density of spherical microdomains. Macromolecules 2010;43:6946-6949.

[22] Salim NV, Hanley T, Guo Q. Microphase separation through competitive hydrogen bonding in double crystalline diblock copolymer/homopolymer blends. Macromolecules 2010;43:7695-7704.

[23] Nagpal U, Kang H, Craig GSW, Nealey PF, de Pablo JJ. Pattern dimensions and feature shapes of ternary blends of block copolymer and low molecular weight homopolymers directed to assemble on chemically nanopatterned surfaces. ACS Nano 2011;5:5673-5682.

[24] Ryu JH, Lee SG, Nam JB, Suh KD. Influence of SMA content on the electro-optical properties of polymer-dispersed liquid crystal prepared by monodisperse poly(MMA-co-SMA)/LC microcapsules. Eur. Polym. J. 2007;4:2127-2134.

[25] He J, Yan B, Yu B, Wang S, Zeng Y, Wang Y. The effect of molecular weight of polymer matrix on properties of polymer-dispersed liquid crystals. Eur. Polym. J. 2007;43:2745-2749.

[26] Yagi R, Katae H, Kuwahara Y, Kim SN, Ogata T, Kurihara S. On-off switching properties of one-dimensional photonic crystals consisting of azo-functionalized polymer liquid crystals having different methylene spacers and polyvinyl alcohol. Polymer 2014;55:1120-1127.

[27] Khaligh HH, Liew K, Han Y, Abukhdeir NM, Goldthorpe IA. Silver nanowire transparent electrodes for liquid crystal-based smart windows. Sol. Energ. Mat. Sol. C 2015;132:337-341.

[28] Hoppe CE, Galante MJ, Oyanguren PA, Williams RJJ. Polymer-dispersed liquid crystals based on polystyrene and EBBA: Analysis of phase diagrams and morphologies generated. Macromol. Chem. Phys. 2003;204:928-935.

[29] Ahmad F, Jamil M, Lee JW, Ri YH, Jeon YJ. Characteristics of di- and tri-block copolymers: Polymer disperse liquid crystal display. J. Mod. Optic. 2014;61:1027-1032.

[30] Tercjak A, Serrano E, Garcia I, Ocando C, Mondragon I. Self-assembled block copolymers as matrix for multifunctional materials modified with low-molecular-weight liquid crystals. Acta Mater. 2007;55:6436-6443.

[31] Tercjak A, Gutierrez J, Mondragon I. Conductive properties of photoluminescent Au/Ps-b-PEO inorganic/organic hybrids containing nematic liquid crystals. J. Phys. Chem. 2011;115:1643-1648.

[32] Valenti B, Turturro A, Losiob S, Falqui L, Costa G, Cavazza B, Castellano M. Styrene-diene block copolymers as embedding matrices for polymer-dispersed liquid crystal films. Polymer 2001;42:2427-2438.

[33] Rodrigues JRS, Kaito A, Soldi V, Pires ATN. Behaviour of the miscibility of poly(ethylene oxide)/liquid crystal blends. Polym. Int. 1998;46:138-142.

[34] Filip D, Simionescu CI, Macocinschi D. Thermal behaviour of liquid crystal-

polymer blends. Polym. Degrad. Stabil. 2001;72:377-380.

[35] Filip D, Simionescu CI, Macocinschi D. Thermogravimetric analysis of liquid crystal-polymer blends. Thermochim. Acta 2003;395:217-223.

[36] Tantishaiyakul V, Worakul N, Wongpoowarak W. Prediction of solubility parameters using partial least square regression. Int. J. Pharm. 2006;325:8-14.

[37] Van Krevelen DW, Nijenhuis TK. Properties of polymers. Their correlation with chemical structure: Their numerical estimation and prediction from additive group contributions. Fourth Ed., Elsevier. Oxford (UK), 2009.

Thermo-optical responsive PE-b-PEO block copolymer dispersed liquid crystal blends

4

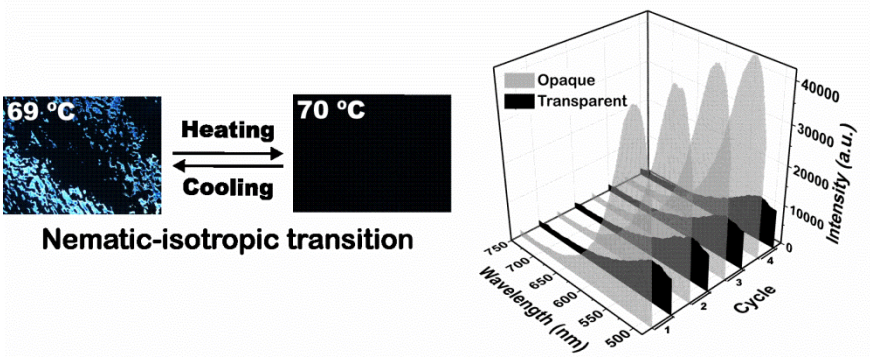

4. Thermo-optical responsive PE-b-PEO block copolymer dispersed liquid crystal blends

The Chapter 4 will deal with thermo-optical responsive behavior of the PDLC blends based on the PE-b-PEO block copolymer and the HOBC and EBBA nematic liquid crystals investigated before in the Chapter 3 however with higher NLCs content. The nematic-isotropic transition will be discussed based on DSC results. The reversible switching process of the prepared PDLC blends will be study by PL and UV-vis spectroscopies. Moreover, the influence of the addition of the PE-b-PEO block copolymer on the thermo-optical responsive of the PDLC blends will be also discussed.

4.1. Introduction

The capability of the NLCs to switch from a highly scattering state (OFF-state) to a transparent state (ON-state) is an attractive property from the point of view of their potential application in electronic devices and sensors [1-20]. The possibility of controlling this reversible optical property in materials based on NLCs make them a fascinating research field and this enables to combine their properties to broaden their potential range of applications [6,21,22].

As it is well known, one of the drawbacks of the low molecular weight NLCs is their temperature dependent crystallization process. In order to overcome this handicap, block copolymers can be used to hinder the crystallization process of liquid crystal phase in the PDLC blends and consequently achieved good dispersion of the nematic liquid crystals, which have strong influence on their optical properties [21-28].

The main objective of this Chapter was the study of thermo-optical reversible behavior of the PDLC blends based on the PE-b-PEO block copolymer and the HOBC and EBBA nematic liquid crystals as a function of temperature.

Different techniques were used to study even HOBC and EBBA nematic liquid crystals maintain their optical properties in the PDLC blends. DSC technique was used to detect the presence of the nematic-isotropic transition in PDLC blends. Moreover, in this Chapter photoluminescence and UV-visible spectroscopies were employed to investigate the thermo-optical reversible behavior of the PDLC blends as a function of the temperature.

4.2. Materials and characterization techniques

4.2.1. Materials

The PE-b-PEO block copolymer and the HOBC and EBBA nematic liquid crystals employed in this Chapter were the same as in the Chapter 3. The only difference was the formulation of the PDLC blends since in this Chapter the high content HOBC and EBBA nematic liquid crystals PDLC blends were prepared and investigated.

4.2.2. Sample preparation

The PE-b-PEO block copolymer dispersed liquid crystal blends were prepared by melting different quantity of PE-b-PEO block copolymer (1, 5 and 10 wt %) with HOBC and EBBA nematic liquid crystals. These PDLC blends were denominated 1PE-b-PEO/LC, 5PE-b-PEO/LC and 10PE-b-PEO/LC, respectively, being LC equal to HOBC or EBBA nematic liquid crystals.

The PDLC blends were fabricated by heating in an oven at 100 °C during 1 h and stirred manually to encourage their mixing, as in the Chapter 3.

The thermo-optical reversible behavior of neat NLCs and the investigated PDLC blends was studied in bulk conditions. The required quantity of the investigated materials was placed between two microscope glass slides and separate using an aluminum frame to control the thickness of the prepared samples (1 mm).

4.2.3. Characterization techniques

4.2.3.1. Differential scanning calorimetry

DSC measurements were performed using a Mettler Toledo DSC 822e differential scanning calorimeter under a nitrogen flow of 25 mL min^{-1}. The calibration was done as described in the Chapter 3. The investigated blends were encapsulated in aluminum pans with the weight around 6 mg. In order to avoid the thermal history, all investigated materials were first heated from -25 to 90 °C at 5 °C min^{-1}, then were cooled from 90 to -25 ºC at 5 °C min^{-1} and finally, the melting was performed heating the samples up to 90 °C at 5 °C min^{-1}. Only the last heating scan was taken into consideration. The melting temperature (T_m), the crystallization temperature (T_c) and the nematic-isotropic temperature (T_{N-I}) were determined in the same way as in the Chapter 3.

4.2.3.2. Photoluminescence spectroscopy

PL properties of neat HOBC and EBBA nematic liquid crystals and the investigated PDLC blends were determined using a Felix32 spectrofluorometer of Photon Technology International (PTI) equipped with a temperature controller. The excitation wavelengths at room temperature were 333 and 467 nm for the HOBC and EBBA nematic liquid crystals, respectively. Photoluminescence emissions spectra of neat HOBC and EBBA nematic liquid crystals and their PDLC blends were recorded during heating/cooling cycles from 10 to 80 °C at a rate of 5 °C min^{-1}. Measurements were repeated four times to study of the photoluminescence switchable ability of the investigated PDLC blends.

4.2.3.3. UV-visible spectroscopy

The UV-vis transmission spectra of the investigated PDLC blends as a function of the temperature were performed using a UV-3600, Shimadzu UV-VIS-NIR spectrophotometer equipped with a thermoelectric single cell holder to control the temperature. Measurements were collected at 10 and 80 ºC in the wavelength range between 200 and 800 nm.

4.2.3.4. Optical microscopy

OM micrographs were taken using a Nikon Eclipse E600W microscope equipped with a hot stage (Mettler FP 82 HT) using crossed polarizers. Required quantity of neat HOBC and EBBA nematic liquid crystals and their PDLC blends placed between two clean microscope glass slides was heated/cooled from 30 to 90 ºC at a rate of 5 ºC min. OM micrographs were collected during heating and cooling processes using the software analySIS docu FIVE.

4.3. Results and discussion

4.3.1. Thermal behaviour of the PDLC blends by DSC

DSC thermograms of the heating and cooling processes of the HOBC nematic liquid crystal and their PDLC blends with the PE-b-PEO block copolymer are shown in Figure 4.1. As can be seen in Figure 4.1a, the T_m of the HOBC nematic liquid crystal was at 58 °C and its T_c at 22 °C as reported in the Chapter 3. The T_{N-I} of the HOBC

nematic liquid crystal was identified at 77 ºC during heating process and almost at the same temperature during cooling process confirming the reversible switching behavior of the HOBC liquid crystal.

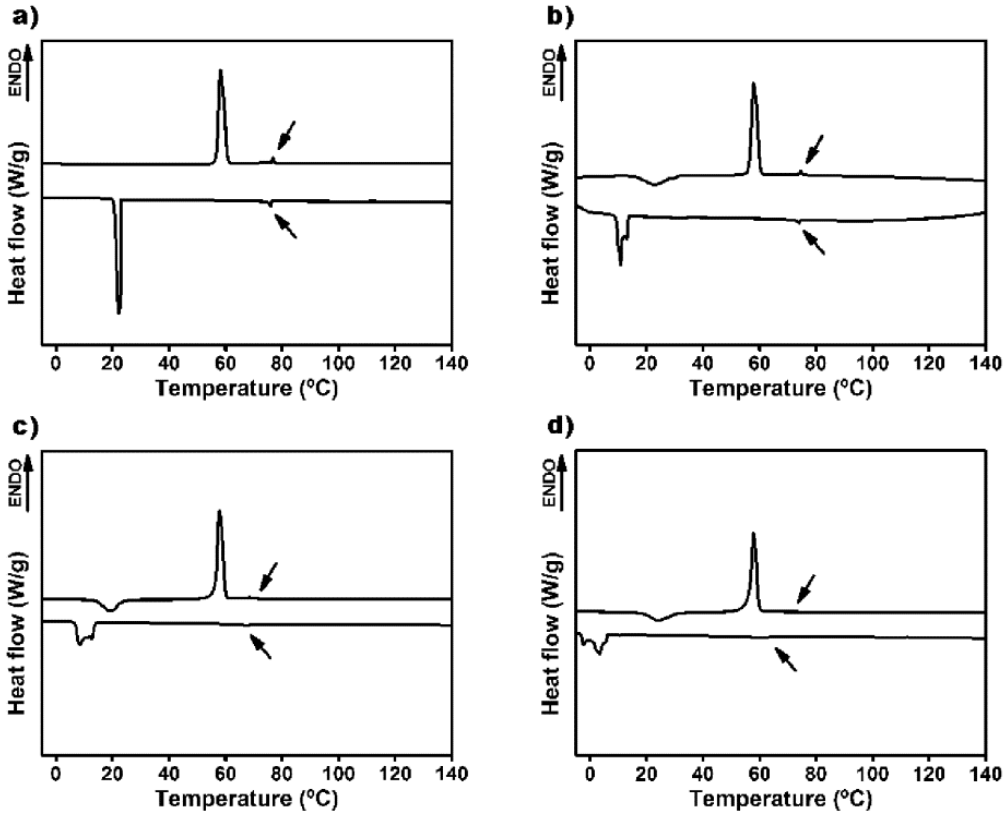

Figure 4.1. DSC thermograms of the a) HOBC nematic liquid crystal and b) 1PE-b-PEO/HOBC, c) 5PE-b-PEO/HOBC and d) 10PE-b-PEO/HOBC blends during heating/cooling processes.

The T_m of the HOBC liquid crystal phase in the PE-b-PEO/HOBC blends was maintained at 58 °C with the addition of 1 and 5 wt % of PE-b-PEO block copolymer. However, the addition of 10 wt % of PE-b-PEO block copolymer provoked a slight decreased of the T_m indicating a partial miscibility between the HOBC nematic liquid crystal and the PEO block of the PE-b-PEO block copolymer. The partial miscibility between components of the PDLC blends was proved for the higher PE-b-PEO block copolymer content in the Chapter 3.

An increase of the PE-b-PEO block copolymer content provoked a decrease of the T_c of the HOBC liquid crystal phase, shifting the crystallization temperature 3, 8 and 11 °C to lower values for 1, 5 and 10 wt % of PE-b-PEO block copolymer, respectively, if compare to the T_c of neat HOBC nematic liquid crystal as shown in Figure 4.1. Thus, the addition of the PE-b-PEO block copolymer hinders the crystallization process of the HOBC liquid crystal phase, once more confirming the partial miscibility between

components in the PE-b-PEO/HOBC blends. Concerning the PE-b-PEO block copolymer phase, neither their melting nor crystallization transitions were detected in the investigated PE-b-PEO/HOBC blends. This phenomenon is probably related to both the partial miscibility between the PE-b-PEO block copolymer and the HOBC nematic liquid crystal, and the low PE-b-PEO block copolymer content in the investigated PDLC blends.

The T_{N-I} of the HOBC liquid crystal phase in the PE-b-PEO/HOBC blends were decreased 2, 8 and 12 °C with the addition of 1, 5 and 10 wt % of PE-b-PEO block copolymer, respectively, if compare with the T_{N-I} of the HOBC nematic liquid crystal (Figure 4.1a-d). Additionally, for all investigated PDLC blends, the nematic-isotropic transition of the HOBC liquid crystal phase occurred almost at the same temperature, regardless of the process, heating or cooling. This behavior indicates that the HOBC nematic liquid crystal maintain its ability to switch from opaque to transparent state in the PE-b-PEO/HOBC blends. Scheme 4.1 shows the orientation changes of the liquid crystal molecules as a function of the temperature.

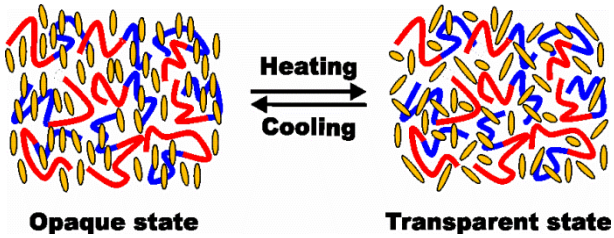

Scheme 4.1. Schematic illustration of the orientation changes of the nematic liquid crystal phase in the PDLC blends during switching from opaque to transparent state.

Similar thermal behavior, as described above for the PE-b-PEO/HOBC blends, was also achieved for the EBBA nematic liquid crystal and their PDLC blends with PE-b-PEO block copolymer as shown in Figure 4.2. As was reported in the Chapter 3, the T_m of the EBBA nematic liquid crystal was 36 °C and its T_c was 5 °C. As expected, the T_{N-I} of the EBBA nematic liquid crystal was clearly detected during both the heating and cooling processes, at 76 ºC, indicating the reversible capability of this nematic liquid crystal.

The addition of 1 wt % of PE-b-PEO block copolymer to the PDLC blend did not provoke changes in the T_m of the EBBA liquid crystal phase. Nevertheless, the addition of 5 and 10 wt % of PE-b-PEO block copolymer resulted in a slight decrease of the T_m of the EBBA liquid crystal phase. This thermal behavior of the PE-b-PEO/EBBA blends can be related to the partial miscibility between the PE block of the PE-b-PEO

block copolymer and the EBBA nematic liquid crystal as was mentioned also in the Chapter 3. The crystallization transition of the EBBA liquid crystal phase shifted to lower temperature with the increase of the PE-b-PEO block copolymer content as an effect of the partial miscibility between the PDLC components. Thus, as showed in Figure 4.2, the T_c of the EBBA liquid crystal phase decreased 1, 3 and 4 ºC with the addition of 1, 5 and 10 wt % of PE-b-PEO block copolymer, respectively, if compare to the T_c of the EBBA nematic liquid crystal.

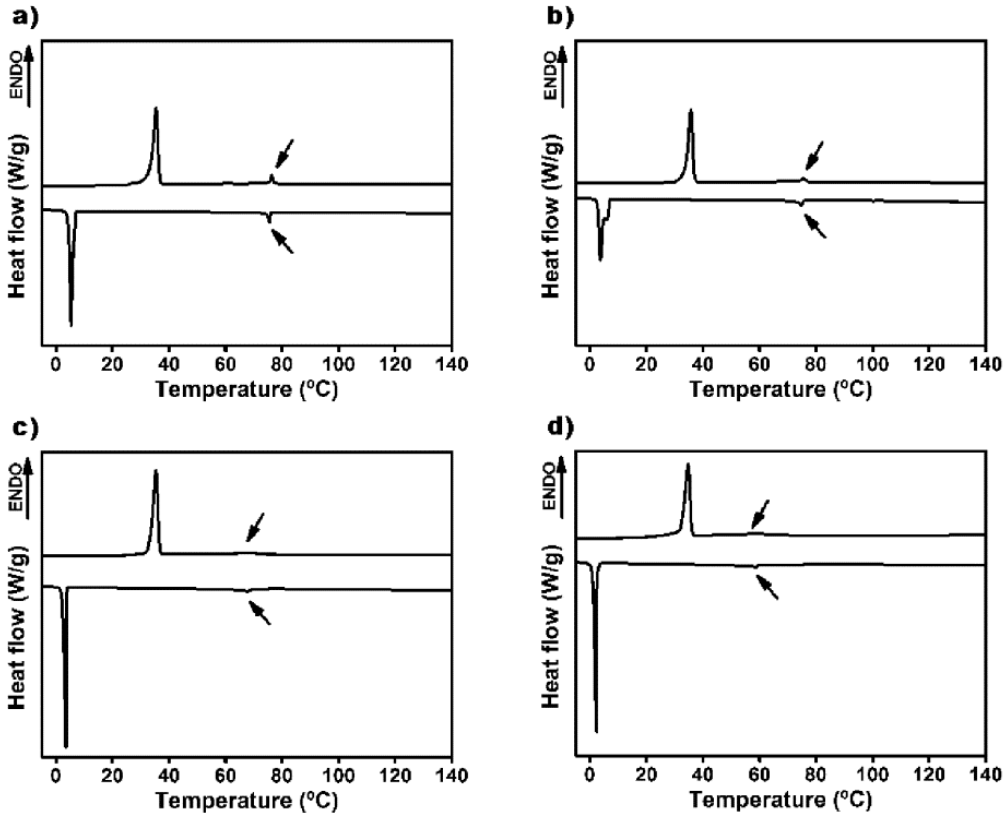

Figure 4.2. DSC thermograms of the a) EBBA nematic liquid crystal and b) 1PE-b-PEO/EBBA, c) 5PE-b-PEO/EBBA and d) 10PE-b-PEO/EBBA blends during the heating/cooling processes.

Moreover, it should be mentioned that due to the partial miscibility between the PDLC components or the low PE-b-PEO block copolymer content in the investigated PDLC blends, their melting and crystallization transition temperatures were not detected.

The nematic-isotropic transition of the EBBA liquid crystal phase was maintained in the PE-b-PEO/EBBA blends. The T_{N-I} of the EBBA liquid crystal phase moved to lower temperatures with the increase of the PE-b-PEO block copolymer content being 75, 68 and 57 ºC for the 1PE-b-PEO/EBBA, 5PE-b-PEO/EBBA and 10PE-b-PEO/EBBA blends, respectively.

For each investigated PDLC blend, the T_{N-I} of the EBBA liquid crystal phase appeared almost at the same temperature, regardless of the heating or cooling process, which affirmed that the EBBA nematic liquid crystal maintained their properties in these PDLC blends.

4.3.2. Structure of the PDLC blends by OM

OM images of the PE-b-PEO/HOBC blends at room temperature (30 ºC) and at the nematic-isotropic transition temperature are shown in Figure 4.3. As expected, in solid state (30 ºC) spherulites of neat HOBC nematic liquid crystal were observed. Moreover, a decrease of the size of the spherulites of the HOBC liquid crystal phase in the PE-b-PEO/HOBC blends with an increase of the PE-b-PEO block copolymer if compare to the size of the spherulites of neat HOBC liquid crystal were also visualized. This behavior was related to the partial miscibility between the HOBC liquid crystal phase and the PEO block of the PE-b-PEO block copolymer which can hinder the crystallization process in the PDLC blends with the increase of the PE-b-PEO block copolymer content.

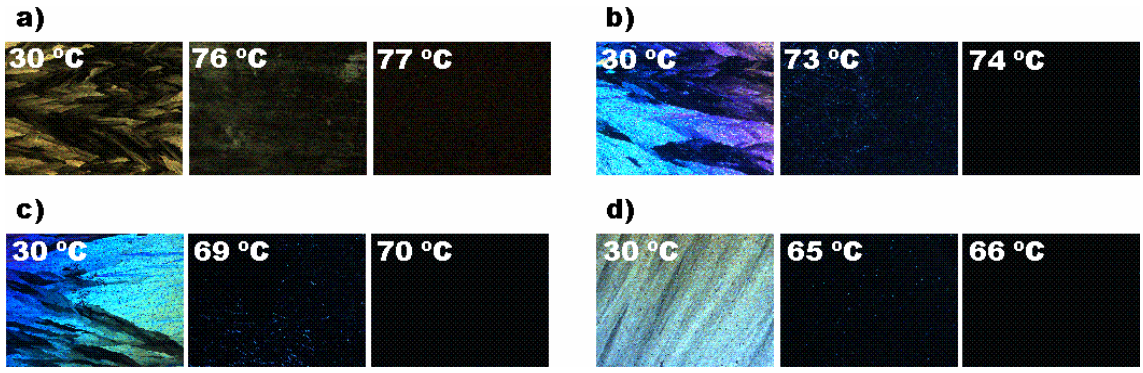

Figure 4.3. OM micrographs taken with crossed polarizers at solid, liquid crystal and liquid state of the a) HOBC nematic liquid crystal and b) 1PE-b-PEO/HOBC c) 5PE-b-PEO/HOBC and d) 10PE-b-PEO/HOBC blends.

As observed by OM, the nematic-isotropic transition took place almost at the same temperature as temperature measured by DSC. Previous to switch from opaque to transparent state (at liquid crystal state) all investigated PE-b-PEO/HOBC blends showed drop-like texture typical for the nematic liquid crystal phase in the PDLC blends [17, 28].

OM images of the PE-b-PEO/EBBA blends at room temperature and at the nematic-isotropic transition temperature are presented in Figure 4.4.

Similarly, to neat HOBC nematic liquid crystal and their blends, at solid state,

the EBBA nematic liquid crystal formed spherulites, which became smaller in the PE-b-PEO/EBBA blends with the addition of the PE-b-PEO block copolymer. Moreover, the addition of 10 wt % of PE-b-PEO led to drop-like texture characteristic for the PDLC blends. This behavior suggested stronger partial miscibility between the EBBA nematic liquid crystal and the PE block of the PE-b-PEO block copolymer than between the HOBC nematic liquid crystal and the PEO block of the PE-b-PEO block.

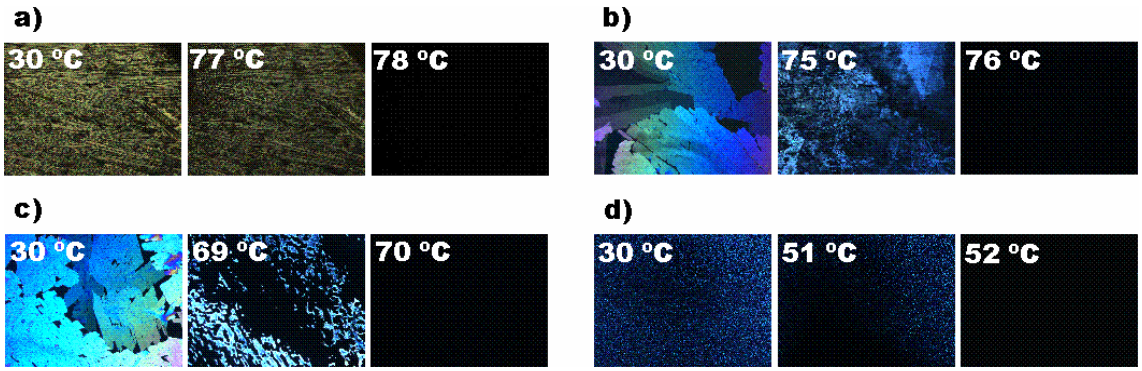

Figure 4.4. OM micrographs taken with crossed polarizers at solid, liquid crystal and liquid state of the a) EBBA nematic liquid crystal and b) 1PE-b-PEO/EBBA c) 5PE-b-PEO/EBBA and d) 10PE-b-PEO/EBBA blends.

As in the case of neat HOBC nematic liquid crystals and its PDLC blends, the changes in the texture as a function of the temperature indicated that the nematic-isotropic transition took place almost at the same temperature as was reported also based on DSC measurement.

The addition of 1 wt % of PE-b-PEO block copolymer did not change the nematic texture if compare with the texture of the EBBA nematic liquid crystal in liquid crystal state. On the contrary, the addition of 5 and 10 wt % of PE-b-PEO block copolymer led to drop-like texture characteristic for the nematic liquid crystals [17,28].

4.3.3. Optical reversible behavior of the HOBC and EBBA liquid crystals

Optical properties of the HOBC and EBBA nematic liquid crystals were studied using PL and UV-vis spectroscopy recording their photoluminescence emission spectra and transmittance spectra as a function of the temperature. The maximums of photoluminescence emission peaks of investigated liquid crystals at 10 and 80 ºC are summarized in Table 4.1 and the photoluminescence emission spectra of the HOBC and EBBA nematic liquid crystals taken at 10 and 80 ºC are shown in Figures 4.5aI and 4.5bI.

The HOBC nematic liquid crystal possessed a well-defined, narrow emission peak 352 nm and high PL intensity at 10 ºC. At 80 ºC, temperature higher than the T_{N-I} of the

HOBC nematic liquid crystal (Figure 4.1), the emission peak of the HOBC nematic liquid crystal shifted slightly to higher wavelength, 358 nm, and simultaneously the PL intensity of this peak was half times lower if compare with the PL intensity at 10 ºC.

Table 4.1. The maximums of photoluminescence emission peaks of the investigated materials at 10 and 80 ºC.

Sample	Wavelength at 10 ºC (nm)	Wavelength at 80 ºC (nm)
HOBC	352	358
1PE-b-PEO/HOBC	352	354
5PE-b-PEO/HOBC	352	356
10PE-b-PEO/HOBC	356	373
EBBA	512	498
1PE-b-PEO/EBBA	512	524
5PE-b-PEO/ EBBA	510	510
10PE-b-PEO/ EBBA	504	504

The PL intensity of the HOBC nematic liquid crystal emission spectra reversibly changed when the temperature changed from 10 to 80 ºC. Figure 4.5aII clearly shows this reversible behavior during four consecutive heating/cooling cycles.

This reversible switching of the HOBC nematic liquid crystal emission spectra could be strongly related to reversible capability of the HOBC nematic liquid crystal [17,21,24], which is able to switch from highly scattering state (opaque) at 10 ºC to transparent state at 80 ºC provoked by applied temperature gradient. This fact is due to the different internal scattering of the excitation light at different temperature when passing through the PE-b-PEO/EBBA blends. At 10 ºC (OFF-state), the excited photons are scattered from the surface of the opaque PE-b-PEO/EBBA blends (1 mm thick film) and the probability that some exited photons pass throughout the PDLC blends is very low. On the contrary, at 80 ºC (ON-state) most excited photons pass through the transparent 1 mm thick PE-b-PEO/EBBA blends [9, 13].

In the case of the EBBA nematic liquid crystal the emission peak at 10 ºC was at higher wavelength, 512 nm, if compare with the emission peak of the HOBC liquid crystal. Moreover, the PL intensity of neat EBBA nematic liquid crystal was more than thirty times lower if compare to the PL intensity of the HOBC nematic liquid crystal at the same temperature (10 ºC). This phenomenon could be linked to the chemical structure of the EBBA nematic liquid crystal, which has an aniline group as quencher. Quenchers are molecules that decrease the PL intensity without changing the emission spectrum. These molecules are able to capture the excessive energy of the excited state and dissipate it completely as heat, decreasing the emitted PL intensity [29,30].

The emission peak of neat EBBA nematic liquid crystal at 80 ºC moved slightly to lower wavelength (512 and 498 nm at 10 and 80 ºC, respectively) and the PL intensity dropped four times if compare to the PL intensity at 10 ºC. As showed in Figure 4.5bII, the PL intensity of the EBBA liquid crystal emission spectra at 10 and 80 ºC reversibly changed from high to low intensity in several cycles switching from one temperature to other indicating that this process was reversible as well as in the case of HOBC nematic liquid crystal.

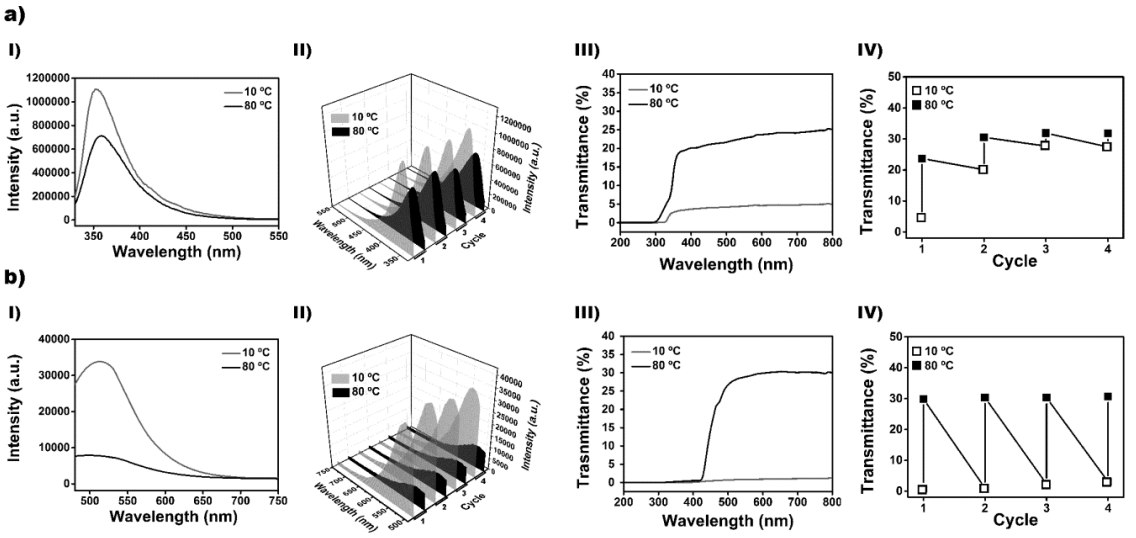

Figure 4.5. Photoluminescence emission spectra at 10 and 80 ºC of the HOBC nematic liquid crystal of aI) heating/cooling cycle, and aII) four heating/cooling cycles. UV-visible transmission spectra at 10 and 80 ºC of the HOBC nematic liquid crystal of aIII) heating/cooling cycle, and aIV) four heating/cooling cycles. Photoluminescence emission spectra at 10 and 80 ºC of the EBBA nematic liquid crystal of bI) heating/cooling cycle, and bII) four heating/cooling cycles. UV-visible transmission spectra at 10 and 80 ºC of the EBBA nematic liquid crystal of bIII) heating/cooling cycle, and bIV) four heating/cooling cycles.

Reversible changes in optical transparency of the HOBC and EBBA nematic liquid crystals as a function of temperature were also investigated by means of UV-vis transmission spectroscopy. As shown in Figures 4.5aIII and 4.5bIII, the UV-vis transmission spectra of the HOBC and EBBA nematic liquid crystals were taken at highly scattering state at 10 ºC (opaque state) and at transparent state at 80 ºC. Moreover, Figures 4.5aIV and 4.5bIV showed that the changes in transparency as a function of temperature were reversible after several heating/cooling cycles varying temperature from 10 to 80 ºC.

The variation of transmittance of neat HOBC nematic liquid crystals, measured at 600 nm wavelength, changed from the very low value, 5 % at 10 ºC (HOBC liquid

crystal was in OFF-state) to the highest optical transparency, 25 % at 80 ºC (HOBC liquid crystal was in ON-state) as shown in Figure 4.5aIII. Under the same UV-vis measurement conditions, the transparency of neat EBBA nematic liquid crystal changed from 0 % at 10 ºC to 30 % at 80 ºC as shown in Figure 4.5bIII. If compare the reversible opaque/transparent switch during several repetitive cycles (see Figures 4.5aIV and 4.5bIV), neat HOBC nematic liquid crystal was losing its reversibility during the repeated cycles while neat EBBA liquid crystal maintained its thermo-optical reversible behavior.

The higher stability in reversible changes in optical transparency in the case of the EBBA liquid crystal can be once more related to presence of the aniline group in its chemical structure, which can make the reversible switching process of EBBA liquid crystal more stable [29,30].

Here, it should be mention that both neat HOBC and EBBA nematic liquid crystals showed UV-shielding properties regardless of temperature, the transmittance was equal 0 % up to 300 and 425 nm for neat HOBC and EBBA nematic liquid crystals, respectively.

4.3.4. Photoluminescence properties of the PDLC blends

The effect of the addition of PE-b-PEO block copolymer on photoluminescence properties of the HOBC and EBBA liquid crystal phases in the PDLC blends were also investigated.

Figures 4.6aI to 4.6fI showed photoluminescence emission spectra of each investigated PDLC blend recorded at 10 and 80 ºC. Reversible photoluminescence change as a function of the temperature during four heating/cooling cycles, from 10 to 80 °C, was shown in Figures 4.6aII to 4.6fII.

The maximum emission intensity peaks at 10 and 80 °C during four consecutive heating/cooling cycles were plotted for each PDLC blend. 3D PL spectra of each investigated PLDC blend during heating/cooling cycles are also presented in Figures 4.7 and 4.8 as additional information.

Here it should be mentioned that the PE-b-PEO block copolymer did not show any emission peak in photoluminescence emission spectra taken for excitation wavelengths equal to 333 and 467 nm characteristic for the HOBC and EBBA nematic liquid crystals, respectively.

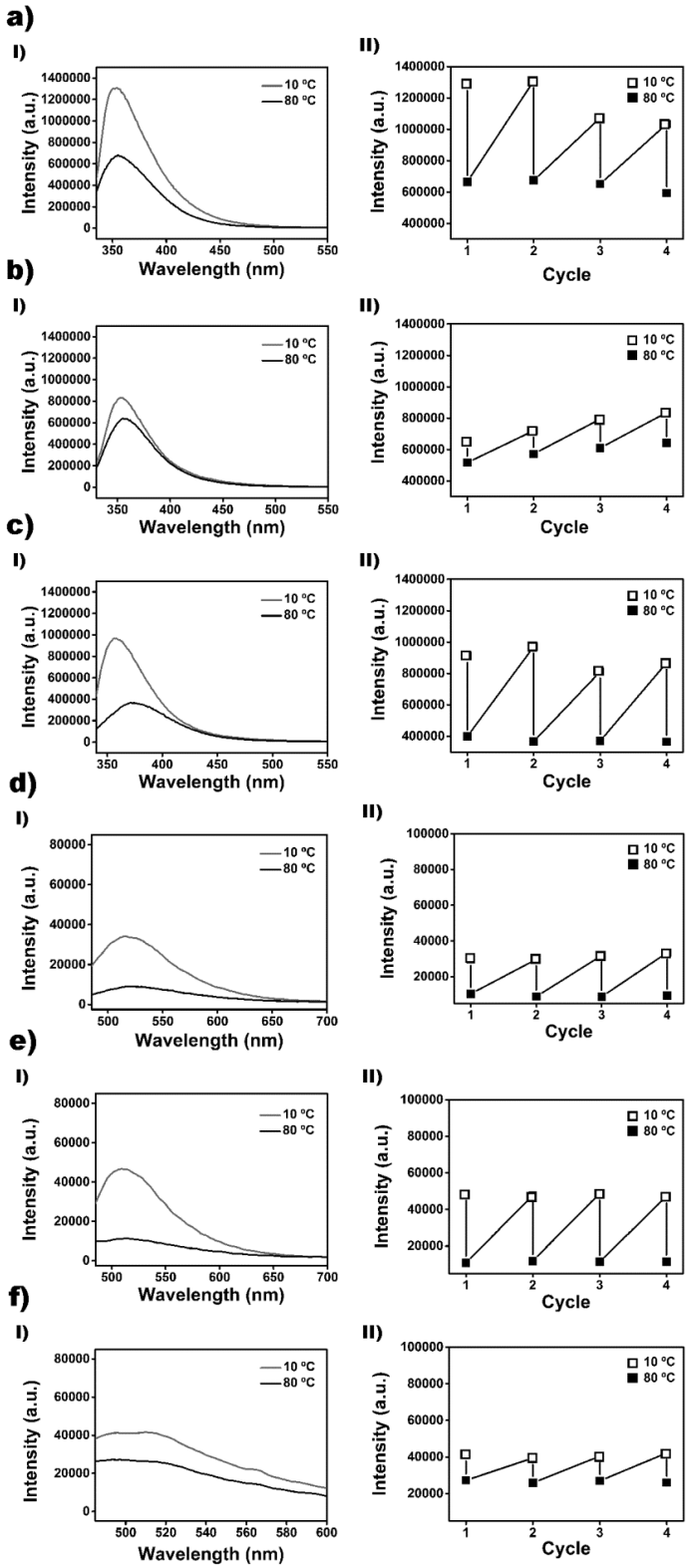

Figure 4.6. PL emission spectra at 10 and 80 °C during a heating/cooling cycle of the PE-b-PEO/HOBC blends with aI) 1, bI) 5 and cI) 10 wt % of PE-b-PEO block copolymer content and of the PE-b-PEO/EBBA blends with dI) 1, eI) 5 and fI) 10 wt % of PE-b-PEO block copolymer content. Maximums emission peaks at 10 and 80 °C during four heating/cooling cycles of the PE-b-PEO/HOBC blends with aII) 1, bII) 5 and cII) 10 wt % of PE-b-PEO block copolymer content and of the PE-b-PEO/EBBA blends with dII) 1, eII) 5 and fII) 10 wt % of PE-b-PEO block copolymer content.

As shown in Figures 4.6aI to 4.6cI, the maximum emission peak of the PE-b-PEO/HOBC blends shifted slightly to higher wavelength being 356 nm at 10 ºC and 373 nm at 80 ºC for the 10PE-b-PEO/HOBC blend. The PL intensity of all investigated PE-b-PEO/HOBC blends decreased almost two times in the case of the 10PE-b-PEO/HOBC blend if compare to the emission spectrum taken at 10 ºC for each blend. Additionally, as shown in Figures 4.6aII to 4.6cII, HOBC liquid crystal phase maintained its reversible photoluminescence switch as a function of temperature in the PE-b-PEO/HOBC blends.

The 3D PL spectra of the PE-b-PEO/HOBC blends showed in Figure 4.7 more deeply visualized the photoluminescence switching.

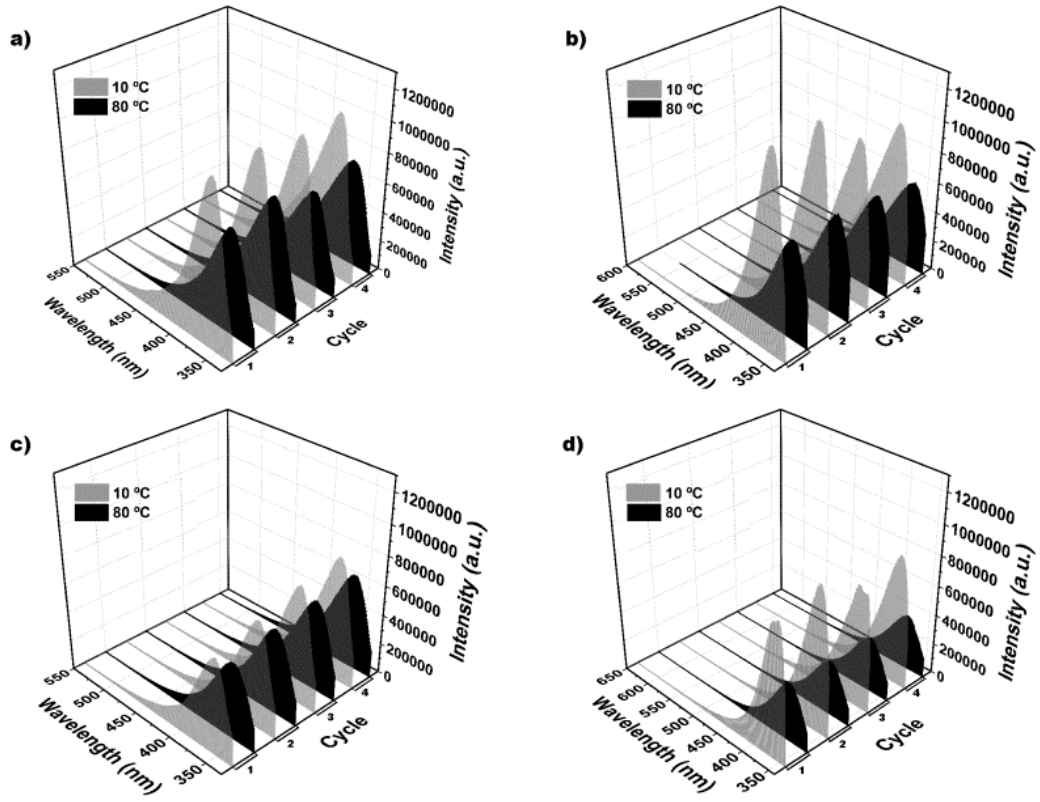

Figure 4.7. 3D photoluminescence emission spectra at 10 and 80 ºC of the a) HOBC nematic liquid crystal and of the PE-b-PEO/HOBC blends with b) 1, c) 5 and d) 10 wt % of PE-b-PEO block copolymer content during four heating/cooling cycles.

The addition of the PE-b-PEO block copolymer to the PE-b-PEO/EBBA blends caused a shift in the maximum emission peak to slightly lower wavelengths (Figure 4.6dI to 4.6fI) at both temperatures, being almost the same for all investigated PDLC blend based on the EBBA nematic liquid crystal, as collected in Table 4.1.

Moreover, PL intensity was also affected by the addition of the PE-b-PEO block

copolymer. The PL intensity at 10 ºC increased with the increase of the PE-b-PEO block copolymer content if compare to the PL intensity of the emission spectrum of EBBA nematic liquid crystal.

Simultaneously, as well as for the PDLC blends based on the HOBC nematic liquid crystal, the PL intensity of the PE-b-PEO/EBBA blends recorded at 80 ºC decreased if compare to the PL intensity recorded at 10 ºC for the same PE-b-PEO block copolymer content, being four times lower for the 1PE-b-PEO/EBBA and 5PE-b-PEO/EBBA blends and more than one time lower for the 10PE-b-PEO/EBBA blend.

Nevertheless, as can be clearly visualized in Figures 4.6IId-4.6IIf, all PE-b-PEO/EBBA blends maintained reversible switching process of the EBBA liquid crystal phase while the 5PE-b-PEO/EBBA blend showed the best photoluminescence switching properties. For better visualization of the photoluminescence switching, 3D PL spectra of the PE-b-PEO/EBBA blends are shown in Figure 4.8.

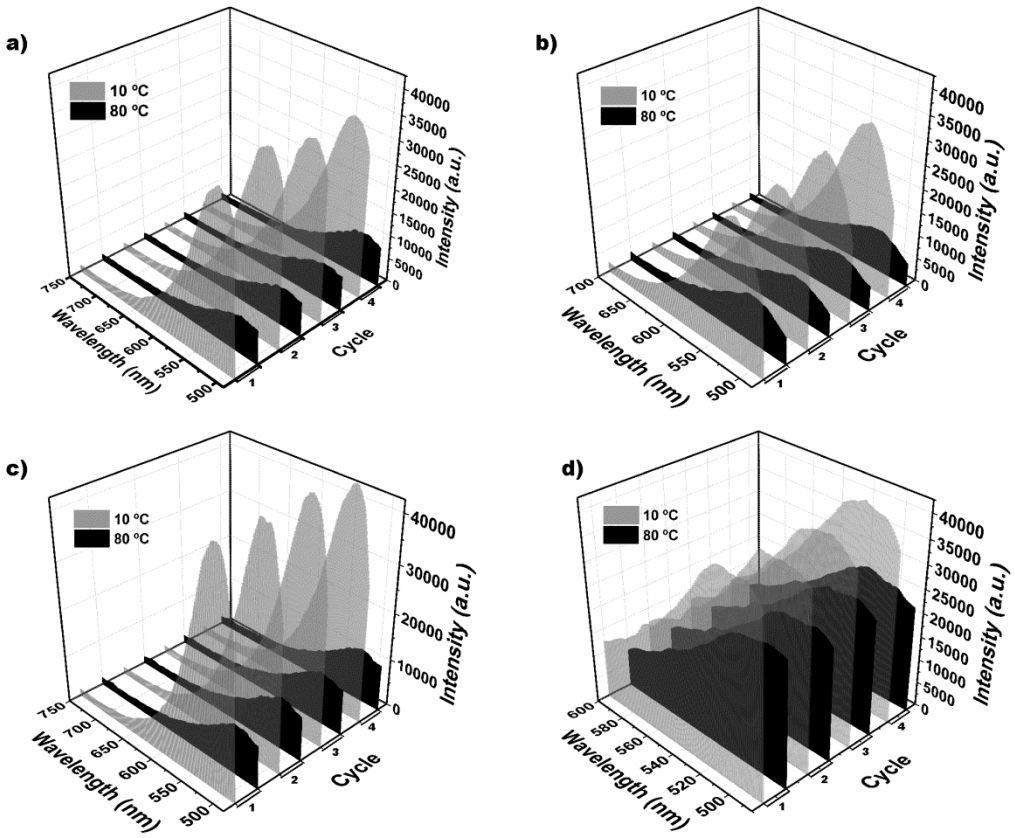

Figure 4.8. 3D photoluminescence emission spectra at 10 and 80 ºC of the a) EBBA nematic liquid crystal and the PE-b-PEO/EBBA blends with b) 1, c) 5 and d) 10 wt % of PE-b-PEO block copolymer content during four heating/cooling cycles.

Generally, taken into account the experimental values, it can be concluded that the addition of the PE-b-PEO block copolymer to the PE-b-PEO/HOBC blends shifted

the maximum emission peak to a higher wavelengths and lower photoluminescence intensities. By contrast, in the PE-b-PEO/EBBA blends, the addition of the PE-b-PEO block copolymer shifted the maximum emission peak to lower wavelengths and slightly higher photoluminescence intensities. This behavior is probably related to the fact that each liquid crystal is miscible with a different block of the PE-b-PEO block copolymer.

As was reported in the Chapter 3, the PEO block is more miscible with the HOBC nematic liquid crystal while the PE block is more miscible with the EBBA nematic liquid crystal. Consequently, for the PE-b-PEO/HOBC blends a part of the PEO block domains microphase separated within the HOBC liquid crystal phase and in the case of the PE-b-PEO/EBBA blends a part of the PE block domains microphase separated within the EBBA liquid crystal phase. Accordingly, the orientation changes of the HOBC and EBBA nematic liquid crystal phases in the PDLC blends during switching from opaque to transparent state are strongly affected as shown in Scheme 4.2.

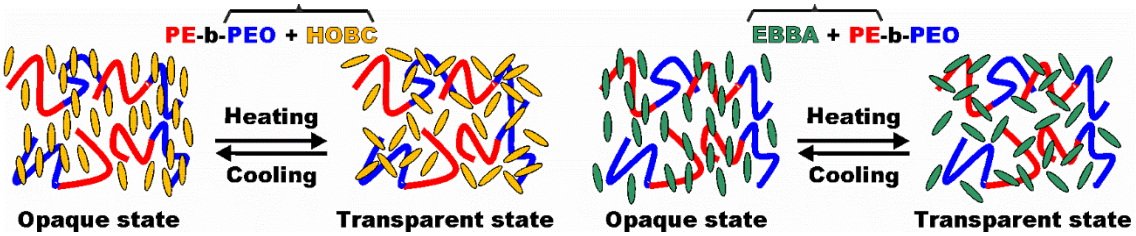

Scheme 4.2. Schematic illustration of the orientation changes of the HOBC and EBBA liquid crystal phases in the PDLC blends during switching from opaque to transparent state.

The miscibility of the liquid crystals with the different blocks of the PE-b-PEO block copolymer can be responsible for the different photoluminescence behavior of the PDLC blends based on the HOBC and EBBA nematic liquid crystals.

4.3.5. Optical reversibility of the PDLC blends as a function of temperature

The transparency and the reversible switching process from opaque to transparent of the PDLC blends based on the HOBC and EBBA nematic liquid crystals as a function of temperature was also studied using UV-vis spectroscopy. Figures 4.9aI to 4.9fI and 4.9aII to 4.9fII showed the UV-vis transmittance spectra of these PDLC blends at 10 ºC (highly scattering state-opaque) and at 80 ºC (transparent state). Moreover, the transmittance values were taken at 600 nm during four heating/cooling cycles to quantify the reversibility of this process.

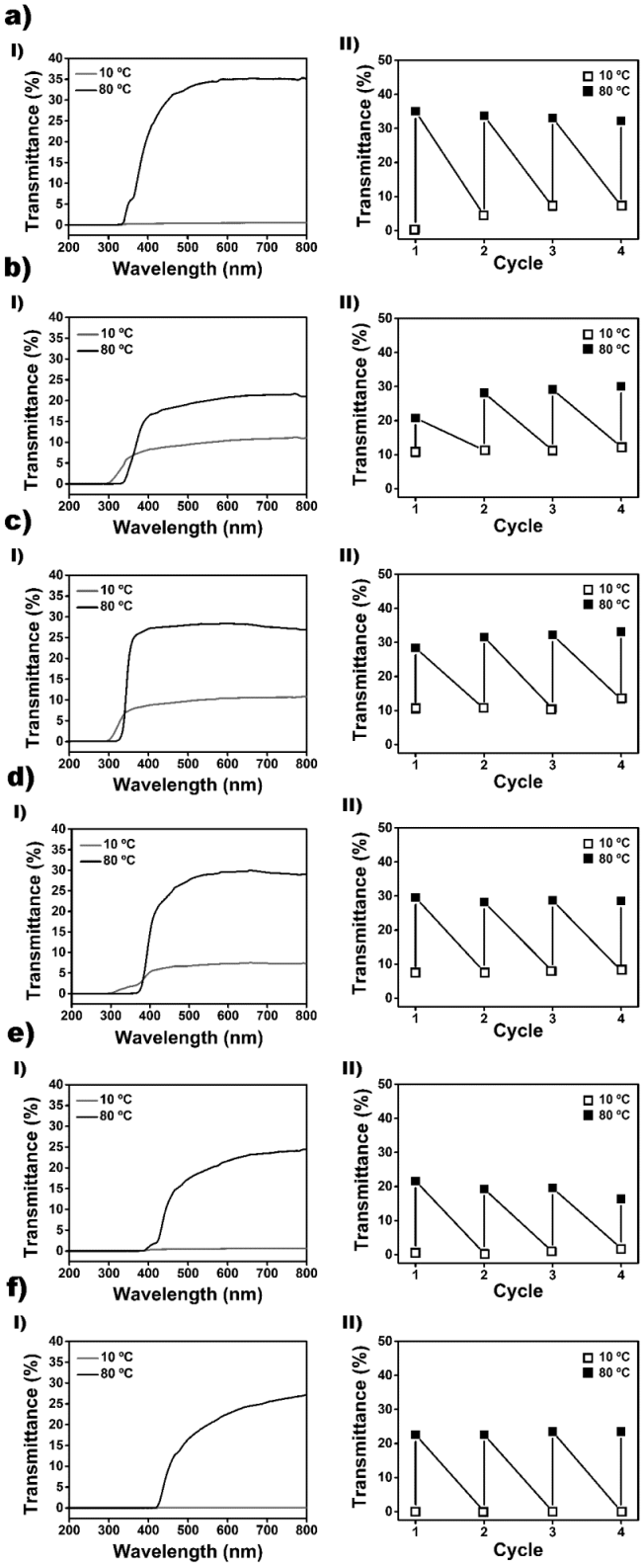

Figure 4.9. UV-visible transmittance spectra at 10 and 80 °C during a heating/cooling cycle of PE-b-PEO/HOBC blends with aI) 1, bI) 5 and cI) 10 wt % PE-b-PEO block copolymer content, and PE-b-PEO/EBBA blends with dI) 1, eI) 5 and fI) 10 wt % PE-b-PEO block copolymer content. Transmittance values, measured at a wavelength of 600 nm, during four heating/cooling cycles at 10 and 80 °C of PE-b-PEO/HOBC blends with aII) 1 , bII) 5 and cII) 10 wt % PE-b-PEO block copolymer content and PE-b-PEO/EBBA blends with dII) 1, eII) 5 and fII) 10 wt % PE-b-PEO block copolymer content.

As shown in Figures 4.9aI to 4.9cI, the transparency of the PE-b-PEO/HOBC blends at 10 ºC increased slightly with the increasing of the PE-b-PEO block copolymer content. This can be related to presence of the PE-b-PEO block copolymer or to the miscibility of the HOBC liquid crystal phase with the PEO-block of the PE-b-PEO block copolymer.

Simultaneously, the transparency of the PE-b-PEO/HOBC blends at 80 ºC decrease considerably with the addition of the PE-b-PEO block copolymer, being 35, 21 and 28 % for the 1PE-b-PEO/HOBC, 5PE-b-PEO/HOBC and 10PE-b-PEO/HOBC blends, respectively. As can be seen in Figures 4.9aII-4.9cII, all investigated PDLC blends based on the HOBC nematic liquid crystal presented good optical reversibility switching from opaque to transparent state during several heating/cooling cycles.

On the contrary to the PE-b-PEO/HOBC blends, at 10 ºC the transmittance of the PE-b-PEO/EBBA blends decreased with the increasing of the PE-b-PEO block copolymer content, being 0 % for 5 and 10 wt % of PE-b-PEO block copolymer as shown in Figures 4.9dI to 4.9fI.

The difference between the transparence tendency of the PDLC blends based on the HOBC and EBBA nematic liquid crystals was probably related to the presence of the PE-b-PEO block copolymer and particularly with the fact that the HOBC nematic liquid crystal was more miscible with the PEO block while the EBBA nematic liquid crystal was more miscible with the PE block.

Similar to the PE-b-PEO/HOBC blends, at 80 ºC the transparency of the PE-b-PEO/EBBA blends decrease slightly with the increasing of the PE-b-PEO block copolymer content, being 30 % for the addition of 1 wt % of PE-b-PEO block copolymer (see Figure 4.9dI) and 25 % for the addition of 5 and 10 w t% of PE-b-PEO block copolymer (see Figures 4.9eI and 4.9fI). Moreover, all PE-b-PEO/EBBA blends kept up the reversible properties of the EBBA liquid crystal phase switching from opaque state at 10 ºC to transparent state at 80 ºC. As can be seen in Figures 4.9dII to 4.9fII this process was reversible after four heating/cooling cycles.

The addition of the PE-b-PEO block copolymer did not modify significantly the UV-shielding properties of the HOBC an EBBA liquid crystals phase in designed PDLC blends.

The transmittance value was equal to 0 %, at both 10 and 80 ºC, up to ~300 and ~425 nm for the PE-b-PEO/HOBC blends and PE-b-PEO/EBBA blends, respectively.

4.4. Conclusions

Thermo-optical responsive behavior of the PDLC blends based on the high HOBC and EBBA nematic liquid crystals content was investigated.

DSC thermograms showed that the increase of the PE-b-PEO block copolymer in the investigated PDLC blends, leads to decrease of nematic-isotropic temperature.

The presence of the nematic-isotropic transition in all investigated PDLC blends, indicate their ability to reversible switching during temperature changes. Thus, liquid crystal phase maintained the nematic-isotropic transition of the HOBC or EBBA nematic liquid crystals in all investigated PDLC blends confirming their ability to switch from opaque to transparent state applying a temperature gradient.

The texture changes as a function of temperature for the investigated HOBC and EBBA nematic liquid crystals and their blends during switching form opaque to transparent state were visualized using OM.

PL intensity of the HOBC liquid crystal is much higher than the EBBA liquid crystal. This behavior can be related to the fact that the EBBA liquid crystal phase can act as quencher due to the aniline group in it chemical structure. Consequently, the EBBA liquid crystal maintained the thermo-optical reversibility during four heating/cooling cycles while the HOBC liquid crystal was losing its reversibility during the repeated heating/cooling cycles. The aniline group presents in the EBBA liquid crystal chemical structure acted as quencher and provoked a lower PL intensity than in the HOBC liquid crystal, however was also responsible of the durability of the thermo-optical reversibility when repeated heating/cooling cycles were applied.

The addition of the PE-b-PEO block copolymer shifted the maximum emission peak to higher wavelength and lower PL intensity for the PE-b-PEO/HOBC blends and shifted the maximum emission peak to lower wavelength and higher PL intensity for the PE-b-PEO/EBBA blends. This behavior was strongly related to the fact that the HOBC nematic liquid crystal is miscible with the PEO block while the EBBA nematic liquid crystal is miscible with the PE block of the PE-b-PEO block copolymer.

Obtained results proved that all investigated PDLC blends maintain reversible switching from opaque to transparent state confirming that they can be employed as thermo-reversible recording materials, thermo-optical devices and temperature sensors.

4.5. References

[1] Giese M, De Witt JC, Shopsowitz KE, Manninng AP, Dong RY, Michal CA, Hamad WY, MacLachlan MJ. Thermal switching of the reflection in chiral nematic mesoporous organosilica films infiltrated with liquid crystals. ACS Appl. Mater. Inter. 2013;5:6854-6859.

[2] Chen L, Liu Z, Che K, Bu Y, Li S, Zhou Q, Xu H, Cai Z. Thermo-switchable multiwavelength laser emission from a dye doped nematic liquid crystal device. Thin Solid Films 2012;520:2971-2975.

[3] Shiraishi Y, Uehara T, Sawai H, Kakiuchi H, Kobayashi S, Toshima N. Electro-optic properties of liquid crystal devices doped with cucurbit(6)uril protected zirconia zanowires. Colloids Surf. A 2014;460:90-94.

[4] Liu Y, Jiang D, Cao W, Yang T, Xia T, Xu R. Microwave tunable split ring resonator bandpass filter using nematic liquid crystal materials. Optik 2016;127:10216-10222.

[5] Yildirim M, Köysal O, Önsal G, Gümüş E. Effect of iron phthalocyanine (FePc) concentration on electrical and dielectric properties of the nematic liquid crystal composites. J. Mol. Liq. 2016;223:868-872.

[6] Pal K, Mohan MLN, Thomas S. Dynamic application of novel electro-optic switchable device modulation by graphene oxide dispersed liquid crystal cell assembling CdS nanowires. Org. Electron. 2016;39:25-37.

[7] Hsiao YC, Huang SM, Yeh ER, Lee W. Temperature dependent electrical and dielectric properties of nematic liquid crystals doped with ferroelectric particles. Displays 2016;44:61-65.

[8] Kee CS, Kim K, Lim H. Tuning of anisotropic optical properties of two dimensional dielectric photonic crystals. Physica B 2003;338:153-158.

[9] Tong X, Zhao Y. Liquid-crystal gel-dispersed quantum dots: reversible modulation of photoluminescence intensity using an electric field. J. Am. Chem. Soc. 2007;129:6372-6373.

[10] Yamane H, Kikuchi H, Kajiyama T. Bistable electro-optical fast switching for induced smectic (liquid crystalline polymer/liquid crystals) and (pseudo liquid crystalline copolymer/liquid crystals) composite systems. Macromolecules 1997;30:3234-3241.

[11] Roy JS, Majumder TP, Dabrowski R, Dey A, Ray PP. Tuning photoluminescence

of liquid crystals doped ZnS nanoflakes. Opt. Mater. 2015;46:467-471.

[12] Yoshino K, Shimoda Y, Kawagishi Y, Nakayama K, Ozaki M. Temperature tuning of the stop band in transmission spectra of liquid crystal infiltrated synthetic opal as tunable photonic crystal. Appl. Phys. Lett. 1999;75:932-934.

[13] Cheng MC, Chu CC, Su YC, Chang WT, Hsiao VKS, Yong KT, Law WC, Prasad PN. Light-induced photoluminescence switching using liquid crystal-dispersed quantum dots. IEEE Photonic. J. 2011;4:19-25.

[14] Lin CC, Huang TC, Chu CC, Hsiao VKS. Optically switchable and axially symmetric half-wave plate based on photoaligned liquid crystal films. Opt. Mater. 2016;57:23-27.

[15] Davis R, Mallia VA, Das S. Reversible photochemical phase transition behavior of alkoxy-cyano-substituted diphenylbutadiene liquid crystals. Chem. Mater. 2003;15:1057-1063.

[16] Fang G, Shi Y, Maclennan JE, Clark NA. Photo-reversible liquid crystal alignment using azobenzene-based self-assembled monolayers: comparison of the bare monolayer and liquid crystal reorientation dynamics. Langmuir 2010;26:17482-17488.

[17] Tercjak A, Serrano E, Mondragon I. Thermally reversible materials based on thermosetting systems modified with polymer dispersed liquid crystals for optoelectronic application. Polym. Adv. Technol. 2006;17:835-840.

[18] Hoppe CE, Galante MJ, Oyanguren PA, Williams RJJ. Thermally reversible light scattering films based on droplets of a liquid crystal (N-4-ethoxybenzylidene-4´-n-butylaniline)/polystyrene solution dispersed in an epoxy matrix. Macromolecules 2004;37:5352-5357.

[19] Hoppe CE, Galante MJ, Oyanguren PA, Williams RJJ. Thermally optical properties of novel thermally switched PDLC films composed of a liquid crystal distributed in a thermoplastic/thermoset polymer blend. Mater. Sci. Eng. C 2004;24:591-594.

[20] Alves VM, Nakamatsu S, Oliveira EA, Zappone B, Richetti P. Anisotropic reversible aggregation of latex nanoparticles suspended in a lyotropic nematic liquid crystal: Effect of gradients of biaxial order. Langmuir 2009;25:11849-11856.

[21] Tercjak A, Gutierrez J, Barud HS, Ribeiro SJL. Switchable photoluminescence liquid crystal coated bacterial cellulose films with conductive response. Carbohyd. Polym. 2016;143:188-197.

[22] Mirzaei J, Reznikov M, Hegmann T. Quantum dots as liquid crystal dopants. J

Mater. Chem. 2012;22:22350-22365.

[23] Tercjak A, Gutierrez J, Mondragon I. Conductive properties of photoluminescent Au/PS-b-PEO inorganic/organic hybrids containing nematic liquid crystals. J. Phys. Chem. C 2011;115:1643-1648.

[24] Tercjak A, Gutierrez J, Ocando JC, Mondragon I. Conductive properties of switchable photoluminescence thermosetting systems based on liquid crystals. Langmuir 2010;26:4296-4302.

[25] Meuer S, Fischer K, Mey I, Janshoff A, Schmidt M, Zentel R. Liquid crystals from polymer-functionalized TiO_2 nanorod mesogens. Macromolecules 2008;41:7946-7952.

[26] Tercjak A, Serrano E, Mondragon I. Multifunctional thermally reversible nanostructured thermosetting materials based on block copolymers dispersed liquid crystal. Macromol. Rapid. Comm. 2007;28:937-941.

[27] Tercjak A, Gutierrez J, Ocando JC, Peponi L, Mondragon I. Thermoresponsive inorganic/organic hybrids based on conductive TiO_2 nanoparticles embedded in poly(styrene-b-ethylene oxide) block copolymer dispersed liquid crystals. Acta Mater. 2009;57:4624-4631.

[28] Tercjak A, Serrano E, Larrañaga M, Mondragon I. Polymer dispersed liquid crystals based on poly(styrene-b-ethylene oxide), poly(bisphenol a carbonate) or poly(methylphenylsiloxane), and 4´(hexyloxy)-4-biphenyl-carbonitrile: analysis of phase diagrams and morphologies generated. J. Appl. Polym. Sci. 2008;108:1116-1125.

[29] Turro NJ, Engel R. Quenching of biacetyl fluorescence and phosphorescence. J. Am. Chem. Soc. 1969;91:7113-7121.

[30] Guo J, Ren T, Zhang J, Li G, Li W, Yang L. Crystal structure characterization as well as theoretical study of spectroscopic properties of novel Schiff bases containing pyrazole group. Spectrochim. Acta 2012;95:135-142.

Hybrid PE-b-PEO/EBBA fibers by electrospinning

5

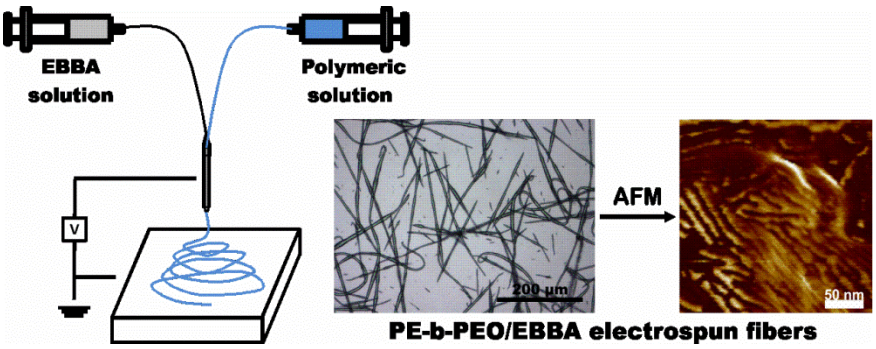

5. Hybrid PE-b-PEO/EBBA fibers by electrospinning

In the present Chapter, the PE-b-PEO block copolymer will be used as matrix for fabrication of the hybrid PE-b-PEO/EBBA and PLA/PE-b-PEO/EBBA electrospun fibers by co-electrospinning technique. Optimization of the electrospinning processing-window will be carried out by varying the concentration of the PE-b-PEO block copolymer solution and playing with three different electrospinning parameters such as voltage, solvent and the PE-b-PEO block copolymer solution flow rate. The hybrid PE-b-PEO/EBBA electrospun fibers will be also fabricated modifying the PE-b-PEO block copolymer fibers with the low molecular weight EBBA nematic liquid crystal using coaxial electrospinning technique. Moreover, the hybrid PLA/EBBA and PLA/PE-b-PEO/EBBA electrospun fibers will be also fabricated by electrospinning technique. The morphology of the fabricated fibers will be investigated from micro to nanoscale using OM, SEM and AFM microscopies.

5.1. Introduction

Nowadays, the need to produce novel materials, for example for packaging, tiny electronic devices and biomedical applications, has helped to develop innovative techniques and improve others.

As was explained in the Chapter 2, the electrospinning technique allows the obtaining of micro and nanofibers playing with different electrospinning parameters. This technique can be considered an easy and versatile technique since a wide range of polymers [1-7] and different block copolymers [8-14] can be used to fabricate electrospun fibers. These kinds of fibers can found applications in different fields such as medical prosthesis (grafts, vessels, and tissues), filtration systems, or electrical and optical devices [14-18].

Co-electrospinning technique is able to simultaneously electrospun different polymers obtaining core-shell structure nanofibers [19-34]. Additionally, liquid crystal molecules have also been used to design hybrid fibers with conductive properties, in order to fabricate electronic devices or sensors.

Many research groups have studied different polymers to obtain electrospun fibers confirming that PLA homopolymer is a good candidate for achieved continuous single fibers with regular and controllable diameters and defect free surface [3,8,13,25-27].

PLA is one of the most used commercial biodegradable polymer derived from renewable resources, the PLA electrospun fibers generated nonwoven mats has shown a great potential in various applications such as drug delivery, fibrous-sensor applications, tissue engineering scaffolds and in the packaging sector [2,3,13,24-26].

One of the aims of this Chapter was the verification of the possibility of fabrication of the hybrid PE-b-PEO/EBBA electrospun fibers. The optimization of the processing-window for fabrication of the PE-b-PEO block copolymer and hybrid PE-b-PEO/EBBA electrospun fibers by co-electrospinning technique was study at the macro and nanoscale by different microscopy techniques such as OM, SEM and AFM microscopies. Moreover, the PLA homopolymer was employed as matrix in order to check even the hybrid PLA/EBBA and PLA/PE-b-PEO/EBBA electrospun fibers are able to form fiber mats. One of the specific objectives of this investigation work was check the liquid crystal character of fabricated electrospun fibers.

5.2. Materials and characterization techniques

5.2.1. Materials

The PE-b-PEO block copolymer with a molecular weight of 2250 g mol^{-1} and 80 wt % of PEO block content, the PLA homopolymer 3051D with a molecular weight of 93500 g mol^{-1} and the EBBA nematic liquid crystal, were employed in this Chapter.

Moreover, chloroform and dimethylformamide (DMF) were used as solvents during the co-electrospinning process.

5.2.2. Sample preparation

The PE-b-PEO block copolymer electrospun fibers and the hybrid PE-b-PEO/EBBA electrospun fibers were performed using an Electrospinner Yflow 2.2.D-350 (Nanotechnology Solutions) with a coaxial vertical standard configuration and connected to a high voltage power. The polymer solution flowed through the inner needle and the same solvent solution used for the polymer solution flows through the outer one. In this case, the solvent solution was used in order to avoid the obstruction of the inner needle during the electrospun process.

To fabricate PE-b-PEO block copolymer electrospun fibers by co-electrospinning process, two groups of parameters were mainly considered, one related with the polymer solution and the other one with the processing conditions.

Regarding the polymer solution, several PE-b-PEO block copolymer concentrations (C_p (wt %)), between 20 and 50 wt %, were prepared in a mixture of chloroform/DMF solvents, with different ratios from 3:1 to 1:0. The polymeric solutions were stirred during 24 h at room temperature.

During the electrospinning process, the block copolymer solution was pushed using a pump through a capillary up to the inner needle of the concentric needle, while solvents, flowed through the outer one.

For comparison, both the PE-b-PEO and hybrid PE-b-PEO/EBBA electrospun fibers were obtained using a coaxial nozzle.

Additionally, processing conditions were optimized, playing with solvent flow rate, Q_s (mL h^{-1}), block copolymer solution flow rate, Q_p (mL h^{-1}), and with the electric field applied between needle and the collector. The needle-collector distance was fixed to 18 cm.

The solvent and block copolymer solution flow rates were varied from 0 to 0.5 mL h^{-1} and from 0.1 to 5 mL h^{-1}, respectively. In the case of the electric field, the positive voltage (V^+) applied over the double needle was between 3 and 14 kV and the negative voltage (V^-) applied over the collector ranged between 3 and 14 kV.

Table 5.1 summarized the preparation conditions employed to fabricate the PE-b-PEO block copolymer fibers.

Table 5.1. Summary of the experimental conditions used during co-electrospinning process of the PE-b-PEO block copolymer fibers.

Number of samples	PE-b-PEO concentration (wt %)	Solvent ratio Chloroform:DMF	PE-b-PEO flow rate Q_p (mL h^{-1})	Chloroform flow rate Q_s (mL h^{-1})	Positive voltage V^+ (kV)	Negative voltage V^- (kV)
330	24 (10-50)	5 (3:1-1:0)	6 (0.1-5)	4 (0-0.5)	8 (3-14)	7 (3-14)

On the other hand, for the development of the hybrid PE-b-PEO/EBBA electrospun fibers, block copolymer solution flowed through the inner needle of the equipment and a solution of 5 wt % of EBBA nematic liquid crystal in chloroform through the outer one.

For this purpose, the best conditions for the fabrication of the block copolymer fibers have been chosen as starting point. Thus, as explained below in Results and Discussion section, the most suitable concentration for fibers fabrication was 46 wt % of PE-b-PEO block copolymer in a mixture of chloroform/DMF solvents.

Table 5.2 summarized the preparation conditions employed to fabricate the hybrid PE-b-PEO/EBBA electrospun fibers.

Table 5.2. Summary of the experimental conditions used during co-electrospinning process of the hybrid PE-b-PEO/EBBA fibers.

Number of samples	Solvent ratio Chloroform/DMF	EBBA flow rate Q_{LC} (mL h^{-1})	PE-b-PEO flow rate Q_p (mL h^{-1})	Positive voltage V^+ (kV)	Negative voltage V^- (kV)
12	5:1	(0.1-0.5)	(0.1-5)	11	11
5	4:1	(0.1-0.5)	(0.1-5)	11	11

As well as in the case of the PE-b-PEO block copolymer electrospun fibers for the hybrid PE-b-PEO/EBBA electrospun fibers the solvent used for the PE-b-PEO block copolymer was a mixture of chloroform/DMF solvents with different solvents ratio.

The experimental conditions to fabricate the hybrid PLA/EBBA and PLA/PE-b-PEO/EBBA electrospun fibers were chosen taking into account previous studies related to the optimization of the PLA electrospun fibers [24-26] and consequently, the conditions of the preparation of the PE-b-PEO block copolymer and hybrid PE-b-PEO/EBBA electrospun fibers were optimized. The materials were prepared in the same way as the PE-b-PEO block copolymer and hybrid PE-b-PEO/EBBA electrospun fibers.

Regarding hybrid the PLA/EBBA, two solutions, one with a 10 wt % of PLA, and the other one, with a 10 wt % of EBBA nematic liquid crystal were prepared in a mixture of chloroform/DMF solvents with a ratio of 4:1. These solutions were stirred during 24 h at room temperature. During the electrospinning process, the PLA solution was pushed using a pump through a capillary up to the inner needle of the concentric needle, while the EBBA liquid crystal solution, flowed through the outer one. The PLA solution flow rate was fixed in 2 mL h^{-1} and the EBBA liquid crystal solution flow rate was varied from 0 to 5 mL h^{-1}.

In respect of the hybrid PLA/PE-b-PEO/EBBA electrospun fibers, two solutions, one with 10 wt % of PLA and 10 wt % of PE-b-PEO block copolymer with the molar ratio 50:50, and the other one, with 10 wt % of EBBA nematic liquid crystal, were prepared in a mixture of chloroform/DMF solvents with a ratio of 4:1. All prepared solutions were stirred during 24 h at room temperature. The PLA/PE-b-PEO solution was pushed using a pump through a capillary up to the inner needle of the concentric needle, while the EBBA liquid crystal solution, flowed through the outer one. The PLA/PE-b-PEO solution flow rate was fixed in 2 mL h^{-1} and the EBBA solution flow

rate was varied from 0 to 5 mL h^{-1}. For the fabrication of the hybrid PLA/EBBA electrospun fibers, as well as for the fabrication of the hybrid PLA/PE-b-PEO/EBBA electrospun fibers, the electric field was 6 kV for the positive voltage (V^+) applied over the double needle and 8 kV for the negative voltage (V^-) applied over the collector.

5.2.3. Characterization techniques

5.2.3.1. Optical microscopy

OM images were captured using a Nikon Eclipse E600W microscope at room temperature. In order to determine the average diameters and lengths of the fibers, 10 independent fibers for each OM image were taken into account and the diameter and length of each fiber was determined using AnalySIS Auto 3.2 software (Soft Imaging System GmbH).

5.2.3.2. Scanning electron microscopy

Morphology and structure of designed electrospun fibers were observed using a PHILIPS XL30 scanning electron microscope.

5.2.3.2. Atomic force microscopy

Fibers surface morphology was investigated by AFM technique under ambient conditions. AFM images were obtained operating in tapping mode with a scanning probe microscope (Nanoscope IIIa, Multimode from Digital Instruments) equipped with an integrated silicon tip/cantilever having a resonance frequency of 300 kHz from the same manufacturer.

5.3. Results and discussion

5.3.1. OM of the PE-b-PEO and hybrid PE-b-PEO/EBBA electrospun fibers

OM technique was used to study the appearance of the fabricated fibers. First of all, it should be mentioned that for PE-b-PEO block copolymer concentrations below 40 wt % electrospray was not obtained since these concentrations were too low for the fiber fabrication.

The electrospray drops were closer and became bigger with the increasing of the block copolymer concentrations, around 40 wt %, which led to the formation of the very

short electrospun fibers with beads. The formation of the fibers was easier employing the mixture of chloroform/DMF as solvent instead of chloroform.

The optical microscopy technique illustrates that the best conditions to fabricate the PE-b-PEO block copolymer electrospun fibers were with concentrations between 45 and 47 wt % of PE-b-PEO block copolymers and a mixture of chloroform/DMF solvents with the ratio of 4:1 and 5:1, as shown in Figures 5.1 to 5.4.

For PE-b-PEO block copolymer concentrations higher than 47 wt % the needle was blocked hindering the flow of the block copolymer solution and therefore the formation of fibers.

The PE-b-PEO block copolymer electrospun fibers obtained for 45 wt % of PE-b-PEO block copolymers in a mixture of chloroform/DMF (4:1) solvents, applying a voltage difference of 22 kV, a chloroform flow rate of 0.1 mL h^{-1} and a block copolymer solution flow rate of 5 mL h^{-1} are shown in Figure 5.1.

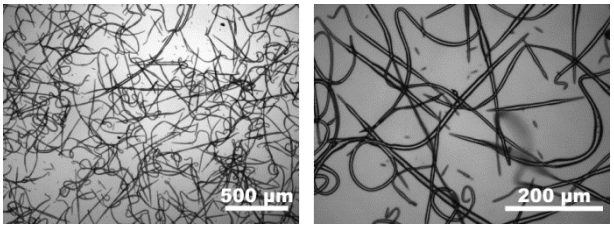

Figure 5.1. OM micrographs of the PE-b-PEO block copolymer electrospun fibers obtained for 45 wt % of PE-b-PEO block copolymer in a mixture of chloroform/DMF solvents (4:1), applying a voltage difference of 22 kV, chloroform flow rate of 0.1 mL h^{-1} and block copolymer solution flow rate of 5 mL h^{-1}.

These electrospinning conditions allowed the fabrication of the fibers with an average diameter of 5 ± 1 µm and the average length of 350 ± 40 µm. It should be noted that the fiber length was homogeneous; in contrast, the diameters were different along each fiber and between them. This heterogeneity was related to the beads that appeared under these processing conditions.

In the case of the PE-b-PEO block copolymer electrospun fibers prepared using 46 wt % of block copolymer in a mixture of chloroform/DMF (5:1) solvents, applying a voltage difference of 22 kV and a chloroform flow rate of 0.1 mL h^{-1}, different sizes of the PE-b-PEO block copolymer fibers were obtained playing with the block copolymer flow rate.

Figure 5.2a shows the PE-b-PEO block copolymer electrospun fibers fabricated with a block copolymer flow rate of 1 mL h^{-1}. The average diameter was 5 ± 2 µm and the average length was 270 ± 90 µm. For the PE-b-PEO block copolymer electrospun

fibers generated with a block copolymer flow rate of 3 and 5 mL h^{-1}, in Figures 5.2b and 5.2c, respectively, similar sized fibers were produced with an average diameter of 4 ± 1 µm and an average length of 200 ± 50 µm. Thus, the increase in the block copolymer flow rate led to a decrease in both the fiber diameter and the length.

Moreover, as shown in Figure 5.2, for the block copolymer flow rate 1 mL h^{-1}, the fibers were more abundant than in the case of the higher block copolymer flow rate.

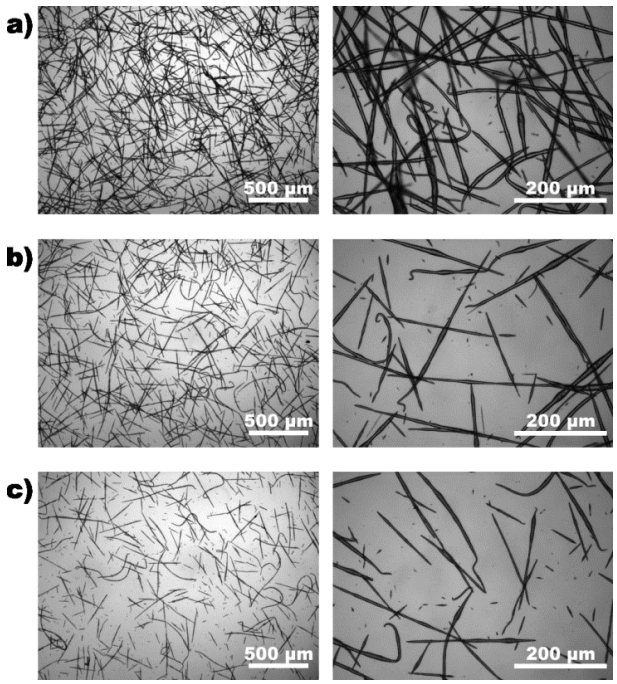

Figure 5.2. OM micrographs of the PE-b-PEO block copolymer electrospun fibers obtained for 46 wt % of PE-b-PEO block copolymer in a mixture of chloroform/DMF solvents (5:1), applying a voltage difference of 22 kV, chloroform flow rate of 0.1 mL h^{-1} and block copolymer solution flow rate of a) 1, b) 3 and c) 5 mL h^{-1}.

Additionally, the PE-b-PEO block copolymer electrospun fibers were also prepared maintaining both, the same PE-b-PEO block copolymer concentration (46 wt %) and a chloroform flow rate of 0.1 mL h^{-1}, and changing the chloroform/DMF ratio to 4:1.

To obtain the PE-b-PEO block copolymer electrospun fibers under these experimental conditions, both the block copolymer flow rate and the applied voltage difference were varied.

Figure 5.3 shows the PE-b-PEO block copolymer electrospun fibers obtained from an applied voltage difference and a block copolymer flow rate of 22 kV and 0.1 mL h^{-1}, and 21 kV and 5 mL h^{-1}, respectively.

On the one hand, the PE-b-PEO block copolymer electrospun fibers prepared

with 22 kV and 0.1 mL h^{-1} (Figure 5.3a) resulted in an average diameter of 3 ± 2 μm and an average length of 320 ± 50 μm. Moreover, employing 21 kV and 5 mL h^{-1} (Figure 5.3b), the size of the PE-b-PEO block copolymer fibers was ~5 ± 2 μm in diameter and ~290 ± 50 μm in length.

Consequently, as show in Figure 5.3a, in the first preparation conditions, thinner and larger fibers were observed if compared with the second preparation conditions as visualized in Figure 5.3b.

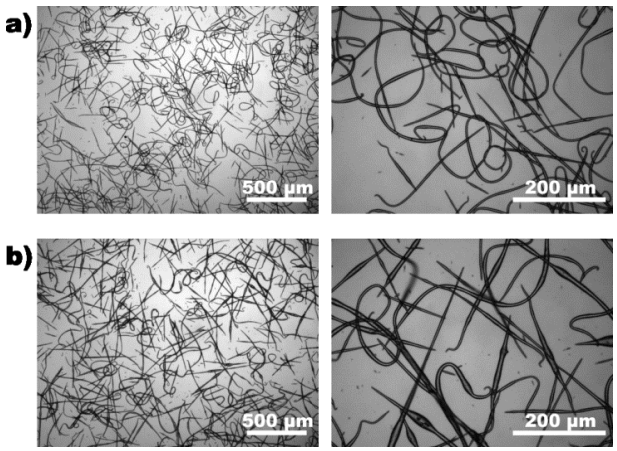

Figure 5.3. OM micrographs of the PE-b-PEO block copolymer electrospun fibers obtained for 46 wt % of PE-b-PEO block copolymer in a mixture of chloroform/DMF solvents (4:1), chloroform flow rate of 0.1 mL h^{-1} applying a voltage difference and block copolymer solution flow rate of a) 22 kV and 0.1 mL h^{-1} and b) 21 kV and 5 mL h^{-1}.

The PE-b-PEO block copolymer electrospun fibers were also achieved by the increase of the block copolymer concentration up to 47 wt %, using solvents ratio of 5:1 and a block copolymer flow rate of 0.5 mL h^{-1} and varying the rest of the electrospinning parameters.

Figure 5.4a, shows the PE-b-PEO block copolymer fibers employing a chloroform flow rate of 0.1 mL h^{-1} and applying a voltage difference of 22 kV. The fabricated fibers possessed an average diameter of 5 ± 1 μm and an average length of 410 ± 90 μm.

In the case of Figure 5.4b, the chloroform flow rate was 0.5 mL h^{-1} and applying a voltage difference of 21 kV. These experimental conditions were responsible for a decrease in the average fiber diameter as well as in the corresponding length, being 4 ± 1 μm and 270 ± 90 μm, respectively.

Comparing the results achieved using different preparation conditions, it can be concluded that the longest and widest fibers were obtained for 47 wt % of PE-b-PEO

block copolymer concentration in a mixture of chloroform/DMF solvents, a block copolymer solution flow rate of 0.5 mL h^{-1}, a chloroform flow rate of 0.1 mL h^{-1} and by applying a voltage difference of 22 kV.

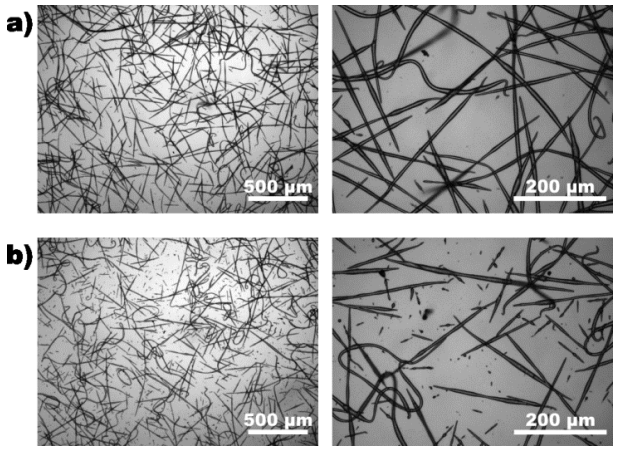

Figure 5.4. OM micrographs of the PE-b-PEO block copolymer electrospun fibers obtained for 47 wt % of PE-b-PEO block copolymer in a mixture of chloroform/DMF solvents (5:1), block copolymer solution flow rate of 0.5 mL h^{-1}, applying a voltage difference and chloroform flow rate of a) 22 kV and 0.1 mL h^{-1} and b) 21 kV and 0.5 mL h^{-1}.

Taking into account the ideal target stabilized for the fibers designed by the electrospinning technique, the PE-b-PEO block copolymer concentration of 46 wt % in a mixture of chloroform/DMF solvents (5:1) solution showed the best results.

These good results are related with, on the one hand, the diameter of fibers obtained under these conditions was consistent and controllable, and on the other hand, the variation of the other electrospinning parameters (block copolymer, solvent flow rates, and applied voltage differences) did not significantly affect the final fiber properties providing a permissible widespread electrospinning processing-window.

According to the promising results obtained for the PE-b-PEO block copolymer electrospun fibers, a 46 wt % of PE-b-PEO block copolymer concentration in a mixture of chloroform/DMF solvents (5:1) solution was used to design the hybrid PE-b-PEO/EBBA electrospun fibers.

In this regard, is interesting to mention the work developed by Rajgarhia et al. [37] in which the relationship between solvent evaporation rate and the morphology of the obtained hybrid fibers was studied. Authors find strong influence of the evaporation rate and the solubility parameter of the solvents on the morphology.

Different hybrid PE-b-PEO electrospun fibers were developed by playing with

the block copolymer flow rate (1, 3 and 5 mL h^{-1}). As well as in the case of the 46 wt % of PE-b-PEO block copolymer in a mixture of chloroform/DMF (5:1) solvents, applied voltage difference and chloroform flow rate remained constant at 22 kV and 0.1 mL h^{-1}, respectively.

Figure 5.5a shows the hybrid PE-b-PEO/EBBA electrospun fibers fabricated with a block copolymer flow rate of 1 mL h^{-1}. The average diameter of the hybrid fibers was 4 ± 1 μm and the average length was 200 ± 30 μm.

By increasing the block copolymer flow rate up to 3 mL h^{-1}, Figure 5.5b, the average length of the hybrid fibers increased up to 230 ± 30 μm conversely, the average diameter remained the same, at 4 ± 1 μm.

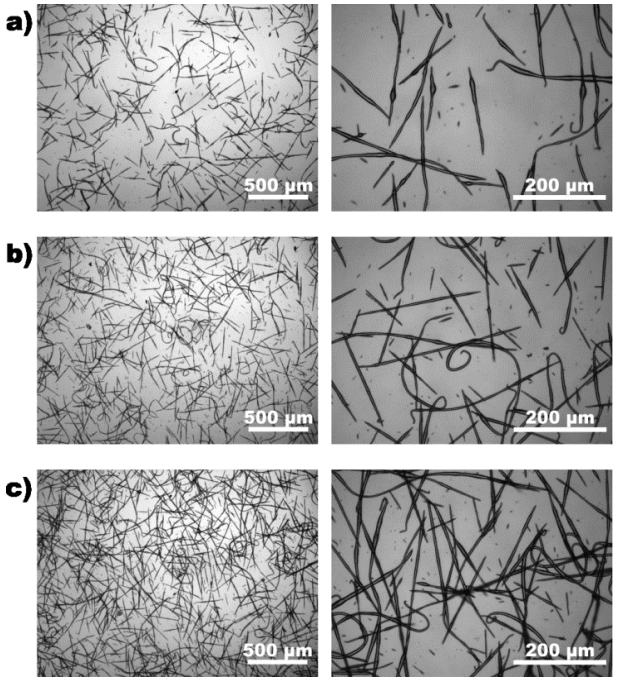

Figure 5.5. OM micrographs of the hybrid PE-b-PEO/EBBA electrospun fibers obtained for 46 wt % of PE-b-PEO block copolymer in a mixture of chloroform/DMF solvents (5:1), applying a voltage difference of 22 kV, EBBA liquid crystal solution flow rate of 0.1 mL h^{-1} and block copolymer solution flow rate of a) 1, b) 3 and c) 5 mL h^{-1}.

For the hybrid PE-b-PEO/EBBA fibers created with a block copolymer flow rate of 5 mL h^{-1}, in Figure 5.5c, the average diameter was 4 ± 1 μm and the average length was 260 ± 80 μm. Therefore, this block copolymer flow rate resulted in an increase in both, the fiber diameter and the length.

Moreover, as shown in Figure 5.5 for the block copolymer flow rate of 5 mL h^{-1}, the hybrid PE-b-PEO/EBBA electrospun fibers were more abundant than in the case of a lower block copolymer flow rate.

A comparison between the PE-b-PEO block copolymer electrospun fibers and the hybrid PE-b-PEO/EBBA electrospun fibers obtained following the same electrospinning processing-window (Figures 5.2 and 5.5) showed a completely opposite behavior. In the case of the PE-b-PEO electrospun fibers without EBBA nematic liquid crystal, an increase in the block copolymer flow rate led to a decrease in fiber diameter and length.

On the contrary, for hybrid PE-b-PEO/EBBA electrospun fibers, an increase in the block copolymer flow rate allowed obtaining longer and wider hybrid fibers. This phenomenon could be explained taken into account the EBBA nematic liquid crystal chemical structure (Chapter 2, Table 2.1).

Its configuration is based on two aromatic rings and an imine group, both of them with delocalized electrons which facilitate electrical conduction. Thus, these electrons contributed to the applied voltage difference and resulted in an increase of fiber length.

Consequently, the addition of the EBBA nematic liquid crystal could improve the electrospinning process.

5.3.2. SEM of the PE-b-PEO block copolymer and hybrid PE-b-PEO/EBBA electrospun fibers

SEM technique was employed to perform a deeper study of obtained fibers using the broader electrospinning processing-window, which corresponds to the 46 wt % of block copolymers in a mixture of chloroform/DMF (5:1) solvents.

SEM images of the PE-b-PEO block copolymer and the hybrid PE-b-PEO/EBBA electrospun fibers based on the 46 wt % of block copolymers in chloroform/DMF solvents (5:1) are shown in Figures 5.6 and 5.7, respectively.

In the case of the PE-b-PEO block copolymer electrospun fibers, once again the fiber diameter was regular and controllable. Moreover, the decrease in the abundance of the fibers due to the increase of the block copolymer flow rate was also observed.

Similarly as for OM results, the best conditions for fiber production were achieved with 46 wt % of PE-b-PEO block copolymers in chloroform/DMF (5:1) solvents therefore this fiber was employed to fabrication of the hybrid PE-b-PEO/EBBA electrospun fibers.

Figure 5.7 shows the SEM images of the hybrid PE-b-PEO/EBBA electrospun fibers obtained for the 46 wt % of PE-b-PEO block copolymers in a mixture of

chloroform/DMF solvents (5:1), applying a voltage difference of 22 kV, an EBBA liquid crystal solution flow rate of 0.1 mL h^{-1} and a block copolymer solution flow rate of 1 mL h^{-1} (Figure 5.7a), 3 mL h^{-1} (Figure 5.7b) and 5 mL h^{-1} (Figure 5.7c).

In agreement with the behavior observed using the OM technique, the SEM images confirmed that an increase in the block copolymer flow rate caused an increase in the fiber diameter and in the abundance of the fibers.

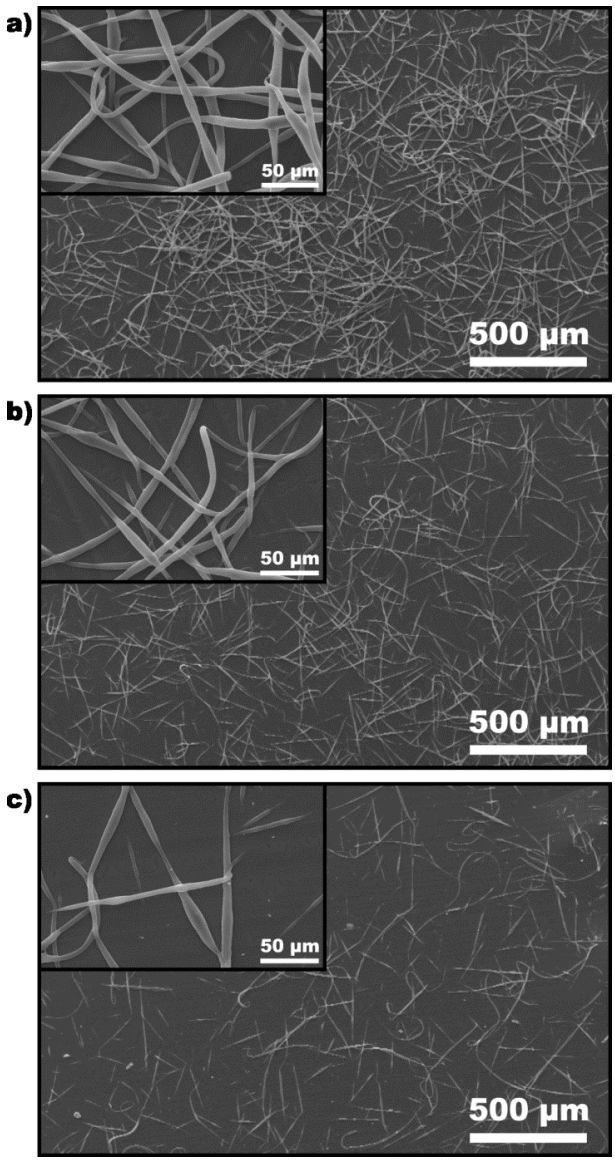

Figure 5.6. SEM images of the PE-b-PEO block copolymer electrospun fibers obtained for 46 wt % of PE-b-PEO block copolymer in a mixture of chloroform/DMF solvents (5:1), applying a voltage difference of 22 kV, chloroform flow rate of 0.1 mL h^{-1} and block copolymer solution flow rate of a) 1, b) 3 and c) 5 mL h^{-1}.

Thus, the behavior is completely opposite if compared with the results obtained for the PE-b-PEO electrospun fibers without the EBBA nematic liquid crystal.

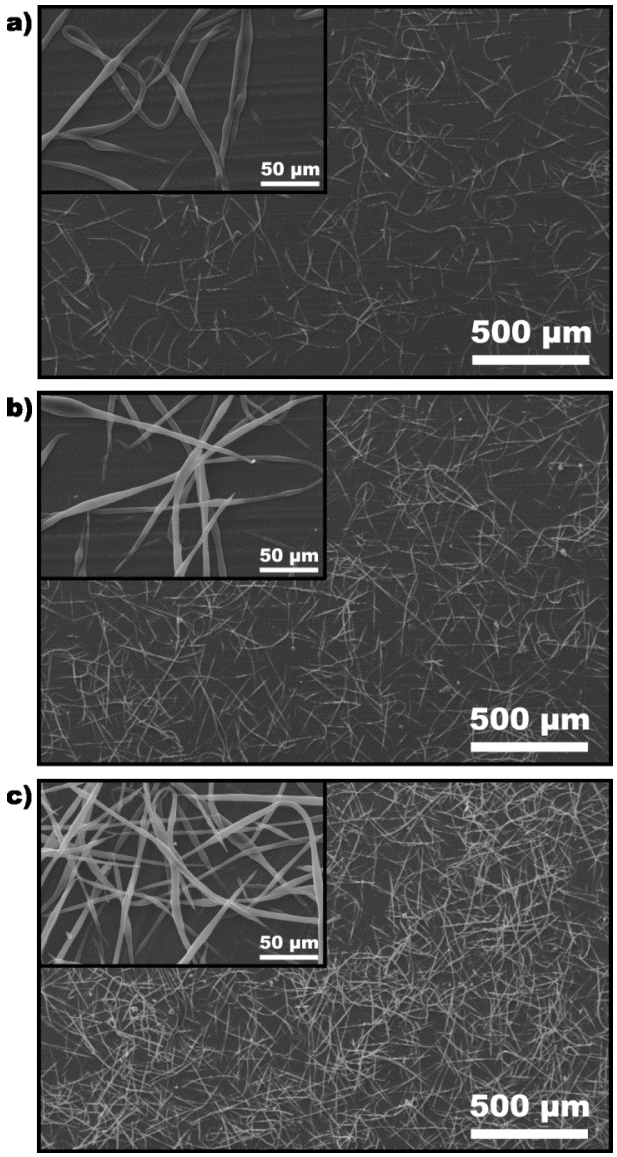

Figure 5.7. SEM images of the hybrid PE-b-PEO/EBBA electrospun fibers obtained for 46 wt % of PE-b-PEO block copolymer in a mixture of chloroform/DMF solvents (5:1), applying a voltage difference of 22 kV, EBBA liquid crystal solution flow rate of 0.1 mL h^{-1} and block copolymer solution flow rate of a) 1, b) 3 and c) 5 mL h^{-1}.

5.3.3. AFM of the PE-b-PEO block copolymer and hybrid PE-b-PEO/EBBA electrospun fibers

With the aim of analyzing the surface morphology of the fabricated PE-b-PEO block copolymer and hybrid PE-b-PEO/EBBA electrospun fibers, AFM measurements were also carried out. Figure 5.8a shows an AFM phase image of the PE-b-PEO electrospun fibers based on the 46 wt % of PE-b-PEO block copolymers in a mixture of chloroform/DMF solvents (5:1), applying a voltage difference of 22 kV, a chloroform flow rate of 0.1 mL h^{-1} and a block copolymer solution flow rate of 1 mL h^{-1}.

Under these electrospinning conditions, the PE-b-PEO block copolymer electrospun fibers showed a microphase separation. Taking into account that the Young´s modulus of the PE is higher than that for the PEO at room temperature [35,36], the darker areas correspond to the PEO block domains and the brightest areas correspond to the PE block domains. As can be observed in Figure 5.8a, the electrospun PE-b-PEO fibers exhibit a cylindrical structure with parallel and perpendicularly oriented cylinders. Moreover, the PEO block nanocrystals (~ 15 nm in size) within the cylindrical PEO domains can be also detected.

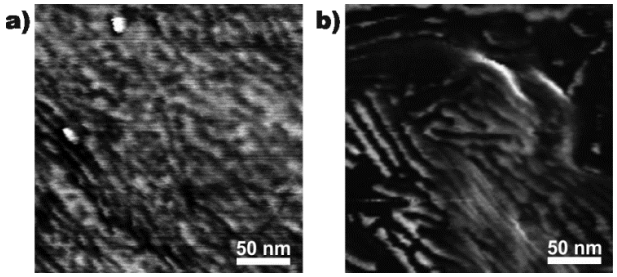

Figure 5.8. AFM phase images of the a) PE-b-PEO electrospun fiber and b) hybrid PE-b-PEO/EBBA electrospun fiber.

In the case of the hybrid PE-b-PEO/EBBA electrospun fibers fabricated under the same processing conditions, the addition of the EBBA nematic liquid crystal led to a significant change in the morphology; from a cylindrical structure to a lamellar one (Figure 5.8b).

This fact can be explained taken into account that, on the one hand, the EBBA nematic liquid crystal is more miscible with the PE blocks than with the PEO blocks, consequently the EBBA nematic liquid crystal was positioned in the PE block domains, as deeply studied in the Chapters 1 and 2. On the other hand, the EBBA nematic liquid crystal chemical structure could also have an influence on the self-assembly process, since, as pointed out before, it affects the electrospinning processing conditions.

5.3.4. OM of the hybrid PLA/EBBA and PLA/PE-b-PEO/EBBA electrospun fibers

The appearance of the fabricated hybrid PLA/EBBA and PLA/PE-b-PEO/EBBA electrospun fibers was studied by OM. Moreover, in order to check the presence of the EBBA nematic liquid crystal in the fabricated fibers, OM with crossed polarizers was employed. The OM micrographs of the all mats were taken at room temperature.

For the hybrid PLA/EBBA electrospun fibers, the EBBA liquid crystal solution flow rate was varied from 0 to 5 mL h^{-1} while the rest of parameters were fixed as

explained above. In the preparation conditions, when the EBBA liquid crystal solution flow rate was equal to 0, the PLA electrospun fibers possessed numerous beads. The increase of the flow rate of the EBBA solution to 0.1 mL h^{-1} led to the decrease of the size and the amount of beads. Moreover, some parts of these PLA/EBBA electrospun fibers was covered by the EBBA nematic liquid crystal as visualized in the cross-polarized OM micrograph. The increase of the EBBA nematic liquid crystal solution flow rate to 0.5 mL h^{-1} allow to reach the fibers without bead, however the fiber length and diameter were not homogeneous. Additionally, the most part of the PLA electrospun fibers were covered by the EBBA nematic liquid crystal as visualize by OM micrographs taken with cross polarized. The increase of the EBBA nematic liquid crystal solution flow rate from 1 to 3 mL h^{-1} resulted in more homogeneous and longer hybrid PLA/EBBA electrospun fibers. The best results were obtained for a flow rate equal to 5 mL h^{-1} as shown in Figure 5.9.

The fibers length and diameter achieved with an EBBA nematic liquid crystal solution flow rate of 5 mL h^{-1} were more homogeneous than in the case of lower EBBA nematic liquid crystal solution flow rates. Moreover, in this case the great part of the fibers was covered by the EBBA nematic liquid crystal.

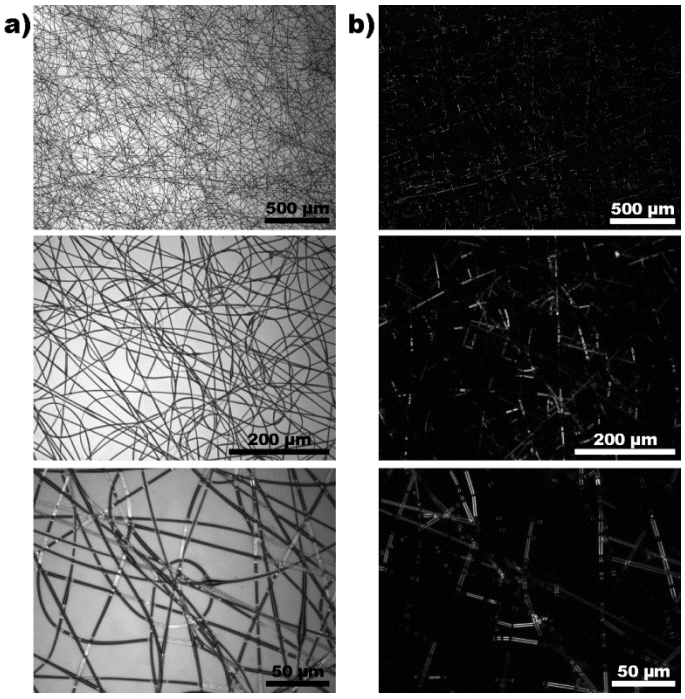

Figure 5.9. OM micrographs a) without crossed polarized and b) with crossed polarizers of the hybrid PLA/EBBA electrospun fibers obtained for 10 wt % of PLA and EBBA nematic liquid crystal with the molar ratio 50:50 in a mixture of chloroform/DMF solvents (4:1) applying a voltage difference of 14 kV, PLA solution flow rate of 2 mL h^{-1} and EBBA solution flow rate of 5 mL h^{-1}.

For the fabrication of the hybrid PLA/PE-b-PEO/EBBA electrospun fibers, the PLA/PE-b-PEO solution flow rate and the rest of electrospinning conditions were maintained and the only EBBA liquid crystal solution flow rate was varied.

For an EBBA liquid crystal solution flow rate equal to 0 mL h^{-1}, the obtained hybrid PLA/PE-b-PEO fibers showed a homogeneous fiber in both length and diameter along the fiber. It seems to be that the addition of the PE-b-PEO block copolymer improved the fibers formation if compare with the PLA fibers.

The increase of the EBBA liquid crystal flow rate to 0.1 mL h^{-1} decreased the fibers diameter and some parts of the hybrid PLA/PE-b-PEO electrospun fibers was covered by the EBBA nematic liquid crystal. For the flow rate of 0.5 mL h^{-1}, the fiber length and the diameter was maintained and the fibers were covered by the EBBA nematic liquid crystal. With the increase of the EBBA liquid crystal solution flow rate (1,2 and 3 mL h^{-1}), the hybrid PLA/PE-b-PEO/EBBA electrospun fibers became more numerous, obtaining thicker mats. The best results were obtained for an EBBA liquid crystal solution flow rate of 5 mL h^{-1} as in the case of the hybrid PLA/EBBA electrospun fibers (Figure 5.10).

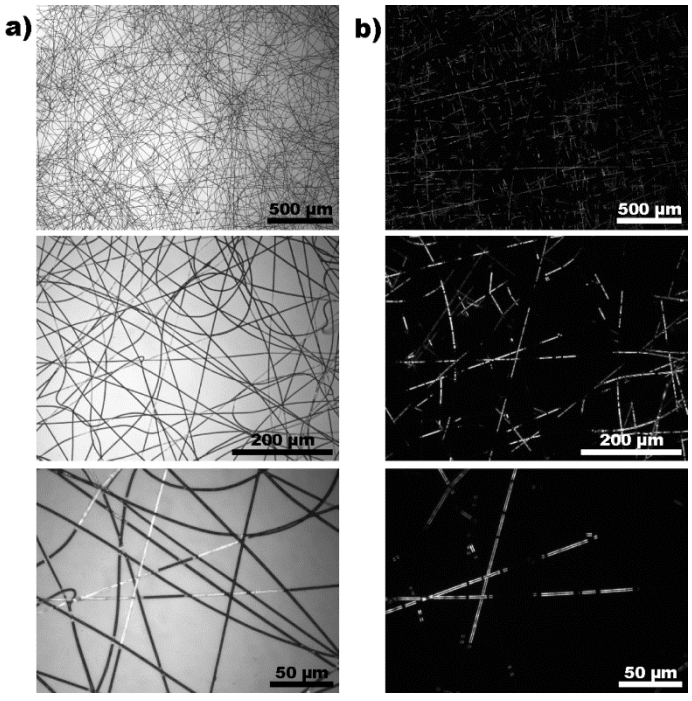

Figure 5.10. OM micrographs a) without crossed polarized and b) with crossed polarizers of the hybrid PLA/PE-b-PEO/EBBA electrospun fibers obtained for 10 wt % of PLA and 10 wt % of PE-b-PEO block copolymer with the molar ratio 50:50 in a mixture of chloroform/DMF solvents (4:1) and 10 wt % of EBBA nematic liquid crystal in a mixture of chloroform/DMF solvents (4:1), applying a voltage difference of 14 kV, PLA solution flow rate of 2 mL h^{-1} and EBBA liquid crystal solution flow rate of 5 mL h^{-1}.

5.4. Conclusions

Nanostructured PE-b-PEO block copolymer electrospun fibers were fabricated using electrospinning technique. Block copolymer solution concentration and in consequence their viscosity, have strong influence on the characteristics of obtained fibers.

Concentrations of around 40 wt % of block copolymer in chloroform or the mixture of chloroform/DMF solvents led to electrospun fibers. According to the OM images, these fibers were better formed in a mixture of chloroform/DMF solvents than using chloroform as solvent. Consequently, DMF improved the electrospun fibers formation.

According to obtained results the best PE-b-PEO block copolymer fibers were fabricated using the 46 wt % of PE-b-PEO block copolymer in a mixture of chloroform/DMF solvents (5:1), applying a voltage difference of 22 kV, solvent flow rate of 0.1 mL h^{-1} and block copolymer solution flow rate of 1 mL h^{-1}.

Moreover, the hybrid PE-b-PEO/EBBA electrospun fibers were also developed following the same electrospinning processing window. The EBBA nematic liquid crystal improved the hybrid PE-b-PEO/EBBA electrospun fibers formation in width and length for the higher block copolymer flow rate (5 mL h^{-1}).

The addition of the EBBA nematic liquid crystal provokes changes in the fiber morphology resulted in well-ordered lamellar structure. Regarding the hybrid PE-b-PEO/EBBA electrospun fibers developed following the same electrospinning processing window, was observed that the EBBA nematic liquid crystal improved the hybrid PE-b-PEO/EBBA electrospun fibers formation in width and length for the higher block copolymer flow rate (5 mL h^{-1}), provoking changes on fiber morphology resulting in well-ordered lamellar structure.

The addition of the PE-b-PEO block copolymer to the PLA solution improved the PLA/PE-b-PEO/EBBA electrospun fibers formation if compare to the PLA/EBBA electrospun fibers. The beads which appeared in the hybrid PLA/EBBA electrospun fibers disappeared with the addition of the PE-b-PEO block copolymer.

EBBA nematic liquid crystal covered the surface of the PLA/EBBA and

PLA/PE-b-PEO/EBBA electrospun fibers as confirmed by OM.

This investigation work proved that co-electrospinning technique can be successfully employed for fabrication of the hybrid materials based on the PE-b-PEO block copolymer and the EBBA nematic liquid crystal, maintaining the nematic liquid crystal character in the obtained hybrid electrospun fibers.

5.5. References

[1] Kongkhlang T, Kotaki M, Kousaka Y, Umemura T, Nakaya D, Chirachanchai S. Electrospun polyoxymethylene: Spinning conditions and its consequent nanoporous nanofiber. Macromolecules 2008;41:4746-4752.

[2] Sonseca A, Peponi L, Sahuquillo O, Kenny JM, Giménez E. Electrospinning of biodegradable polylactide/hydroxyapatite nanofibers: Study on the morphology, crystallinity structure and thermal stability. Polym. Degrad. Stabil. 2012;97:2052-2059.

[3] Li Y, Lim CT, Kotaki M. Study on structural and mechanical properties of porous PLA nanofibers electrospun by channel-based electrospinning system. Polymer 2015;56:572-580.

[4] Katsogiannis KAG, Vladisavljevic GT, Georgiadou S. Porous electrospun polycaprolactone (PCL) fibres by phase separation. Eur. Polym. J. 2015;69:284-295.

[5] Wang B, Li B, Xiong J, Li CY. Hierarchically ordered polymer nanofibers via electrospinning and controlled polymer crystallization. Macromolecules 2008;41:9516-9521.

[6] Li WJ, Cooper Jr JA, Mauck RL, Tuan RS. Fabrication and characterization of six electrospun poly(α-hydroxy ester)-based fibrous scaffolds for tissue engineering applications. Acta Biomater. 2006;2:377-385.

[7] Tao J, Shivkumar S. Molecular weight dependent structural regimes during the electrospinning of PVA. Mater. Lett. 2007;61:2352-2328.

[8] Luu YK, Kim K, Hsiao BS, Chu B, Hadjiargyrou M. Development of a nanostructured DNA delivery scaffold via electrospinning of PLGA and PLA-PEG block copolymers. J. Control. Release. 2003;89:341-353.

[9] Chen X, Dong B, Wang B, Shah R, Li CY. Crystalline block copolymer decorated, hierarchically ordered polymer nanofibers. Macromolecules 2010;43:9918-9927.

[10] Cho SJ, Jung SM, Kang M, Shin HS, Youk JM. Preparation of hydrophilic PCL nanofiber scaffolds via electrospinning of PCL/PVP-b-PCL block copolymers for enhanced cell biocompatibility. Polymer 2015;69:95-102.

[11] Valtola L, Koponen A, Karesoja M, Hietala S, Laukkanen A. Tailored surface properties of semi-fluorinated block copolymers y electrospinning. Polymer 2009;50:3103-3110.

[12] Bayley GM, Mallon PE. Porous micro fibers by the electrospinning of amphiphilic graft copolymer solutions with multi-walled carbon nanotubes. Polymer 2012;53:5523-5539.

[13] Luu YK, Kim K, Hsiao BS, Chu B, Hadjiargyrou M. Development of a nanostructured DNA delivery scaffold via electrospinning of PLGA and PLA-PEG block copolymers. J. Control. Realase 2003;89:341-353.

[14] Mascia L, Su R, Clarke J, Lou Y, Mele E. Fibres from blends of epoxidized natural rubber and polylactic acid by the electrospinning process: Compatibilization and surface texture. Eur. Polym. J. 2017;241:241-254.

[15] Schiffman JD, Schauer CL. A review: Electrospinning of biopolymer nanofibers and their applications. Polym. Rev. 2008;48:317-352.

[16] Enz E, Lagerwall J. Electrospun microfibres with temperature sensitive iridescence from encapsulated cholesteric liquid crystal. J. Mater. Chem. 2010;20:6866-6872.

[17] Enz E, Beumeister U, Lagerwall J. Coaxial electrospinning of liquid crystal-containing poly(vinylpyrrolidone) microfibers. J. Org. Chem. 2009;5:1-8.

[18] Kye Y, Kim C, Lagerwall J. Multifunctional responsive fibers produced by dual liquid crystal core electrospinning. J. Mater. Chem. C 2015;3:8979-8985.

[19] Bazilevsky AV, Yarin AL, Megaridis CM. Co-electrospinning of core-shell using a single-nozzle technique. Langmuir 2007;23:2311-2314.

[20] Jiang G, Qin X. An improved free surface electrospinning for high through put manufacturing of core-shell nanofibers. Mater. Lett. 2014;128:259-262.

[21] Sun Z, Zussman E, Yarin AL, Wendorff JH, Greiner A. Compound core-shell polymer nanofibers by co-electrospinning. Adv. Mater. 2003;22:1929-1932.

[22] Zhang JF, Yang DZ, Xu F, Zhang ZP, Yin RX, Nie J. Electrospun core-shell structure nanofibers from homogeneous solution of poly(ethylene oxide)/chitosan. Macromolecules 2009;42:15278-5284.

[23] Llorens E, Ibañez H, del Valle LJ, Puiggalí J. Biocompatibility and drug release behavior of scaffolds prepared by coaxial electrospinning of poly(butylene succinate) and polyethylene glycol. Mater. Sci. Eng. 2015;49:472-484.

[24] Mujica-Garcia A, Navarro-Baena I, Kenny JM, Peponi L. Influence of the processing parameters on the electrospinning of biopolymeric fibers. J. Renew. Mater. 2014;2:23-34.

[25] Arrieta MP, López J, López D, Kenny JM, Peponi L. Development of flexible materials based on plasticized electrospun PLA-PHB blends: Structural, thermal, mechanical and disintegration properties. Eur. Polym. J. 2015;73:433-446.

[26] Jiménez A, Peltzer M, Ruseckaite R. Electrospinning of PLA, poly(lactic acid) science and technology: Processing, properties, additives and applications. Royal

Society of Chemistry. Cambridge (UK), 2015.

[27] Rogina A. Electrospinning process: Versatile preparation method for biodegradable and natural polymers and biocomposite systems applied in tissue engineering and drug delivery. App. Surf. Sci. 2014;296:221-230.

[28] Nista SVG, Bettini J, Mei LHI. Coaxial nanofibers of chitosan-alginate-PEO polycomplex obtained by electrospinning. Carbohyd. Polym. 2015;127:222-228.

[29] Tian L, Ziqiang S, Jianquan W, Mujia G. Fabrication of hydroxyapatite nanoparticles decorated cellulose triacetate nanofibers for protein adsorption by coaxial electrospinning. Chem. Eng. J. 2015;260:818-825.

[30] Castillo-Ortega MM, Montaño-Figueroa AG, Rodriguez-Félix DE, Munive GT, Herrera-Franco PJ. Amoxicillin embedded in cellulose acetate-poly (vinyl pyrrolidone) fibers prepared by coaxial electrospinning: Preparation and characterization. Mater. Lett. 2012;76:250-254.

[31] Longson TJ, Bhowmick R, Gu C, Cruden BA. Core-shell interactions in coaxial electrospinning and impact on electrospun multiwall carbon nanotube core, poly(methyl methacrylate) shell fibers. J. Phys. Chem. 2011;115:12742-12750.

[32] Sung YK, Ahn BW, Kang TJ, Magnetic nanofibers with core (Fe_3O_4 nanoparticlesuspension)/sheath (polyethyleneterephthalate) structure fabricated by coaxial electrospinning. Magn. J. 2012;324:916-922.

[33] Song T, Zhang YZ, Zhou TJ. Fabrication of magnetic composite nanofibers of poly(ε-caprolactone) with FePt nanoparticles by coaxial electrospinning. J. Magn. Magn Mater. 2006;303:e286-e289.

[34] Tiwari SK, Tzezana R, Zussman E, Venkatraman SS. Optimizing partition-controlled drug release from electrospun core-shell fibers. Int. J. Pharmaceut. 2010;392:209-217.

[35] Brandrup J, Immergut EH, Grulke EA, Abe A, Bloch DR. Polymer handbook. Forth Ed., John Wiley & Sons. New York (USA), 1999.

[36] Soule SA, Cashman KV. The mechanical properties of solidified polyethylene glycol 600, an analog for lava crust. J. Volcanol. Geoth. Res. 2004;129:139-153.

[37] Rajgarhia SS, Benavides RE, Jana SC. Morphology control of bi-component polymer nanofibers produced by gas jet process. Polymer 2016;93:142-151.

PE-b-PEO block copolymer nanostructured thermosetting system as template for TiO_2 nanoparticles

6

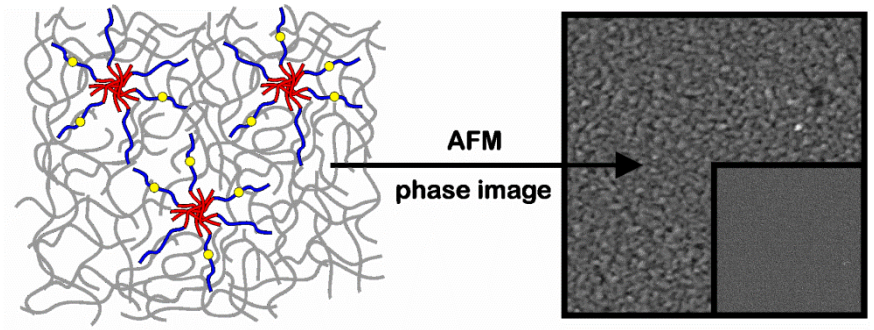

DGEBA/MCDEA system modified with PE-b-PEO and TiO_2 nanoparticles

6. PE-b-PEO block copolymer nanostructured thermosetting system as template for TiO_2 nanoparticles

In this Chapter, two different molecular weight and blocks molar ratio PE-b-PEO block copolymers will be used as nanostructuration agent for the epoxy based thermosetting system and as surfactant for the sol-gel synthesized titanium dioxide (TiO_2) nanoparticles. The miscibility between the DGEBA epoxy resin and the PE-b-PEO block copolymers and the influence of the addition of the PE-b-PEO block copolymers on the curing reaction time of the epoxy based thermosetting systems will be studied by DSC technique. The morphology of the epoxy based thermosetting systems and the dispersion of the TiO_2 nanoparticles in these systems will be investigated by the AFM phase images. UV-vis spectroscopy will be employed to analyze the transparency of these thermosetting systems, and the surface properties of these epoxy based thermosetting systems will be characterized by the water contact angle.

6.1. Introduction

Epoxy based thermosetting systems used as matrix display an excellent chemical resistance, good mechanical properties and thermal stability. However, their main drawback is the brittleness [1-4]. In order to decrease the brittleness and increase the toughness, these thermosetting systems are modified with block copolymers [4,5-14] or with inorganic nanoparticles [3,15-19].

As it is well known, the addition of block copolymer reduced the modulus of the epoxy based thermosetting systems and the use of the rigid inorganic particles can increased the toughness without affecting the high glass transition temperature of the epoxy based thermosetting matrix. This is a desirable property of many applications of these materials [1,14,18,20-28].

On the one hand, the use of amphiphilic block copolymers resulted in its self-assembly during polymerization reaction and in the partial miscibility of one of blocks of block copolymer with the epoxy resin. In this work, the amphiphilic PE-b-PEO block copolymer was used as both nanostructuration agent and as template for TiO_2 nanoparticles. Moreover, the PEO block of the PE-b-PEO block copolymer was

miscible with both, the DGEBA epoxy resin [4,33,34] and the sol-gel synthesized inorganic nanoparticles [2,23,28].

The use of the block copolymers allows to obtain different nanostructures as a function of the composition and the molecular weight [4,5,8-10,12,13,21-24,29-32].

On the other hand, the addition of inorganic nanoparticles permits to obtain epoxy based thermosetting systems with combined optical, mechanical, magnetic and optoelectronic properties [2,3,15,17,18]. It is crucial to achieve a homogeneous dispersion of the inorganic nanoparticles since the final properties are closely related to this point [2,15,17-19,23,26].

The use of the block copolymers and the inorganic nanoparticles jointly is an effective pathway to achieve epoxy based thermosetting systems with synergistic and tunable properties [2,15,17,18,23,26-28]. In this kind of thermoset materials the block copolymer acted as nanostructuration agent and as surfactant for the dispersion of inorganic nanoparticles, leading to well-dispersed inorganic nanoparticles in the nanostructured thermosetting systems.

The purpose of this Chapter was the use of the PE-b-PEO nanostructured thermosetting systems as template for dispersion and localization of the TiO_2 nanoparticles. The effect of the molecular weight and molar ratio between the blocks of the PE-b-PEO block copolymer on the dispersion of the TiO_2 nanoparticles was also investigated. The miscibility between the DGEBA epoxy resin as well as the DGEBA/MCDEA matrix and the PE-b-PEO block copolymers was study as key parameter responsible for the dispersion of the TiO_2 nanoparticles.

6.2. Materials and characterization techniques

6.2.1. Materials

Two different PE-b-PEO diblock copolymers, one with an average molecular weight of 920 g mol^{-1} and 50 wt % of PEO block content and the other one with an average molecular weight of 2250 g mol^{-1} and 80 wt % of PEO block content, were employed in this Chapter as modifiers. The PE-b-PEO block copolymer with lower molecular weight was denominated LPE-b-PEO while higher molecular weight block copolymer was named HPE-b-PEO.

Additionally, the DGEBA epoxy resin was cured with a stoichiometric amount of the aromatic amine curing agent MCDEA.

For the fabrication of the TiO_2 nanoparticles via sol-gel synthesis, titanium isopropoxide ($Ti(OCH(CH_3)_2)_4$) was used as precursor and was provided by Sigma-Aldrich. In addition, isopropanol, hydrochloric acid (HCl, 37 %) and toluene were analytical grade. All these materials were used as received, without further purification.

6.2.2. Sample preparation

6.2.2.1. Sol-gel synthesis

The titanium sol-gel solution was obtained according to the procedure published by Gutierrez et al. [2,35]. The sol-gel solution was prepared mixing 0.125 mmol of titanium isopropoxide, 5 mL of isopropanol, 0.125 mmol of an aqueous HCl and 5 mL of toluene under vigorous stirring for 1 h.

6.2.2.2. Blending protocol

The thermosetting systems modified with the PE-b-PEO block copolymers were prepared as follows. First, adequate amount of the PE-b-PEO block copolymer and the DGEBA epoxy resin were mixed and manually stirred at 80 °C in an oil bath until a homogenous mixture was achieved. Then, the curing agent, MCDEA, was added and stirred 30 s before curing reaction.

On the other hand, thermosetting systems modified with both PE-b-PEO block copolymers and the sol-gel synthesized TiO_2 nanoparticles were also prepared. First, the desired amount of the sol-gel solution was added to the DGEBA epoxy resin and mixed at 80 °C for 10 min. Then, an adequate amount of the PE-b-PEO block copolymer was added to the mixture and after mixing with manual stirring, MCDEA was added and stirred 30 s before curing reaction. Finally, all investigated thermosetting systems were degassed in vacuum and cured at 190 °C for 4 h.

Apart from neat DGEBA/MCDEA system, the thermosetting systems modified with the PE-b-PEO block copolymers (5, 10, 20 and 40 wt % of LPE-b-PEO or HPE-b-PEO block copolymers) and the same PE-b-PEO block copolymers and the sol-gel synthesized TiO_2 nanoparticles were prepared. The thermosetting systems modified with both the PE-b-PEO block copolymers and synthesized TiO_2 nanoparticles were prepared with a molar ratio 50:50.

All investigated thermosetting systems were carried out in 1 mm thick mold, consequently obtained results are referred to the bulk conditions.

6.2.3. Characterization techniques

6.2.3.1. Differential scanning calorimetry

DSC measurements were performed using a Mettler Toledo DSC 822e differential scanning calorimeter under a nitrogen flow of 25 mL min^{-1}. All investigated epoxy based thermosetting systems were encapsulated in aluminum pans using a weight of all samples around 10 mg.

The curing reaction of neat DGEBA/MCDEA system and the PE-b-PEO block copolymer modified thermosetting systems was analyzed by means of an isothermal scan at 190 ºC during 2 h.

In order to study the miscibility of two different PE-b-PEO block copolymers with the DGEBA epoxy resin, a dynamic scan was performed from -25 to 150 °C at 5 °C min^{-1}.

Thermal transition temperatures of all investigated thermosetting systems were determined using dynamic scans performed from -50 to 220 ºC with a heating rate of 5 ºC min^{-1}. Prior to this scan, a heating from -50 to 220 ºC followed by a cooling from 220 to -25 ºC at 5 ºC min^{-1} were carried out in order to remove the thermal history of the investigated material.

The crystallization degree (X_c) was calculated using the following equation [36,37]:

$$X_c = \frac{\Delta Hex}{\omega \Delta H100\%} \text{ x } 100$$

where ω was the weight fraction of the component of mixture for which the degree of crystallization was calculated and $\Delta H_{100\%}$ was the theoretical melting enthalpy of investigated material in the 100 % crystalline state. The experimental enthalpy of the melting transition, ΔH_{ex}, was calculated from the area of the endothermic peak during heating.

Moreover, the Fox equation was applied with the aim of confirming the partial miscibility between the PE-b-PEO block copolymer and the DGEBA epoxy resin [38]. The T_g of the PEO block and the PE block of the PE-b-PEO block copolymer were -65 and -33 ºC, respectively [39,40].

6.2.3.2. Fourier transform infrared spectroscopy

FTIR was performed using a Nicolet Nexus 670 spectrometer equipped with a single horizontal Golden Gate cell (ATR). Spectra were recorded in the range from 600 to 4000 cm^{-1}, with 2 cm^{-1} resolution and an accumulation of 20 scans.

6.2.3.3. UV-visible spectroscopy

The optical transparency of all investigated thermosetting systems was studied using a UV-3600, Shimadzu UV-VIS-NIR spectrophotometer in the range from 200 to 800 nm.

6.2.3.4. Atomic force microscopy

The morphology of all investigated thermosetting systems was studied by AFM. For AFM measurements, the investigated thermosetting systems were cut using an ultramicrotome Leica Ultracut R with a diamond blade. Transversal cross-section surface of all investigated thermosetting systems was analyzed. AFM images were obtained using a scanning probe microscope (Nanoscope IIIa Multimode^{TM}, Digital Instruments). Tapping mode (TM) was employed in air using an integrated tip/ cantilever (125 mm in length with ca. 300 kHz resonant frequency).

6.2.3.5. Water contact angle

Water contact angle measurements of the DGEBA/MCDEA cured system and the DGEBA/MCDEA based thermosetting systems were carried out using Data Physics OCA 20 contact angle system at ambient temperature. 3 mL distilled water drop was used for each measurement. At least five measurements were made for each investigated thermosetting system.

6.3. Results and discussion

6.3.1. Miscibility of the PE-b-PEO/ DGEBA uncured mixtures by DSC

The miscibility of the DGEBA epoxy resin with the PE-b-PEO block copolymers was studied by DSC technique. DSC thermograms of the PE-b-PEO/DGEBA uncured mixtures are shown in Figure 6.1.

All investigated PE-b-PEO/DGEBA uncured mixtures possessed a unique T_g indicating a partial miscibility between the components. The T_g of the DGEBA epoxy resin, at -18 ºC, shifted to lower temperatures with the increase of the PE-b-PEO block copolymer content independent on the use of the LPE-b-PEO or HPE-b-PEO block copolymers. In both cases, the T_m of the PEO block of the PE-b-PEO block copolymers rich phase was detected only for the 40PE-b-PEO/DGEBA uncured mixtures.

Moreover, in both cases, the T_m of the PEO block of the PE-b-PEO block copolymer rich phase shifted to lower temperature if compare to the T_m of the PEO block of the PE-b-PEO block copolymer. The T_m of the PEO block in the 40LPE-b-PEO/DGEBA uncured mixture moved from 35 ºC for neat LPE-b-PEO block copolymer to 28 ºC. Similar behavior was observed for the 40HPE-b-PEO/DGEBA uncured mixture, where the T_m shifted 7 ºC, being 57 ºC for neat HPE-b-PEO block copolymer and 50 ºC for the 40HPE-b-PEO/DGEBA uncured mixture.

These results confirm the partial miscibility between the PEO block of the PE-b-PEO block copolymer and the DGEBA epoxy resin in the investigated uncured mixtures [4,33,34].

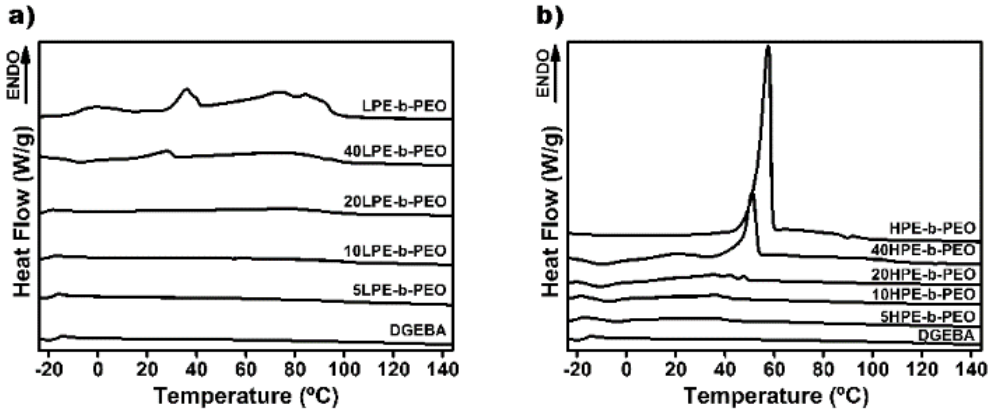

Figure 6.1. DSC thermograms of the DGEBA epoxy resin and the PE-b-PEO/DGEBA uncured mixtures with 5, 10, 20 and 40 wt % of a) LPE-b-PEO and b) HPE-b-PEO block copolymers.

Additionally, the crystallization degree of the PEO block rich phases in the PE-b-PEO/DGEBA uncured mixtures was calculated. Crystallization degree of the PEO block was maintained in the case of the 40LPE-b-PEO/DGEBA blend with respect to the LPE-b-PEO block copolymer, 14 %, and decreased from 68 % to 54 % in the case of the 40HPE-b-PEO/DGEBA blend in comparison with the crystallization degree of the HPE-b-PEO block copolymer, which corroborated the partial miscibility between components.

6.3.2. Effect of the addition of the PE-b-PEO block copolymers on the curing reaction by DSC

In order to study the effect of the addition of the PE-b-PEO block copolymer on the curing reaction, the DGEBA/MCDEA based thermosetting systems modified with 5, 10, 20 and 40 wt % of PE-b-PEO block copolymer were studied as shown in Figure 6.2.

For comparison, isothermal DSC thermograms of neat DGEBA/MCDEA system were also shown.

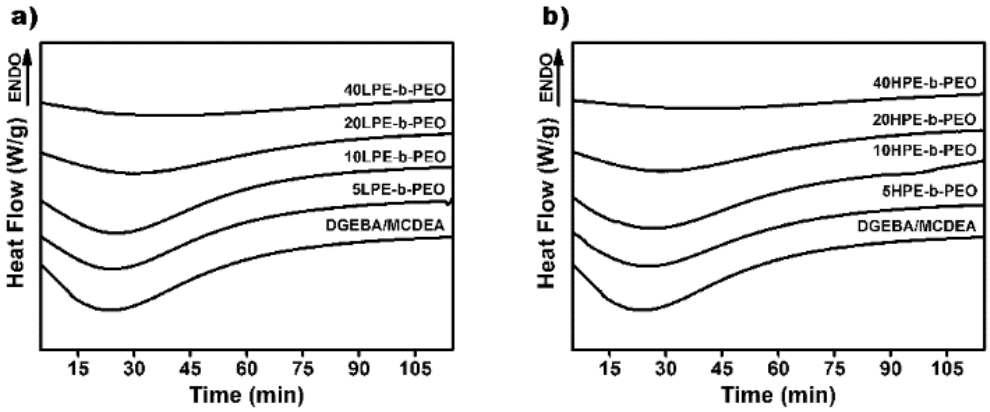

Figure 6.2. Isothermal DSC thermograms at 190 ºC of neat DGEBA/MCDEA system and the PE-b-PEO(DGEBA/MCDEA) systems fabricated using a) LPE-b-PEO and b) HPE-b-PEO block copolymer.

All investigated thermosetting systems modified with the LPE-b-PEO block copolymer (Figure 6.2a) and with the HPE-b-PEO block copolymer (Figure 6.2b) showed a delay of the curing reaction with the increase of the PE-b-PEO block copolymer content if compared to neat DGEBA/MCDEA system, being slightly more pronounced in the case of the HPE-b-PEO(DGEBA/MCDEA) systems.

In the case of neat DGEBA/MCDEA system, the maximum curing reaction time was achieved at 23 min while the highest delay was detected for 40 wt % of LPE-b-PEO block copolymer being the maximum cure reaction time equal to 39 min.

Similar behavior was observed in the thermosetting systems modified with HPE-b-PEO block copolymer, the curing reaction time delayed from 25 to 40 min with the addition of 5 and 40 wt % of PE-b-PEO block copolymer, respectively.

As it is well known, this behavior is related to the dilution effect of the PEO block of the PE-b-PEO block copolymer on the curing reaction of the DGEBA/MCDEA system [4, 33, 34]. Thus, the ether groups of the PEO block of the PE-b-PEO block copolymer can form hydrogen bonds with the OH groups of the DGEBA epoxy resin and, consequently, delayed curing reaction [4,28,35-38].

FTIR spectra of the thermosetting systems modified with both the PE-b-PEO block copolymers and the same block copolymers and TiO_2 nanoparticles, confirmed the formation of these hydrogen bonds.

As can be clearly observed, the OH groups at 3300-3400 cm^{-1} shifted to lower wavelengths as can be visualized in Figure 6.3.

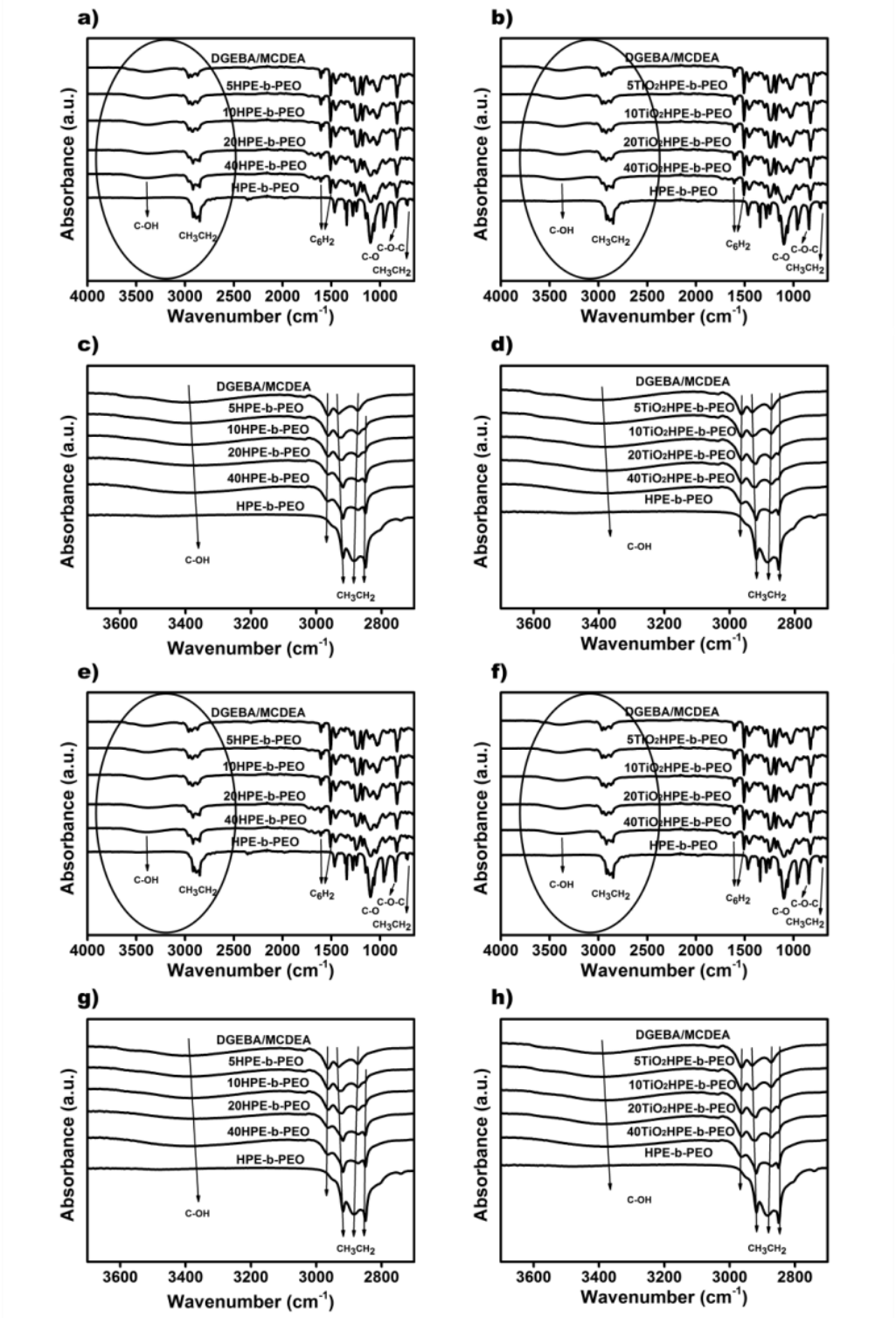

Figure 6.3. FTIR spectra of the a) LPE-b-PEO(DGEBA/MCDEA) b) TiO_2LPE-b-PEO(DGEBA/MCDEA) e) HPE-b-PEO(DGEBA/MCDEA) and f) TiO_2HPE-b-PEO(DGEBA/MCDEA) cured systems and FTIR spectra from 2700 cm^{-1} to 3700 cm^{-1} of the c) LPE-b-PEO(DGEBA/MCDEA) d) TiO_2LPE-b-PEO(DGEBA/MCDEA) g) HPE-b-PEO(DGEBA/MCDEA) h) TiO_2HPE-b-PEO(DGEBA/MCDEA) cured systems. For comparison FTIR spectra of neat LPE-b-PEO and HPE-b-PEO block copolymers and neat DGEBA/MCDEA cured system were added.

6.3.3. Thermal behavior of the DGEBA/MCDEA based thermosetting systems by DSC

DSC thermograms of neat DGEBA/MCDEA cured system and the thermosetting systems modified with the LPE-b-PEO block copolymer and the same block copolymer and TiO_2 nanoparticles are shown in Figure 6.4.

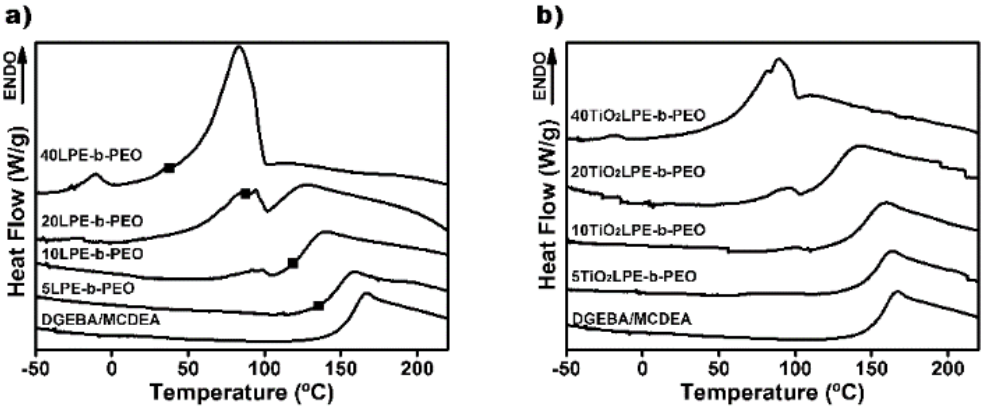

Figure 6.4. DSC thermograms of the a) LPE-b-PEO(DGEBA/MCDEA) cured systems with different LPE-b-PEO content and b) TiO_2LPE-b-PEO(DGEBA/MCDEA) cured systems with different TiO_2LPE-b-PEO content. For comparison DSC thermograms of neat DGEBA/MCDEA cured system was also added. Marked temperatures correspond to the theoretical T_gs calculated by Fox equation.

As can be observed, the T_g of neat DGEBA/MCDEA cured system, at 154 ºC, shifted to lower temperatures in the epoxy modified thermosetting systems. Taken into account the experimental results, showed in Table 6.1, the T_g of the DGEBA/MCDEA matrix decreased with the increasing of both the LPE-b-PEO and TiO_2LPE-b-PEO contents being a higher decreased in the case of neat DGEBA/MCDEA cured system modified only with the LPE-b-PEO block copolymer.

Thus, in the case of neat DGEBA/MCDEA cured systems modified with the LPE-b-PEO block copolymer, the PEO block is the partially miscible with the DGEBA/MCDEA matrix and in the case of the DGEBA/MCDEA cured systems modified with both the LPE-b-PEO block copolymer and TiO_2 nanoparticles, the PEO block is the partially miscible with the DGEBA/MCDEA matrix and acted as surfactant for synthesized nanoparticles.

The theoretical T_gs calculated using Fox equation [38] were highlighted in Figure 6.4a and collected in Table 6.1. The experimental T_gs were approximated to theoretical ones confirming the miscibility between the PEO block and the DGEBA/MCDEA matrix.

Table 6.1. The T_gs of neat DGEBA/MCDEA cured system and of the LPE-b-PEO(DGEBA/MCDEA) and TiO_2LPE-b-PEO(DGEBA/MCDEA) cured systems calculated from DSC thermograms and the theoretical T_g values calculated using the Fox equation.

Sample	Experimental T_g (ºC)	Theoretical T_g (ºC)
DGEBA/MCDEA	154	
5LPE-b-PEO(DGEBA/MCDEA)	145	135*
10LPE-b-PEO(DGEBA/MCDEA)	122	118*
20LPE-b-PEO(DGEBA/MCDEA)	111	88*
40LPE-b-PEO(DGEBA/MCDEA)	30	39*
5TiO_2LPE-b-PEO(DGEBA/MCDEA)	151	-
10TiO_2LPE-b-PEO(DGEBA/MCDEA)	148	-
20TiO_2LPE-b-PEO(DGEBA/MCDEA)	125	-
40TiO_2LPE-b-PEO(DGEBA/MCDEA)	102	-
LPE-b-PEO	-65	

*The theoretical T_gs was calculated only for thermosetting systems modified with the LPE-b-PEO block copolymer.

As expected, the T_m of the PE block rich phase of the LPE-b-PEO(DGEBA/MCDEA) and TiO_2LPE-b-PEO(DGEBA/MCDEA) cured systems was detected only for more than 10 wt % of LPE-b-PEO block copolymer or 10 wt % of TiO_2LPE-b-PEO modifier content being the same for all systems confirming the immiscibility of the PE block of the LPE-b-PEO block copolymer with the DGEBA/MCDEA matrix.

On the contrary, the T_m of the PEO block of the LPE-b-PEO block copolymer was not detected in any investigated thermosetting system. This phenomenon can be related to the partial miscibility between the PEO block of the PE-b-PEO block copolymer and the DGEBA/MCDEA matrix and the low content of PEO block with respect to the whole thermosetting system (2,5 wt % of PEO block for 5 wt % and 20 wt % of PEO block for 40 wt %).

Figure 6.5 shown the DSC thermograms of the HPE-b-PEO(DGEBA/MCDEA) and TiO_2HPE-b-PEO(DGEBA/MCDEA) cured systems with different modifier content. The addition of the HPE-b-PEO block copolymer or the same block copolymer and TiO_2 nanoparticles to the DGEBA/MCDEA matrix, led to shift the T_g of the PEO block/(DGEBA/MCDEA) rich phase to lower temperature as shown Table 6.2.

Taking into account that the molar ratio between the HPE-b-PEO block copolymer and the TiO_2 nanoparticles was fixed to 50:50, for the same modifier amount the PEO block content in the TiO_2HPE-b-PEO(DGEBA/MCDEA) cured systems is two times lower than in the HPE-b-PEO(DGEBA/MCDEA) cured systems.

Consequently, the decrease of the T_g was less pronounced since there is low PEO block content which can interact with the DGEBA/MCDEA matrix.

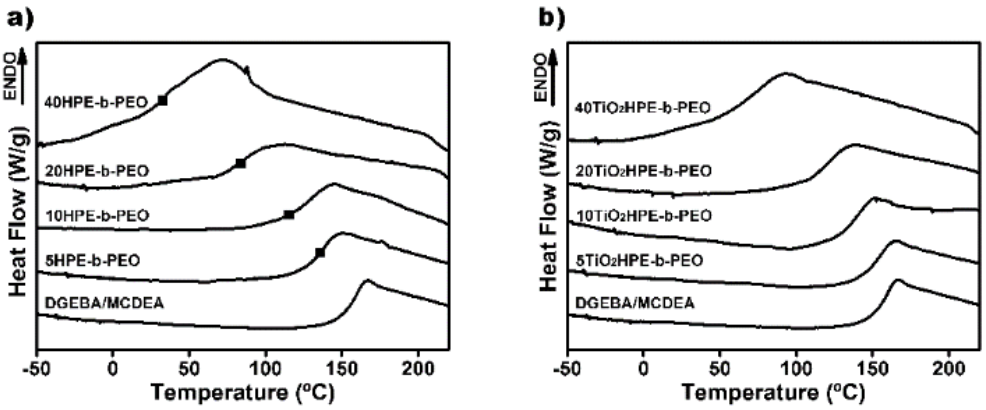

Figure 6.5. DSC thermograms of the a) HPE-b-PEO(DGEBA/MCDEA) cured systems with different HPE-b-PEO content and b) TiO_2HPE-b-PEO(DGEBA/MCDEA) cured systems with different TiO_2HPE-b-PEO content. For comparison DSC thermograms of neat DGEBA/MCDEA cured system was also added. Marked temperatures correspond to the theoretical T_gs calculated by the Fox equation.

Similar to the LPE-b-PEO(DGEBA/MCDEA) cured systems, the experimental T_gs of the HPE-b-PEO(DGEBA/MCDEA) cured systems approximated to the theoretical T_gs confirming the miscibility between the PEO block of the HPE-b-PEO block copolymer and the DGEBA/MCDEA matrix.

Table 6.2. The T_gs of neat DGEBA/MCDEA cured system and of the HPE-b-PEO/(DGEBA/MCDEA) and TiO_2HPE-b-PEO/(DGEBA/MCDEA) cured systems calculated from DSC thermograms and the theoretical T_g values calculated using the Fox equation.

Sample	Experimental T_g (ºC)	Theoretical T_g (ºC)
DGEBA/MCDEA	154	
5HPE-b-PEO(DGEBA/MCDEA)	136	134*
10HPE-b-PEO(DGEBA/MCDEA)	128	115*
20HPE-b-PEO(DGEBA/MCDEA)	85	83*
40HPE-b-PEO(DGEBA/MCDEA)	26	32*
5TiO_2HPE-b-PEO(DGEBA/MCDEA)	151	-
10TiO_2HPE-b-PEO(DGEBA/MCDEA)	139	-
20TiO_2HPE-b-PEO(DGEBA/MCDEA)	122	-
40TiO_2HPE-b-PEO(DGEBA/MCDEA)	108	-
HPE-b-PEO	-65	

*The theoretical T_gs was calculated only for thermosetting systems modified with the HPE-b-PEO block copolymer.

Moreover, the T_m of the PE block rich phase in both the HPE-b-PEO(DGEBA/MCDEA) and TiO_2HPE-b-PEO(DGEBA/MCDEA) cured systems was detected only for 40 wt % of modifier. This fact can be related to the low PE block

content in the HPE-b-PEO block copolymer (20 wt %) or the immiscibility of the PE block and the DGEBA/MCDEA matrix.

6.3.4. Transparency of the thermosetting systems by UV-vis

The optical transparency of the investigated thermosetting systems was studied using UV-vis spectroscopy. UV-vis transmittance spectra of the DGEBA/MCDEA cured system and all the thermosetting systems modified with the LPE-b-PEO block copolymer and the same block copolymer and TiO_2 nanoparticles are shown in Figure 6.6. Moreover, visual appearance of these systems, are displayed on the top of each figure.

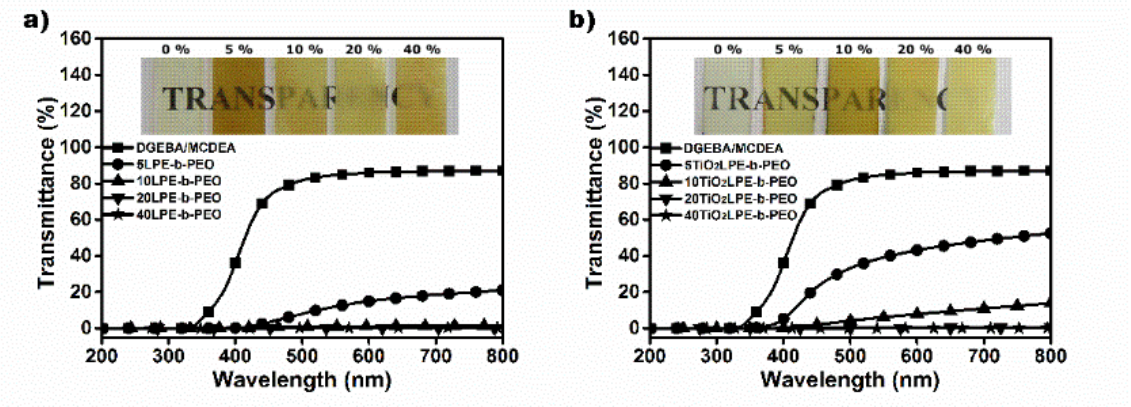

Figure. 6.6. UV-vis transmittance spectra of the different a) LPE-b-PEO(DGEBA/MCDEA) cured systems and b) TiO_2LPE-b-PEO(DGEBA/MCDEA) cured systems. For comparison UV-vis transmittance spectra of neat DGEBA/MCDEA cured system was also added. The inset on the top of each figure corresponds to the visual appearance of the investigated thermosetting systems.

As expected, neat DGEBA/MCDEA cured system was transparent at ambient temperature and possessed a good visible light transmittance, 86 % at 600 nm. The addition of the LPE-b-PEO block copolymer led to a significant decreasing in the transmittance suggesting the presence of heterogeneities or/and refractive index fluctuations in the epoxy based thermosetting systems modified with more than 10 wt % of modifier (Figure 6.6a and 6.6b) [41,42].

The visual appearance of the LPE-b-PEO(DGEBA/MCDEA) and TiO_2LPE-b-PEO(DGEBA/MCDEA) cured systems was showed on the top of Figures 6.6a and 6.6b, respectively. For both investigated thermosetting systems, transparent materials were obtained up to 10 wt % of modifier that is in a good agreement with the UV-vis results.

UV-vis transmittance spectra of the DGEBA/MCDEA cured system and all the thermosetting systems modified with the HPE-b-PEO block copolymer and the same

block copolymer and TiO_2 nanoparticles were shown in Figure 6.7.

Thermosetting systems modified with the HPE-b-PEO block copolymer (Figure 6.7a) showed higher visible light transmittance if compare with the thermosetting systems modified with the LPE-b-PEO block copolymer (Figure 6.6a). This could be due to the higher miscibility between the PEO block and the DGEBA/MCDEA matrix in the case of the HPE-b-PEO block copolymer (80 wt % of PEO block) than in the LPE-b-PEO block copolymer (50 wt % of PEO block).

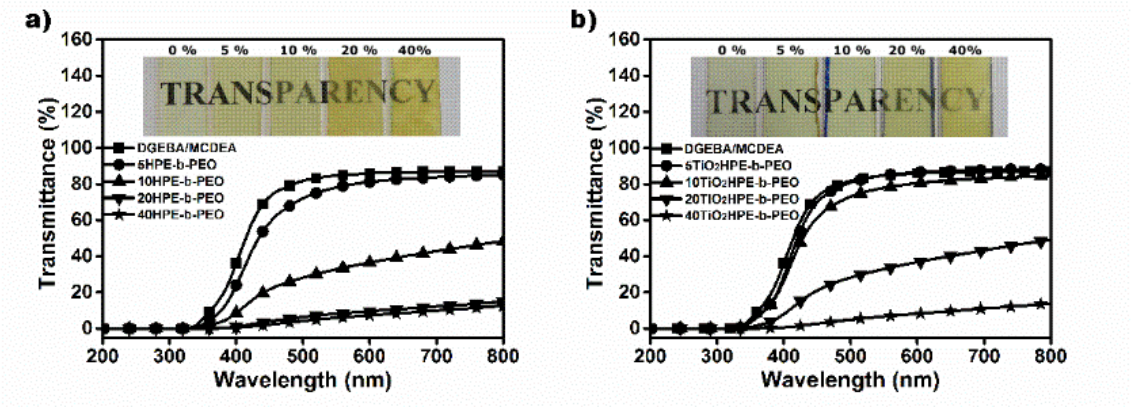

Figure. 6.7. UV-vis transmittance spectra of the different a) HPE-b-PEO(DGEBA/MCDEA) cured systems and b) TiO_2HPE-b-PEO(DGEBA/MCDEA) cured systems. For comparison UV-vis transmittance spectra of neat DGEBA/MCDEA cured system was also added. The inset on the top of each figure corresponds to the visual appearance of the investigated thermosetting systems.

The addition of more than 20 wt % of HPE-b-PEO block copolymer or TiO_2HPE-b-PEO modifier, led to decrease in the visible light transmittance suggesting heterogeneities or/and refractive index fluctuations in these systems, as explained above.

The visual appearance showed that the investigated thermosetting systems were transparent up to 20 wt % modifier, that is in a good agreement with the UV-vis results.

6.3.5. The morphology of the epoxy based thermosetting systems by AFM

The morphology of neat DGEBA/MCDEA cured system as well as all investigated thermosetting systems was analyzed by AFM.

As was expected, the AFM phase image of neat DGEBA/MCDEA cured system showed a regular and uniform morphology, without both micro- and macrophase separation as can be visualized in Figure 6.8.

AFM phase images of the thermosetting systems modified with the LPE-b-PEO block copolymer and the same block copolymer and TiO_2 nanoparticles are presented in Figure 6.9.

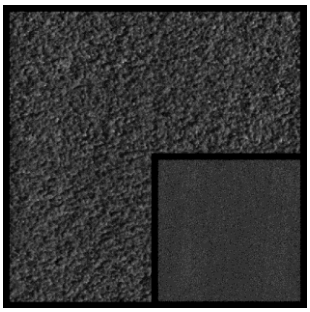

Figure 6.8. AFM phase images (750 nm x 750 nm) of neat DGEBA/MCDEA cured system. The insets at the bottom correspond to 3 μm x 3 μm AFM phase images.

Taken into account that only the PEO block of the PE-b-PEO block copolymer was miscible with the DGEBA/MCDEA matrix, in AFM phase images the PEO block (DGEBA/MCDEA) rich phase appeared as brightest areas while the PE block rich phase correspond to dark areas.

The addition of 5 wt % of LPE-b-PEO block copolymer led to the sphere-like morphology of microseparated PE block with phase domains with the average size of 8 ± 2 nm in diameter. The size of these domains increases with the addition of 10 wt % of LPE-b-PEO block copolymer forming in some case worm-like structure (Figure 6.9b). Similar morphology was observed for the 20LPE-b-PEO(DGEBA/MCDEA) cured system.

The addition of 40 wt % of LPE-b-PEO block copolymer led to a macrophase separated thermosetting system (Figure 6.9d). In this case, some part of the PEO block microseparate within the PE block phase. These results are in a good agreement with the UV-vis results.

AFM phase images of the TiO_2LPE-b-PEO(DGEBA/MCDEA) cured systems with different TiO_2LPE-b-PEO content are shown in Figures 6.9e-h. The molar ratio between the synthesized TiO_2 nanoparticles and the LPE-b-PEO block copolymer was fixed to be 50:50.

For the 5TiO_2LPE-b-PEO(DGEBA/MCDEA) cured system, sphere-like morphology was detected where darker areas correspond to the PE block rich phase domains (Figure 6.9e). The average size of the microseparated PE block rich phase domains was smaller than for the 5LPE-b-PEO(DGEBA/MCDEA) cured system (6 ± 2 nm).

Moreover, small brighter spots observed in AFM phase image correspond to the TiO_2 nanoparticles [2]. Inset of Figure 6.9e confirms the presence of TiO_2 nanoparticle aggregates.

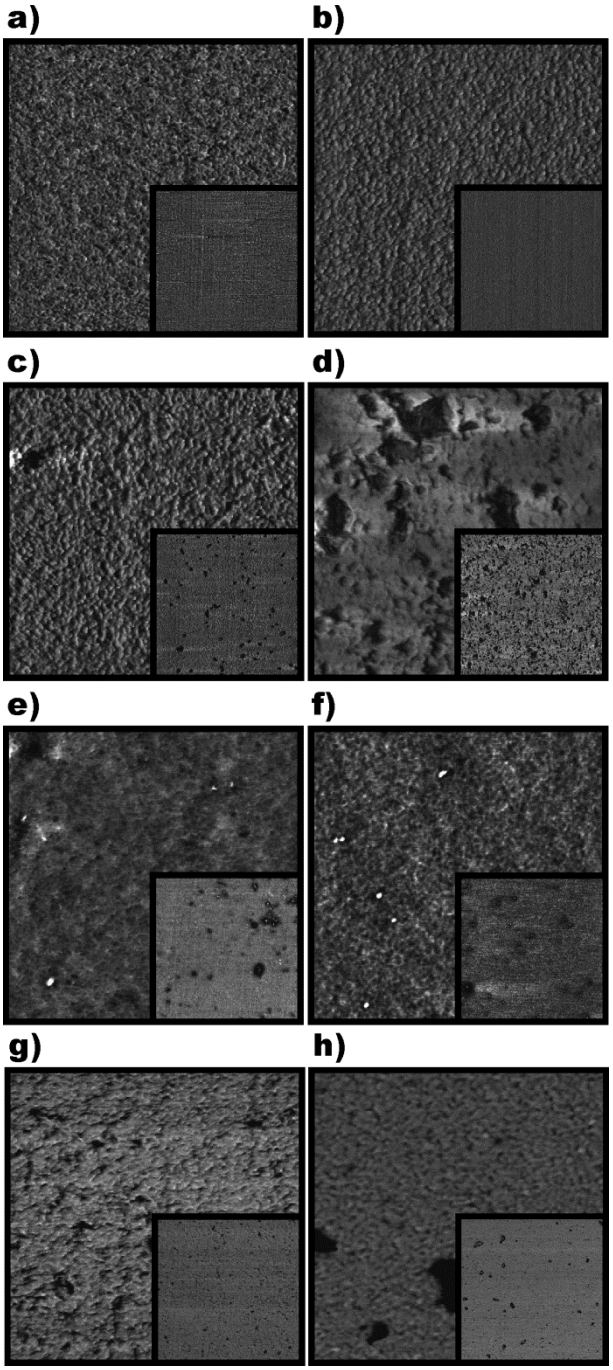

Figure 6.9. AFM phase images (750 nm x 750 nm) of the DGEBA/MCDEA thermosetting systems modified with a) 5, b) 10, c) 20 and d) 40 wt % of LPE-b-PEO block copolymer and e) 5, f) 10, g) 20 and h) 40 wt % of TiO_2LPE-b-PEO modifier. The insets at the bottom correspond to 3 μm x 3 μm AFM phase images.

This behavior can be related to the low PEO block content in the 5TiO_2LPE-b-PEO(DGEBA/MCDEA) cured system, only 1.25 wt %. Consequently, the amount of the PEO block is mostly miscible with the DGEBA/MCDEA matrix is not enough to act as surfactant for TiO_2 nanoparticles. Thus, the aggregation of the TiO_2 nanoparticles can be clearly distinguished, as shown in Figure 6.9e. This behavior was represented in Scheme 6.1.

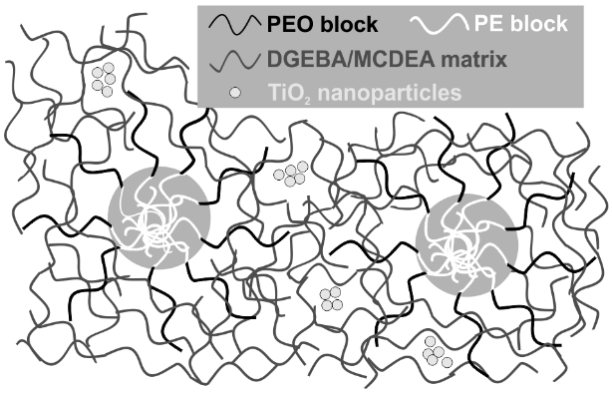

Scheme 6.1. TiO_2 nanoparticles aggregates in the 5TiO_2LPE-b-PEO(DGEBA/MCDEA) cured system.

The addition of 10 wt % of TiO_2LPE-b-PEO provoked an increase of the sphere-like PE block rich phase domains, and simultaneously an improvement of dispersion of the TiO_2 nanoparticles can be also detected (see inset of Figure 6.9f). The modification of the DGEBA/MCDEA cured system with 20 wt % of TiO_2LPE-b-PEO changed the morphology from sphere-like to worm-like one. Small bright spots correspond to the TiO_2 nanoparticles, which are also visible in AFM phase image of this thermosetting system. These TiO_2 nanoparticles were well dispersed in the PEO block (DGEBA/MCDEA) matrix and located preferably in the interface with the microseparated PE block domains (Figure 6.9g). The size of the TiO_2 nanoparticles was smaller in the case of the 20TiO_2LPE-b-PEO(DGEBA/MCDEA) cured system if compare with thermosetting systems modified with less TiO_2LPE-b-PEO modifier content. This can be related to the fact, that in this thermosetting system, one part of the PEO block is miscible with the DGEBA/MCDEA matrix and the other one partially covered the TiO_2 nanoparticles [2]. The thermosetting systems modified with 40 wt % of TiO_2LPE-b-PEO showed not only worm-like structure of the PE block rich phase but also a macroseparation of this phase, see inset of Figure 6.9h.

The difference in the morphology between the LPE-b-PEO(DGEBA/MCDEA) and TiO_2LPE-b-PEO(DGEBA/MCDEA) cured systems with the same LPE-b-PEO block copolymer was also analyzed.

As can be seen, Figures 6.9a and 6.9f, the 5LPE-b-PEO(DGEBA/MCDEA) and 10TiO_2LPE-b-PEO(DGEBA/MCDEA) cured systems, possessed sphere-like morphology with the very similar size. The only difference is in a bright TiO_2 nanoparticles clearly visualized in the 10TiO_2LPE-b-PEO(DGEBA/MCDEA) cured system. Similar tendency was also observed for the morphology of the 10LPE-b-PEO(DGEBA/MCDEA) and 20TiO_2LPE-b-PEO(DGEBA/MCDEA) cured systems.

Thus, the addition of TiO_2 nanoparticles did not affect the nanostructuration of the LPE-b-PEO block copolymer nanostructured thermosetting system.

Moreover, the root mean square roughness, R_q, and the average roughness, R_a, of the LPE-b-PEO block copolymer thermosetting systems were studied and date were collected in the Table 6.3.

Table 6.3. The R_q and R_a parameters corresponding to the LPE-b-PEO(DGEBA/MCDEA) and TiO_2LPE-b-PEO(DGEBA/MCDEA) cured systems.

Sample	R_q (nm)	R_a (nm)
5LPE-b-PEO(DGEBA/MCDEA)	0.9	0.7
10LPE-b-PEO(DGEBA/MCDEA)	1.9	1.6
20LPE-b-PEO(DGEBA/MCDEA)	1.5	1.2
40LPE-b-PEO(DGEBA/MCDEA)	4.5	3.3
5TiO_2LPE-b-PEO(DGEBA/MCDEA)	2.0	1.4
10TiO_2LPE-b-PEO(DGEBA/MCDEA)	0.9	0.7
20TiO_2LPE-b-PEO(DGEBA/MCDEA)	3.4	2.0
40TiO_2LPE-b-PEO(DGEBA/MCDEA)	0.8	0.6

The R_q and R_a of the thermosetting systems modified only with the LPE-b-PEO block copolymer increased with the addition of the LPE-b-PEO block copolymer.

As expected, the highest roughness values, R_q 4.5 and R_a 3.3 nm were found for the 40LPE-b-PEO(DGEBA/MCDEA) cured system. Thus, the macrophase separation of the PE block rich phase provoked an increase of the roughness surface.

The R_q and R_a of the TiO_2LPE-b-PEO(DGEBA/MCDEA) cured systems increased with the addition of 5 and 20 wt % of TiO_2LPE-b-PEO in comparison with the thermosetting systems modified with 10 and 40 wt % of TiO_2LPE-b-PEO.

In the case of the 5TiO_2LPE-b-PEO(DGEBA/MCDEA) cured system, the aggregation of the TiO_2 nanoparticles can be responsible for the increase of the roughness. In the case of the 20TiO_2LPE-b-PEO(DGEBA/MCDEA) cured system, the changes in the morphology from sphere-like to worm-like can increase the roughness of this system.

AFM phase images of the thermosetting systems modified with the HPE-b-PEO block copolymer are shown in Figure 6.10.

As well as for the thermosetting systems modified with the LPE-b-PEO block copolymer, the addition of 5 wt % of HPE-b-PEO block copolymer led to the sphere-like morphology. The size of these domains was smaller than in the thermosetting systems modified with the LPE-b-PEO block copolymer, probably due to the lower PE block

content in the HPE-b-PEO block copolymer (20 wt %). For the 10HPE-b-PEO(DGEBA/MCDEA) cured system the size of the sphere-like PE block rich phase domains increased, which resulted in some worm-like structures as shown in Figure 6.10b.

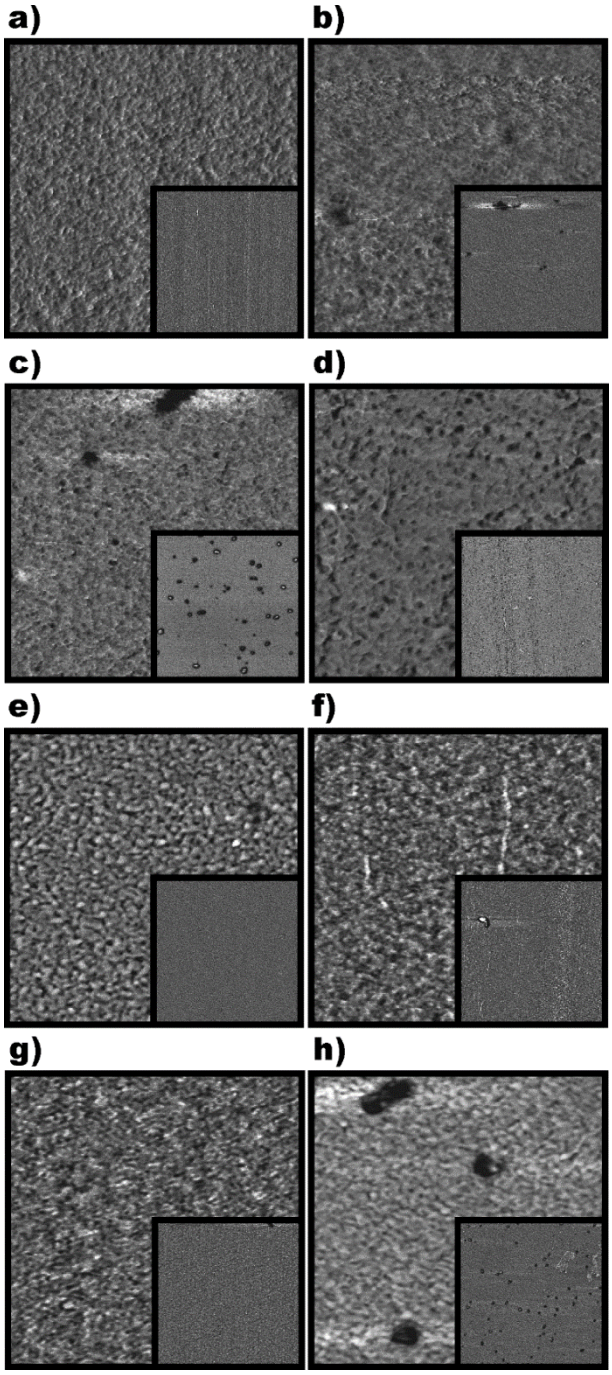

Figure 6.10. AFM phase images (750 nm x 750 nm) of the DGEBA/MCDEA thermosetting systems modified with a) 5, b) 10, c) 20 and d) 40 wt % of HPE-b-PEO block copolymer and e) 5, f) 10, g) 20 and h) 40 wt % of TiO_2HPE-b-PEO content. The insets at the bottom correspond to 3 μm x 3 μm AFM phase images.

The same worm-like morphology was observed for the 20HPE-b-PEO(DGEBA/MCDEA) cured system. Moreover, this thermosetting system showed

also a homogeneously distributed regular in size (50 ± 5 nm) brighter microseparated domains. This morphology is different if compare with the macrophase separated morphology of the 40HPE-b-PEO(DGEBA/MCDEA) cured system. Taken into account higher content of the PEO block in the HPE-b-PEO block copolymer and its higher molecular weight, these regular bright domains can be attributed to the separated PEO block rich phase surrounded by the PE block (inset of Figure 6.10c).

These results are in good agreement with UV-vis since the size of the separated domains is lower than 100 nm and do not altered transparency of the thermosetting systems (compare the UV-vis results of the 20HPE-b-PEO(DGEBA/MCDEA with the 40HPE-b-PEO(DGEBA/MCDEA) cured systems). The addition of 40 wt % of HPE-b-PEO block copolymer led to the sphere-like morphology with regular size 13 ± 2 nm in diameter (Figure 6.10d).

AFM phase images of the TiO_2HPE-b-PEO(DGEBA/MCDEA) cured systems modified with different HPE-b-PEO block copolymer and TiO_2 nanoparticles content are shown in Figures 6.10e-h.

The worm-like darker areas of the separated PE block rich phase domains can be easily distinguished when a 5 wt % of TiO_2HPE-b-PEO modifier was added to the DGEBA/MCDEA matrix (Figure 6.10e). Moreover, bright spots preferably located in the interface between the microphase separated of the PE block rich phase domains and the DGEBA/MCDEA matrix, were distinguished [26]. These bright spots correspond to the TiO_2 nanoparticles, as schematically illustrated in Scheme 6.2.

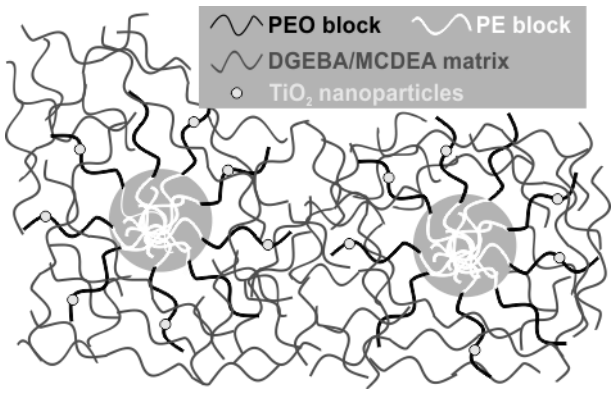

Scheme 6.2. TiO_2 nanoparticles preferably located in the interface between microphase separated PE block rich phase and DGEBA/MCDEA matrix.

The addition of the 10TiO_2HPE-b-PEO and 20TiO_2HPE-b-PEO modifier led to slight increase of the microphase separated PE block rich phase domains and increase of quantity of bright spots corresponding to the TiO_2 nanoparticles (Figures 6.10f and

6.10g). The 40TiO_2HPE-b-PEO(DGEBA/MCDEA) cured system maintained both worm-like morphology of the microphase separated PE block rich phase and good distribution of the TiO_2 nanoparticles (Figure 6.10h). Moreover, as for the 20HPE-b-PEO(DGEBA/MCDEA) cured system (with the same HPE-b-PEO content) smaller in size (35 ± 5 nm) the homogeneously distributed PEO block microphase separated domains was also detected (compare Figure 6.10c and 6.10h).

As for the thermosetting systems modified with the LPE-b-PEO block copolymer also in the case of the thermosetting systems modified with the HPE-b-PEO block copolymer, the R_q and R_a parameters were analyzed and represented in Table 6.4.

Table 6.4. The R_q and R_a parameters corresponding to the HPE-b-PEO(DGEBA/MCDEA) and TiO_2HPE-b-PEO(DGEBA/MCDEA) cured systems.

Sample	R_q (nm)	R_a (nm)
5HPE-b-PEO(DGEBA/MCDEA)	1.0	0.8
10HPE-b-PEO(DGEBA/MCDEA)	1.1	0.9
20HPE-b-PEO(DGEBA/MCDEA)	1.0	0.8
40HPE-b-PEO(DGEBA/MCDEA)	2.9	2.3
5TiO_2HPE-b-PEO(DGEBA/MCDEA)	1.4	1.1
10TiO_2HPE-b-PEO(DGEBA/MCDEA)	1.0	0.8
20TiO_2HPE-b-PEO(DGEBA/MCDEA)	0.5	0.4
40TiO_2HPE-b-PEO(DGEBA/MCDEA)	1.5	1.1

Similar tendency was observed when thermosetting systems were modified with the HPE-b-PEO block copolymer. The R_q and R_a values increased with the addition of the HPE-b-PEO block copolymer content, while 40 wt % of HPE-b-PEO block copolymer was added to the DGEBA/MCDEA matrix the highest roughness values, R_q 2.9 and R_a 2.3 nm, were obtained. This can be related to the macrophase separation.

A different behavior was observed in the case of the epoxy systems modified with the HPE-b-PEO block copolymer and TiO_2 nanoparticles. In the 5TiO_2LPE-b-PEO(DGEBA/MCDEA) and 40TiO_2LPE-b-PEO(DGEBA/MCDEA) cured systems a higher roughness was observed than in the 10TiO_2LPE-b-PEO(DGEBA/MCDEA) and 20TiO_2LPE-b-PEO(DGEBA/MCDEA) cured systems, which showed a lower roughness.

Generally, the roughness values were higher for the thermosetting systems fabricated with the LPE-b-PEO block copolymer if compare to the thermosetting systems fabricated with the HPE-b-PEO block copolymer. This fact can be related to the higher partial miscibility between the PEO block and the DGEBA/MCDEA matrix

in the case of the thermosetting systems modified with the HPE-b-PEO block copolymer, where the higher PEO block content led to more regular morphology and good dispersion of the TiO_2 nanoparticles.

6.3.6. Contact angle of the epoxy based thermosetting systems

The surface properties of the PE-b-PEO(DGEBA/MCDEA) and TiO_2PE-b-PEO(DGEBA/MCDEA) cured systems were investigated by the water contact angle.

The changes in the hydrophilic nature of the thermosetting systems modified with different content of LPE-b-PEO block copolymer or with the same block copolymer and TiO_2 nanoparticles are shown in Figure 6.11.

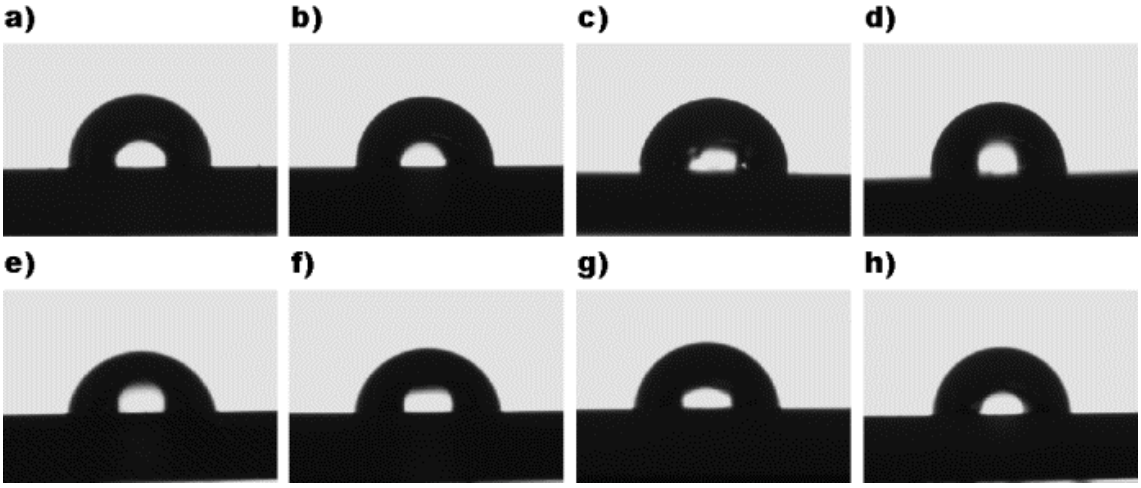

Figure 6.11. Images of a water droplet in contact with the DGEBA/MCDEA thermosetting systems modified with a) 5, b) 10, c) 20 and d) 40 wt % of LPE-b-PEO and e) 5, f) 10, g) 20 and h) 40 wt % of TiO_2LPE-b-PEO.

In the case of the LPE-b-PEO(DGEBA/MCDEA) cured systems, a slightly decreasing in the water contact angle, from 94 º to 91 º, was observed with the increase of 5 to 20 wt % of LPE-b-PEO block copolymer content. In contrast the addition of 40 wt % of LPE-b-PEO block copolymer resulted in an increase of contact angle up to 93 º (Table 6.5).

This behavior can be related to the macrophase separation of the PE block of the PE-b-PEO block copolymer. Thus, the hydrophobic character of the PE block [45] led to slight increase in the water contact angle of the 40LPE-b-PEO(DGEBA/MCDEA) cured system. This is related to fact that, as mentioned in the Chapter 2, the water contact angle higher than 90º indicated hydrophobic character of investigated material.

Similar behavior was also detected for the TiO_2LPE-b-PEO(DGEBA/MCDEA)

cured systems. The water contact angle decreased slightly from 88 to 85 º with the addition of 5 to 20 wt % of TiO_2LPE-b-PEO and increased to 90 º with the addition of 40 wt % of TiO_2LPE-b-PEO (Table 6.5). These phenomena can be related to the macrophase separation of the PE block rich phase from the DGBA/MCDEA matrix.

Table 6.5. The water contact angle of the thermosetting systems modified with the LPE-b-PEO block copolymer and the same block copolymer and the synthetized TiO_2 nanoparticles.

Sample	Contact angle (º)
DGEBA/MCDEA	100 ± 2
5LPE-b-PEO(DGEBA/MCDEA)	95 ± 1
10LPE-b-PEO(DGEBA/MCDEA)	94 ± 2
20LPE-b-PEO(DGEBA/MCDEA)	91 ± 3
40LPE-b-PEO(DGEBA/MCDEA)	93 ± 4
5TiO_2LPE-b-PEO(DGEBA/MCDEA)	88 ± 2
10TiO_2LPE-b-PEO(DGEBA/MCDEA)	86 ± 2
20TiO_2LPE-b-PEO(DGEBA/MCDEA)	85 ± 1
40TiO_2LPE-b-PEO(DGEBA/MCDEA)	90 ± 3

The decrease of the water contact angle in the case of both, the LPE-b-PEO(DGEBA/MCDEA) and TiO_2LPE-b-PEO(DGEBA/MCDEA) cured systems, is directly related with the hydrophilic character of the PEO block rich phase partially miscible with the DGEBA/MCDEA matrix.

Consequently, the addition less than 40 wt % of LPE-b-PEO block copolymer, improved the hydrophilic character of these systems. By contrast, the addition of 40 wt % of LPE-b-PEO block copolymer provoked an increase of the water contact angle due to the hydrophobic character of the macrophase separated PE block rich phase.

Water contact angle of the DGEBA/MCDEA cured systems modified with the HPE-b-PEO block copolymer and with the same block copolymer and the synthesized TiO_2 nanoparticles was also analyzed.

As can be observed in Figure 6.12, in the case of the HPE-b-PEO/(DGEBA/MCDEA) systems, the water contact angle decreased drastically with the increasing of the HPE-b-PEO block copolymer content being 100, 96, 79 and 74 º with the addition of 5, 10, 20 and 40 wt % of HPE-b-PEO block copolymer content, respectively, as collected in Table 6.6. This could be attributed, as mentioned above, to the hydrophilic character of the PEO block of the HPE-b-PEO block copolymer.

In the case of the thermosetting systems modified with both, the HPE-b-PEO block copolymer and TiO_2 nanoparticles, the significant decreasing of the water contact

angle was observed only with the addition of 40 wt % of TiO_2HPE-b-PEO being 95 º for the 5TiO_2HPE-b-PEO(DGEBA/MCDEA) cured system and 75 º for the 40TiO_2HPE-b-PEO(DGEBA/MCDEA) cured system (Table 6.6).

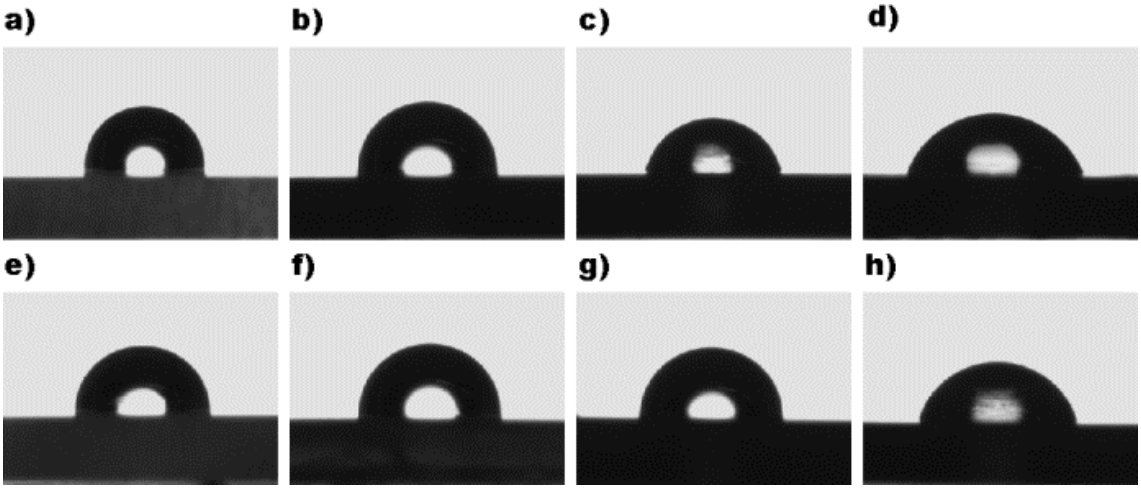

Figure 6.12. Images of a water droplet in contact with the DGEBA/MCDEA thermosetting systems modified with a) 5, b) 10, c) 20 and d) 40 wt % of HPE-b-PEO and e) 5, f) 10, g) 20 and h) 40 wt % of TiO_2HPE-b-PEO.

This behavior can be related with the high PEO block content in the HPE-b-PEO block copolymer, 80 wt %, if comparted to the LPE-b-PEO block copolymer, 50 wt %. Consequently, the PEO block is partially miscible with the DGEBA/MCDEA matrix and act as dispersion agent for the TiO_2 nanoparticles affected hydrophilic character of analyzed surface.

Table 6.6. The water contact angle of the thermosetting systems modified with the HPE-b-PEO block copolymer and the same block copolymer and the synthetized TiO_2 nanoparticles.

Sample	Contact angle (º)
DGEBA/MCDEA	100 ± 2
5HPE-b-PEO(DGEBA/MCDEA)	100 ± 3
10HPE-b-PEO(DGEBA/MCDEA)	96 ± 1
20HPE-b-PEO(DGEBA/MCDEA)	79 ± 3
40HPE-b-PEO(DGEBA/MCDEA)	74 ± 4
5TiO_2HPE-b-PEO(DGEBA/MCDEA)	95 ± 2
10TiO_2HPE-b-PEO(DGEBA/MCDEA)	97 ± 4
20TiO_2HPE-b-PEO(DGEBA/MCDEA)	93 ± 1
40TiO_2HPE-b-PEO(DGEBA/MCDEA)	75 ± 2

Based on the obtained results, it can be summarized that the epoxy based thermosetting systems modified with the HPE-b-PEO block copolymer showed higher hydrophilic character than epoxy based thermosetting systems modified with the LPE-

b-PEO block copolymer due to both the higher PEO block content (80 wt %) and the higher molecular weight of the HPE-b-PEO block copolymer.

6.4. Conclusions

Epoxy based thermosetting systems modified with two different PE-b-PEO block copolymers (different molecular weight and molar ratio between blocks) and the same block copolymers and sol-gel synthetized TiO_2 nanoparticles were prepared and characterized.

DSC results for the PE-b-PEO/DGEBA unreactive mixtures confirmed the partial miscibility between the PEO block and the DGEBA epoxy resin. The addition of the PE-b-PEO block copolymers resulted in a delay of the curing reaction time as a consequence of the dilution effect.

Thermal behavior of the investigated thermosetting systems after curing reaction indicated the partial miscibility between the PEO block of the PE-b-PEO block copolymers and the DGEBA/MCDEA matrix resulted in shift of the T_g of the DGEBA/MCDEA matrix to lower temperatures with increase of the PE-b-PEO block copolymers content.

The T_g of the DGEBA/MCDEA matrix in the case of the TiO_2PE-b-PEO(DGEBA/MCDEA) cured systems were lower if compare to the corresponding cured systems without TiO_2 nanoparticles since in these systems the PEO block not only acted as nanostructuration agent, but also as surfactant for the sol-gel synthesized TiO_2 nanoparticles.

Higher optical transparency was reached for the cured systems modified with the HPE-b-PEO block copolymer and the same block copolymer and TiO_2 nanoparticles as consequence of the higher PEO block copolymer content (50 wt % in the LPE-b-PEO block copolymer and 80 wt % in the HPE-b-PEO block copolymer).

The morphology of the cured systems depends strongly on the PE-b-PEO block copolymer used for fabrication of both the PE-b-PEO(DGEBA/MCDEA) and TiO_2PE-b-PEO(DGEBA/MCDEA) cured systems being the PEO bock content the key parameter for the nanostructuration and for the dispersion of the synthesized TiO_2 nanoparticles. The PEO block content in the PE-b-PEO block copolymers and

consequently in all the investigated thermosetting systems governed not only morphology but also surface properties since the hydrophilic character of the thermosetting systems was strongly affected.

The PE-b-PEO block copolymer nanostructured thermosetting systems, depends on formulation, can acted as template for the TiO_2 nanoparticles resulting in materials with high transparency and hydrophilic surface character.

6.5. References

[1] Johnsen BB, Kinloch AJ, Mohammed RD, Taylor AC. Toughening mechanisms of nanoparticle-modified epoxy. Polymer 2007;48:530-541.

[2] Gutierrez J, Mondragon I, Tercjak A. Morphological and optical behavior of thermoset matrix composites varying both polystyrene-block-poly(ethylene oxide) and TiO_2 nanoparticle content. Polymer 2011;52:5699-5707.

[3] Hsieh TH, Kinloch AJ, Masania K, Taylor AC, Sprenger S. The mechanisms and mechanics of the toughening of epoxy polymers modified with silica nanoparticles. Polymer 2010;51:6284-6294.

[4] Cano L, Builes DH, Tercjak A. Morphological and mechanical study of nanostructured epoxy systems modified with amphiphilic poly(ethylene oxide-b-propylene oxide-b-ethylene oxide) triblock copolymer. Polymer 2014;55:738-745.

[5] Hillmyer MA, Lipic PM, Hajduk DA, Almdal K, Bates FS. Self-assembly and polymerization of epoxy resin-amphiphilic block copolymer nanocomposites. J. Am. Chem. Soc. 1997;119:2749-2750.

[6] Serrano E, Martin MD, Tercjak A, Pomposo JA, Mecerreyes D, Mondragon I. Nanostructured thermosetting systems from epoxidized styrene butadiene block copolymers. Macromol. Rapid Commun. 2005;26:982-985.

[7] Serrano E, Tercjak A, Ocando C, Larrañaga M, Parellada MD, Corona-Galván S, Mecerreyes D, Zafeiropoulos NE, Stamm M, Mondragon I. Curing behavior and final properties of nanostructured thermosetting systems modified with epoxidized styrene-butadiene linear diblock copolymers. Macromol. Chem. Phys. 2007;208:2281-2292.

[8] Mijovic J, Shen M, Sy JW. Dynamics and morphology in nanostructured thermoset network/block copolymer blends during network formation. Macromolecules 2000;33:5235-5244.

[9] Thio YS, Wu J, Bates SF. Epoxy toughening using low molecular weight poly(hexylene oxide)-poly(ethylene oxide) diblock copolymers. Macromolecules 2006;39:7187-7189.

[10] Lipic PM, Bates FS, Hillmyer MA. Nanostructured thermosets from self-assembled amphiphilic block copolymer/epoxy resin mixtures. J. Am. Chem. Soc. 1998;12:8963-8970.

[11] Ocando C, Serrano E, Tercjak A, Peña C, Kortaberria G, Calberg C, Grignard B, Jerome R, Carrasco PM, Mecerreyes D, Mondragon I. Structure and properties of a

semifluorinated diblock copolymer modified epoxy blend. Macromolecules 2007;40:4068-4074.

[12] Liu JD, Thompson ZJ, Sue HJ, Bates FS, Hillmyer MA, Dettloff M, Jacob G, Verghese N, Pham H. Toughening of epoxies with block copolymer micelles of wormlike morphology. Macromolecules 2010;43:7238-7243.

[13] Tercjak A, Larrañaga M, Martin MD, Mondragon I. Thermally reversible nanostructured thermosetting blends modified with poly(ethylene-b-ethylene oxide) diblock copolymer. J. Therm. Anal. Calorim. 2006;86:663-667.

[14] Pérez-Ruiz L, Royston GJ, Fairclough JPA, Ryan AJ. Toughening by nanostructure. Polymer 2008;49:4475-4488.

[15] Chau Hang JL, Liu HW, Su WF. Fabrication of hybrid surface-modified titania-epoxy nanocomposite films. J. Phys. Chem. Solids 2009;70:1385-1389.

[16] Peponi L, Valenti L, Torre L, Mondragon I, Kenny JM. Surfactant assisted selective confinement of carbon nanotubes functionalized with octadecylamine in a poly(styrene-b-isoprene-b-styrene) block copolymer matrix. Carbon 2009;47:2474-2480.

[17] Tercjak A, Gutierrez J, Mondragon I. Conductive properties of inorganic/organic nanostructured systems based on block copolymers. Mater. Sci. Forum 2012;714:153-158.

[18] Carolan D, Ivankovic A, Kinloch AJ, Sprenger S, Taylor AC. Toughening of epoxy-based hybrid nanocomposites. Polymer 2016;97:179-190.

[19] Kobayashi M, Saito H, Boury B, Matsukawa K, Sugahara Y. Epoxy-based hybrids using TiO_2 nanoparticles prepared via a non-hydrolytic sol-gel route. Appl. Organomet. Chem. 2013;27:673-677.

[20] Lim JY, Lee CS, Lee JM, Ahn J, Cho HH, Kim JH. Amphiphilic block-graft copolymer templates for organized mesoporous TiO_2 films in dye-sensitized solar cells. J. Power Sources 2016;301:18-28.

[21] Zhu L, Zhang C, Han J, Zheng S, Li X. Formation of nanophases in epoxy thermosets containing an organic-inorganic macrocyclic molecular brush with poly(ε-caprolactone)-block-polystyrene side chains. Soft Matter 2012;8:7062-7072.

[22] Maiez-Tribut S, Pascault JP, Soule ER, Borrajo J, Williams RJJ. Nanostructured epoxies based on the self-assembly of block copolymers: a new miscible block that can be tailored to different epoxy formulations. Macromolecules 2007;40:1268-1273.

[23] Tercjak A, Gutierrez J, Martin MD, Mondragon I. Transparent titanium

dioxide/block copolymer modified epoxy-based systems in the long scale microphase separation threshold. Eur. Polym. J. 2012;48:16-25.

[24] Meng F, Zheng S, Li H, Liang Q, Liu T. Formation of ordered nanostructures in epoxy thermosets: A mechanism of reaction-induced microphase separation. Macromolecules 2006;39:5072-5080.

[25] Meng F, Zheng S, Liu T. Epoxy resin containing poly(ethylene oxide)-block-poly(ε-caprolactone) diblock copolymer: Effect of curing agents on nanostructures. Polymer 2006;47:7590-7600.

[26] Tercjak A, Gutierrez J, Peponi L, Rueda L, Mondragon I. Arrangement of conductive TiO_2 nanoparticles in hybrid inorganic/organic thermosetting materials using liquid crystal. Macromolecules 2009;42:3386-3390.

[27] Ocando C, Tercjak A, Mondragon I. Nanostructured systems based on SBS epoxidized triblock copolymers and well-dispersed alumina/epoxy matrix composites. Compos. Sci. Technol. 2010;70:1106-1112.

[28] Gutierrez J, Tercjak A, Mondragon I. Transparent nanostructured thermoset composites containing well-dispersed TiO_2 nanoparticles. J. Phys. Chem. C 2010;114:22424-22430.

[29] Guo Q, Thomann R, Gronski W. Nanostructures, semicrytalline morphology, and nanoscale confinement effect on the crystallization kinetics in self-organized block copolymer/thermoset blends. Macromolecules 2003;36:3635-3645.

[30] Guo Q, Liu J, Chen L, Wang K. Nanostructures and nanoporosity in thermoset epoxy blends with an amphiphilic polyisoprene-block-poly (4-vinyl pyridine) reactive diblock copolymer. Polymer 2008;49:1737-1742.

[31] Yi F, Zheng S. Nanostructures and surface hydrophobicity of self-assembled thermosets involving epoxy resin and poly(2,2,2-trifluoroethyl acrylate)-block-poly(ethylene oxide) amphiphilic diblock copolymer. J. Phys. Chem. B 2009;113:1857-1868.

[32] Sun P, Dang Q, Li B, Chen T, Wang Y, Lin H, Jin Q, Ding D. Mobility, miscibility, and microdomain structure in nanostructured thermoset blends of epoxy resin and amphiphilic poly(ethylene oxide)-block-poly(propylene oxide)-block-poly(ethylene oxide) triblock copolymers characterized by solid-state NMR. Macromolecules 2005;38:5654-5667.

[33] Larrañaga M, Gabilondo N, Kortaberria G, Serrano E, Remiro P, Riccardi CC, Mondragon I. Micro- or nanoseparated phases in thermoset blends of an epoxy resin

and PEO-PPO-PEO triblock copolymer. Polymer 2005;46:7082-7093.

[34] Larrañaga M, Serrano E, Martin MD, Tercjak A, Kortaberria G, de la Caba K, Riccardi CC, Mondragon I. Mechanical properties-morphology relationships in nano-/microstructured epoxy matrices modified with PEO-PPO-PEO block copolymers. Polym. Int. 2007;56:1392-1403.

[35] Gutierrez J, Tercjak A, Garcia I, Peponi L, Mondragon I. Hybrid titanium dioxide/PS-b-PEO block copolymer nanocomposites based on sol-gel synthesis. Nanotechnology 2008;19:155607/1-155607/8

[36] Gao C, Zhang S, Li X, Zhu S, Jiang Z. Synthesis of poly(ether ether ketone)-block polyimide copolymer and its compatibilization for poly(etheretherketone)/thermoplastic polyimide blends. Polymer 2014;55:119-25.

[37] Aroguz AZ, Engin HH, Baysal BM. The assessment of miscibility and morphology of poly(ε-caprolactone) and poly(para-chlorostyrene) blends. Eur. Polym. J. 2007;43:403-9.

[38] Larrañaga M, Serrano E, Martin MD, Tercjak A, Kortaberria G, de la Caba K, Riccardi CC, Mondragon I. Mechanical properties-morphology relationships in nano-/microstructured epoxy matrices modified with PEO-PPO-PEO block copolymers. Polym. Int. 2007;56:1392-1403.

[39] Müller AJ, Balsamo V, Arnal ML. Nucleation and crystallization in diblock and triblock copolymers. Adv. Polym. Sci. 2005;190:1-63.

[40] Davis GT, Eby RK. Glass transition of polyethylene: Volume relaxation. J. Appl. Phys. 1973;44:4274-4281.

[41] Builes DH, Hernández-Ortiz JP, Corcuera MA, Mondragon I, Tercjak A. Effect of poly(ethylene oxide) homopolymer and two different poly(ethylene oxide-b-poly(propylene oxide)-b-poly(ethylene oxide) triblock copolymers on morphological, optical, and mechanical properties of nanostructured unsaturated polyester. Appl. Mater. Interfaces 2014;6:1073-1081.

[42] Builes DH, Hernandez H, Mondragon I, Tercjak A. Relationship between the morphology of nanostructured unsaturated polyesters modified with PEO-b-PPO-b-PEO triblock copolymer and their optical and mechanical properties. J. Phys. Chem. C 2013;117:3563-3471.

[43] Korayem AH, Korayem MH. The effect of surface roughness on the vibration behavior of AFM piezoelectric MC in the vicinity of sample surface in air environment

based on MCS theory. Precis. Eng. 2017;47:212:222.

[44] Spencer A, Dobryden I, Almqvist N, Almqvist A, Larsson R. The influence of AFM and VSI techniques on the accurate calculation of tribological surface roughness parameters. Tribol. Int. 2013;57:245-250.

[45] Razmkhah K, Chmel NP, Gibson MI, Rodger A. Oxidized polyethylene films for orienting polar molecules for linear dichroism spectroscopy. Analyst 2014;139:1372-1382.

General conclusions, future work and scientific contributions

7

7. General conclusions, future work and scientific contributions

7.1. General conclusions

The most relevant conclusions of the investigation work related to this thesis are summarized below:

The PE-b-PEO block copolymer dispersed liquid crystal blends were fabricated using two low molecular weight HOBC and EBBA nematic liquid crystals. Obtained results showed that the PEO block of the PE-b-PEO block copolymer is partially miscible with the HOBC nematic liquid crystal while the PE block of the PE-b-PEO block copolymer resulted in stronger miscibility with the EBBA nematic liquid crystal. The miscibility of each nematic liquid crystal with each block of the PE-b-PEO block copolymer had strong influence on the final properties of investigated PDLC blends. Moreover, the investigated PDLC blends maintain the nematic character of the liquid crystal, switching from opaque to transparent state as a function of temperature.

Hybrid PE-b-PEO/EBBA as well as PLA/PE-b-PEO/EBBA electrospun fibers were successfully fabricated optimizing the co-electrospinning processing-window. The combined use of the PLA polymer and PE-b-PEO block copolymer improved the electrospun fibers formation. Moreover, the nematic character of the EBBA liquid crystal was also maintained in the investigated hybrid electrospun fibers based on both, PE-b-PEO block copolymer and PLA homopolymer.

Nanostructured epoxy based thermosetting systems were effectively fabricated using amphiphilic PE-b-PEO block copolymer. The PEO block of the PE-b-PEO block copolymer is miscible with the DGEBA/MCDEA matrix whereas the immiscible PE block, lead to a microphase separation. These PE-b-PEO block copolymer nanostructured thermosetting systems were used as surfactant for the dispersion and localization of the TiO_2 nanoparticles.

The PEO block of the PE-b-PEO block copolymer had strong influence on the morphology and the final properties of the nanostructured thermosetting systems.

Moreover, the molecular weight of the PE-b-PEO block copolymer and molar ratio between blocks, affect to the dispersion and localization of the sol-gel synthesized TiO_2 nanoparticles.

7.2. Future work

In order to continue this investigation work, the following research lines are proposed:

The study of the influence of the self-assembly of the PE-b-PEO block copolymer on the thermo-optical reversible properties of the PE-b-PEO/HOBC and PE-b-PEO/EBBA blends.

The addition of the inorganic nanoparticles into PE-b-PEO/HOBC and PE-b-PEO/EBBA blends in order to enhance thermo-optical reversible behavior of the PE-b-PEO block copolymer dispersed liquid crystal blends.

The use of the PLA or PEO homopolymer as matrix to design hybrid fiber mats modified with both PE-b-PEO block copolymers and nematic liquid crystals. The employment of the PLA or PEO homopolymer as matrix can allow to fabricate compact integrated multifunctional materials with interesting thermo-optical reversible properties of nematic liquid crystal phase.

The study of the mechanical and conductive properties of the PE-b-PEO block copolymer nanostructured thermosetting systems modified with sol-gel synthesized TiO_2 nanoparticles.

The incorporation of nematic liquid crystals into PE-b-PEO block copolymer nanostructured thermosetting systems in order to design materials with thermo-optical respond. The incorporation of both nematic liquid crystals and inorganic nanoparticles into PE-b-PEO block copolymer nanostructured thermosetting systems to design multifunctional materials.

The used of acquired knowledge during the preparation of bulk hybrid polymeric materials based on PE-b-PEO block copolymer for preparation coatings from the point of view of potential applications.

7.3. Scientific contributions

7.3.1. Publications

Scientific publications directly related to presented investigation work are the following:

Carrasco-Hernandez S, Gutierrez J, Tercjak A. Thermo-responsive polymer dispersed liquid crystals based on block copolymers. Nova Science Publishers. Eds L. Peponi, J.-M. Raquez. Under revision.

Carrasco-Hernandez S, Gutierrez J, Tercjak A. PE-b-PEO block copolymer nanostructured thermosetting systems as template for TiO_2 nanoparticles. Eur. Polym. J. Under second revision.

Impact Factor: 3.485, 13 of 85 in Polymer Science (JCR 2015), Q1

Carrasco-Hernandez S, Gutierrez J, Tercjak A. Optical reversible behavior of poly(ethylene-b-ethylene oxide) block copolymer dispersed liquid crystal blends. Eur. Polym. J. 2017;91:187-196.

Impact Factor: 3.485, 13 of 85 in Polymer Science (JCR 2015), Q1

Carrasco-Hernandez S, Gutierrez J, Peponi L, Tercjak A. Optimization of the electrospinning processing-window to fabricate nanostructured PE-b-PEO and hybrid PE-b-PEO/EBBA fibers. Polym. Eng. Sci. 2017. DOI 10.1002/pen.

Impact Factor: 1.719, 40 of 85 in Polymer Science (JCR 2015), Q2

Carrasco-Hernandez S, Gutierrez J, Tercjak A. Thermal and optical behavior of poly(ethylene-b-ethylene oxide) block copolymer dispersed liquid crystals blends. Eur. Poly. J. 2016;74:148-157.

Impact Factor: 3.485, 13 of 85 in Polymer Science (JCR 2015), Q1

Other scientific publications:

Gutierrez J, **Carrasco-Hernandez S**, Barud HS, Oliveira RL, Carvalho RA, Amaral AC, Tercjak A. Transparent nanostructured cellulose acetate films based on the self-assembly of PEO-b-PPO-b-PEO block copolymer. Carbohyd. Polym.

2017;165:437-443.

Impact Factor: 4.219, 9 of 85 in Polymer Science (JCR 2015), Q1

Cano L, Builes DH, **Carrasco-Hernandez S**, Gutierrez J, Tercjak A. Quantitative nanomechanical property mapping of epoxy thermosetting system modified with poly(ethylene oxide-b-propylene oxide-b-ethylene oxide) triblock copolymer. Poly. Test. 2017;57:38-41.

Impact Factor: 2.350, 5 of 33 in Material Science, Characterization and Testing (JCR 2015), Q1

7.3.2. Contributions in conferences

Contributions in conferences directly related to the presented investigation work are the following:

Carrasco Hernández S, Cano L, Gutierrez J, Tercjak A. Reversibility study of polymer dispersed liquid crystals based on PE-b-PEO block copolymer and liquid crystals. ECNP 2016, 9th ECNP International Conference on Nanostructured Polymers and Nanocomposites. Rome (Italy), 2016, contribution: **poster**. Grant from **University of the Basque Country (UPV/EHU).**

Carrasco Hernández S, Peponi L, Tercjak A. Optimization of the processing-window to obtain PE-b-PEO electrospun fibers. 5th International Conference on Biobased and Biodegradable Polymers (BIOPOL-2015). Donostia-San Sebastian (Spain), 2015, contribution: **poster**.

Carrasco Hernández S, Cano L, Gutierrez J, Tercjak A. Polymeric blends based on PE-b-PEO block copolymer and HOBC or EBBA liquid crystals. JIP-JEPO 2015 1st French-Spanish Joint Congress for Young Researchers in Polymer, Donostia-San Sebastian (Spain), 2015, contribution: **oral communication**.

Carrasco Hernández S, Cano L, Gutierrez J, Tercjak A. Preparation and characterization of PE-b-PEO block copolymer and HOBC or EBBA liquid crystals polymeric blends. Imaginenano 2015 (NanoSpain Chemistry). Bilbao (Spain), 2015, contribution: **poster**.

Other contributions in conferences:

Tercjak A, Cano L, **Carrasco-Hernandez S**, Gutierrez J. Multifunctional hybrid inorganic/organic materials. MoDeSt 2016. The 9th International Conference on Modification, Degradation and Stabilization of Polymers. Krakov (Poland), 2016, contribution: **poster**.

Cano L, Gutierrez J, **Carrasco-Hernandez S**, Builies DH, Tercjak A. Epoxi erretxin motako polimero termoegonkorren zailtasunaren hobekuntza blokezko kopolimeroen bidez. Materialen Zientzia eta Teknologia III. Kongresua. Bizkaia (Spain), 2016, contribution: **oral communication**.

Gutierrez J, Cano L, **Carrasco-Hernandez S**, Tercjak A. Multifunctional nanostructured materials based on block copolymer templated sol-gel process. ICM-2016. International Conference on Macromolecules: Synthesis, Morphology, Processing, Structure, Properties and Applications. Kerala (India), 2016, contribution: **invited oral communication**.

Tercjak A, Cano L, **Carrasco-Hernandez S**, Fernandez R, Gutierrez J. Mechanical properties of composite materials by peakforce quantitative nanomechanical mapping technique. ECM4 4th International Symposium on Energy Challenges and Mechanics (ECM4) - working on small scales. Aberdeen (United Kingdom), 2015, contribution: **invited oral communication**.

Tercjak A, Cano L, Builes DH, **Carrasco-Hernandez S**, Gutierrez J. Multiphasic materials based on block copolymers and nanostructured thermosets. Energy Materials Nanotechnology Meeting on Polymers. Orlando (United States), 2015, contribution: **invited oral communication**.

Gutierrez J, Cano L, **Carrasco-Hernandez S**, Tercjak A. Blokezko kopolimeroetan oinarritutako funtzio anitzeko material nanoegituratu berriak. Materialen Zientzia eta Teknologia II. Donostia-San Sebastian (Spain), 2014, contribution: **poster**.

7.3.3. Research stays

Research stay at the Institute of Polymer Science and Technology (ICTP) of the Spanish National Research Council (CSIC) in Madrid (Spain) from April 2015 to June 2015, supervised by Dr. Laura Peponi and funded by the Ministry of Economy and

Competitiveness (MINECO).

Research stay at the Chemistry Department of the University College Cork (UCC) in Cork (Ireland) from March 2016 to May 2016, supervised by Dr. Michael Morris and funded by the Ministry of Economy and Competitiveness (MINECO).

Appendix

1. List of symbols

C_p	block copolymer concentration
f	volume fraction of one block of block copolymer
M_n	number average molecular weight
N	degree of polymerization
N-I	nematic-isotropic
T_c	crystallization temperature
T_g	glass transition temperature
T_m	melting temperature
T_{NI}	nematic-isotropic temperature
Q_p	block copolymer solution flow rate
Q_s	solvent flow rate
R_a	average roughness
R_q	square roughness
V^+	positive voltage
V^-	negative voltage
w	weight fraction
ΔH	enthalpy
Θ	water contact angle
χ	Flory-Huggins interaction parameter
X_c	crystallization degree

2. List of abbreviations

AFM	atomic force microscopy
ATR	attenuated total reflection
BCC	body centered cubic
CLC	cholesteric liquid crystal
DGEBA	diglycidyl ether of bisphenol A
DIS	disordered
DMF	dimethylformamide
DSC	differential scanning calorimetry
EBBA	N-(4-ethoxybenzylidene)-4-butylaniline
FTIR	Fourier transform infrared spectroscopy
GYD	gyroid
HCl	hydrochloric acid
HEX	hexagonal
HOBC	4'-(hexyloxy)-4-biphenylcarbonitrile
LAM	lamellar
LC	liquid crystal
LCD	liquid crystal display
LDG	Laudau-de-Gennes
LED	light emitting diode
MCDEA	4,4’-methylene bis(3-chloro-2,6-diethylaniline)
NLC	nematic liquid crystal
OM	optical microscopy

PCL	polycaprolactone
PDLC	polymer dispersed liquid crystal
PE	polyethylene
PE-b-PEO	poly(ethylene-b-ethylene oxide) diblock copolymer
PEO	polyethylene oxide
PL	Photoluminiscence spectroscopy
PLA	polylactic acid
PMMA	poly(methyl methacrylate)
RIPS	reaction induced phase separation
SEM	scanning electron microscopy
SLC	smectic liquid crystal
TGA	thermal gravimetric analysis
UV-vis	ultraviolet-visible
Wt	weight

3. List of schemes

Chapter 3

Chapter 4

Chapter 6

4. List of tables

Chapter 2

Chapter 3

Chapter 4

Chapter 5

Chapter 6

PEO(DGEBA/MCDEA) and TiO_2HPE-b-PEO(DGEBA/MCDEA) cured systems.

Table 6.5. The water contact angle of the thermosetting systems modified with the LPE-b-PEO block copolymer and the same block copolymer and the synthetized TiO_2 nanoparticles.

Table 6.6. The water contact angle of the thermosetting systems modified with the HPE-b-PEO block copolymer and the same block copolymer and the synthetized TiO_2 nanoparticles.

5. List of figures

Chapter 1

Chapter 2

Chapter 3

copolymer and the HOBC (a, b) and EBBA (c, d) nematic liquid crystals during heating and cooling processes. For comparison the DSC thermograms of neat components were also plotted.

Figure 3.4. DSC thermograms of the a) PEO/HOBC and b) PEO/EBBA blends with different PE-b-PEO block copolymer content during heating process. For comparison the DSC thermograms of neat PEO homopolymer was also plotted.

Figure 3.5. OM micrographs of the a) HOBC nematic liquid crystal and its PDLC blends containing b) 25 wt %, c) 50 wt %, d) 75 wt % of PE-b-PEO block copolymer, and e) EBBA nematic liquid crystal and its PDLC blends containing f) 25 wt %, g) 50 wt %, h) 75 wt % of PE-b-PEO block copolymer. For comparison optical micrograph of the i) PE-b-PEO block copolymer was also presented. All OM micrographs were taken between crossed polarizers.

Chapter 4

Figure 4.1. DSC thermograms of the a) HOBC nematic liquid crystal and b) 1PE-b-PEO/HOBC, c) 5PE-b-PEO/HOBC and d) 10PE-b-PEO/HOBC blends during heating/cooling processes.

Figure 4.2. DSC thermograms of the a) EBBA nematic liquid crystal and b) 1PE-b-PEO/EBBA, c) 5PE-b-PEO/EBBA and d) 10PE-b-PEO/EBBA blends during the heating/cooling processes.

Figure 4.3. OM micrographs taken with crossed polarizers at solid, liquid solid and liquid state of the a) HOBC nematic liquid crystal and b) 1PE-b-PEO/HOBC c) 5PE-b-PEO/HOBC and d) 10PE-b-PEO/HOBC blends.

Figure 4.4. OM micrographs taken with crossed polarizers at solid, liquid solid and liquid state of the a) EBBA nematic liquid crystal and b) 1PE-b-PEO/EBBA c) 5PE-b-PEO/EBBA and d) 10PE-b-PEO/EBBA blends.

Figure 4.5. Photoluminescence emission spectra at 10 and 80 ºC of the HOBC nematic liquid crystal of aI) heating/cooling cycle, and aII) four heating/cooling cycles. UV-visible transmission spectra at 10 and 80 ºC of the HOBC nematic liquid crystal of aIII) heating/cooling cycle, and aIV) four heating/cooling cycles. Photoluminescence emission spectra at 10 and 80 ºC of the EBBA nematic liquid crystal of bI) heating/cooling cycle, and bII) four heating/cooling cycles. UV-visible transmission spectra at 10 and 80 ºC of the EBBA nematic liquid crystal of bIII) heating/cooling cycle, and bIV) four heating/cooling cycles.

Figure 4.6. PL emission spectra at 10 and 80 °C during a heating/cooling cycle of the PE-b-PEO/HOBC blends with aI) 1, bI) 5 and cI) 10 wt % of PE-b-PEO block copolymer content and of the PE-b-PEO/EBBA blends with dI) 1, eI) 5 and fI) 10 wt % of PE-b-PEO block copolymer content. Maximums emission peaks at 10 and 80 °C during four heating/cooling cycles of the PE-b-PEO/HOBC blends with aII) 1, bII) 5 and cII) 10 wt % of PE-b-PEO block copolymer content and of the PE-b-PEO/EBBA blends with dII) 1, eII) 5 and fII) 10 wt % of PE-b-PEO block copolymer content.

Figure 4.7. 3D photoluminescence emission spectra at 10 and 80 ºC of the a) HOBC nematic liquid crystal and of the PE-b-PEO/HOBC blends with b) 1, c) 5 and d) 10 wt % of PE-b-PEO block copolymer content during four heating/cooling cycles.

Figure 4.8. 3D photoluminescence emission spectra at 10 and 80 ºC of the a) EBBA nematic liquid crystal and the PE-b-PEO/EBBA blends with b) 1, c) 5 and d) 10 wt % of PE-b-PEO block copolymer content during four heating/cooling cycles.

Figure 4.9. UV-visible transmittance spectra at 10 and 80 °C during a heating/cooling cycle of PE-b-PEO/HOBC blends with aI) 1, bI) 5 and cI) 10 wt % PE-b-PEO block copolymer content, and PE-b-PEO/EBBA blends with dI) 1, eI) 5 and fI) 10 wt % PE-b-PEO block copolymer content. Transmittance values, measured at a wavelength of 600 nm, during four heating/cooling cycles at 10 and 80 °C of PE-b-PEO/HOBC blends with aII) 1 , bII) 5 and cII) 10 wt % PE-b-PEO block copolymer content and PE-b-PEO/EBBA blends with dII) 1, eII) 5 and fII) 10 wt % PE-b-PEO block copolymer content.

Chapter 5

Figure 5.1. OM micrographs of the PE-b-PEO block copolymer electrospun fibers obtained for 45 wt % of PE-b-PEO block copolymer in a mixture of chloroform/DMF solvents (4:1), applying a voltage difference of 22 kV, chloroform flow rate of 0.1 mL h^{-1} and block copolymer solution flow rate of 5 mL h^{-1}.

Figure 5.2. OM micrographs of the PE-b-PEO block copolymer electrospun fibers obtained for 46 wt % of PE-b-PEO block copolymer in a mixture of chloroform/DMF solvents (5:1), applying a voltage difference of 22 kV, chloroform flow rate of 0.1 mL h^{-1} and block copolymer solution flow rate of a) 1, b) 3 and c) 5 mL h^{-1}.

Figure 5.3. OM micrographs of the PE-b-PEO block copolymer electrospun fibers obtained for 46 wt % of PE-b-PEO block copolymer in a mixture of chloroform/DMF solvents (4:1), chloroform flow rate of 0.1 mL h^{-1}applying a voltage difference and block

copolymer solution flow rate of a) 22 kV and 0.1 mL h^{-1} and b) 21 kV and 5 mL h^{-1}.

Figure 5.4. OM micrographs of the PE-b-PEO block copolymer electrospun fibers obtained for 47 wt % of PE-b-PEO block copolymer in a mixture of chloroform/DMF solvents (5:1), block copolymer solution flow rate of 0.5 mL h^{-1}, applying a voltage difference and chloroform flow rate of a) 22 kV and 0.1 mL h^{-1} and b) 21 kV and 0.5 mL h^{-1}.

Figure 5.5. OM micrographs of the hybrid PE-b-PEO/EBBA electrospun fibers obtained for 46 wt % of PE-b-PEO block copolymer in a mixture of chloroform/DMF solvents (5:1), applying a voltage difference of 22 kV, EBBA liquid crystal solution flow rate of 0.1 mL h^{-1} and block copolymer solution flow rate of a) 1, b) 3 and c) 5 mL h^{-1}.

Figure 5.6. SEM images of the PE-b-PEO block copolymer electrospun fibers obtained for 46 wt % of PE-b-PEO block copolymer in a mixture of chloroform/DMF solvents (5:1), applying a voltage difference of 22 kV, chloroform flow rate of 0.1 mL h^{-1} and block copolymer solution flow rate of a) 1, b) 3 and c) 5 mL h^{-1}.

Figure 5.7. SEM images of the hybrid PE-b-PEO/EBBA electrospun fibers obtained for 46 wt % of PE-b-PEO block copolymer in a mixture of chloroform/DMF solvents (5:1), applying a voltage difference of 22 kV, EBBA liquid crystal solution flow rate of 0.1 mL h^{-1} and block copolymer solution flow rate of a) 1, b) 3 and c) 5 mL h^{-1}.

Figure 5.8. AFM phase images of the a) PE-b-PEO electrospun fiber and b) hybrid PE-b-PEO/EBBA electrospun fiber.

Figure 5.9. OM micrographs a) without crossed polarized and b) with crossed polarizers of the hybrid PLA/EBBA electrospun fibers obtained for 10 wt % of PLA and EBBA nematic liquid crystal with the molar ratio 50:50 in a mixture of chloroform/DMF solvents (4:1) applying a voltage difference of 14 kV, PLA solution flow rate of 2 mL h^{-1} and EBBA solution flow rate of 5 mL h^{-1}.

Figure 5.10. OM micrographs a) without crossed polarized and b) with crossed polarizers of the hybrid PLA/PE-b-PEO/EBBA electrospun fibers obtained for 10 wt % of PLA and 10 wt % of PE-b-PEO block copolymer with the molar ratio 50:50 in a mixture of chloroform/DMF solvents (4:1) and 10 wt % of EBBA nematic liquid crystal in a mixture of chloroform/DMF solvents (4:1), applying a voltage difference of 14 kV, PLA solution flow rate of 2 mL h^{-1} and EBBA liquid crystal solution flow rate of 5 mL h^{-1}.

Chapter 6

Figure 6.1. DSC thermograms of the DGEBA epoxy resin and the PE-b-PEO/DGEBA uncured mixtures with 5, 10, 20 and 40 wt % of a) LPE-b-PEO and b) HPE-b-PEO

block copolymers.

Figure 6.2. Isothermal DSC thermograms at 190 ºC of neat DGEBA/MCDEA system and the PE-b-PEO(DGEBA/MCDEA) systems fabricated using a) LPE-b-PEO and b) HPE-b-PEO block copolymer.

Figure 6.3. FTIR spectra of the a) LPE-b-PEO(DGEBA/MCDEA) b) TiO_2LPE-b-PEO(DGEBA/MCDEA) e) HPE-b-PEO(DGEBA/MCDEA) and f) TiO_2HPE-b-PEO(DGEBA/MCDEA) cured systems and FTIR spectra from 2700 cm^{-1} to 3700 cm^{-1} of the c) LPE-b-PEO(DGEBA/MCDEA) d) TiO_2LPE-b-PEO(DGEBA/MCDEA) g) HPE-b-PEO(DGEBA/MCDEA) h) TiO_2HPE-b-PEO(DGEBA/MCDEA) cured systems. For comparison FTIR spectra of neat LPE-b-PEO and HPE-b-PEO block copolymers and neat DGEBA/MCDEA cured system were added.

Figure 6.4. DSC thermograms of the a) LPE-b-PEO(DGEBA/MCDEA) cured systems with different LPE-b-PEO content and b) TiO_2LPE-b-PEO(DGEBA/MCDEA) cured systems with different TiO_2LPE-b-PEO content. For comparison DSC thermograms of neat DGEBA/MCDEA cured system was also added. Marked temperatures correspond to the theoretical T_gs calculated by Fox equation.

Figure 6.5. DSC thermograms of the a) HPE-b-PEO(DGEBA/MCDEA) cured systems with different HPE-b-PEO content and b) TiO_2HPE-b-PEO(DGEBA/MCDEA) cured systems with different TiO_2HPE-b-PEO content. For comparison DSC thermograms of neat DGEBA/MCDEA cured system was also added. Marked temperatures correspond to the theoretical T_gs calculated by the Fox equation.

Figure. 6.6. UV-vis transmittance spectra of the different a) LPE-b-PEO(DGEBA/MCDEA) cured systems and b) TiO_2LPE-b-PEO(DGEBA/MCDEA) cured systems. For comparison UV-vis transmittance spectra of neat DGEBA/MCDEA cured system was also added. The inset on the top of each figure corresponds to the visual appearance of the investigated thermosetting systems.

Figure. 6.7. UV-vis transmittance spectra of the different a) HPE-b-PEO(DGEBA/MCDEA) cured systems and b) TiO_2HPE-b-PEO(DGEBA/MCDEA) cured systems. For comparison UV-vis transmittance spectra of neat DGEBA/MCDEA cured system was also added. The inset on the top of each figure corresponds to the visual appearance of the investigated thermosetting systems.

Figure 6.8. AFM phase images (750 nm x 750 nm) of neat DGEBA/MCDEA cured system. The insets at the bottom correspond to 3 μm x 3 μm AFM phase images.

Figure 6.9. AFM phase images (750 nm x 750 nm) of the DGEBA/MCDEA

thermosetting systems modified with a) 5, b) 10, c) 20 and d) 40 wt % of LPE-b-PEO block copolymer and e) 5, f) 10, g) 20 and h) 40 wt % of TiO_2LPE-b-PEO modifier. The insets at the bottom correspond to 3 μm x 3 μm AFM phase images.

Figure 6.10. AFM phase images (750 nm x 750 nm) of the DGEBA/MCDEA thermosetting systems modified with a) 5, b) 10, c) 20 and d) 40 wt % of HPE-b-PEO block copolymer and e) 5, f) 10, g) 20 and h) 40 wt % of TiO_2HPE-b-PEO content. The insets at the bottom correspond to 3 μm x 3 μm AFM phase images.

Figure 6.11. Images of a water droplet in contact with the DGEBA/MCDEA thermosetting systems modified with a) 5, b) 10, c) 20 and d) 40 wt % of LPE-b-PEO and e) 5, f) 10, g) 20 and h) 40 wt % of TiO_2LPE-b-PEO.

Figure 6.12. Images of a water droplet in contact with the DGEBA/MCDEA thermosetting systems modified with a) 5, b) 10, c) 20 and d) 40 wt % of HPE-b-PEO and e) 5, f) 10, g) 20 and h) 40 wt % of TiO_2HPE-b-PEO.